DEVELOPMENT OF A SENSOR SYSTEM TO INVESTIGATE THE ARCHING ACTION OF SOIL

Abeykoon Mudiyanselage Deshan Chanuka Bandara

178043L

Thesis submitted in fulfilment of the requirements for the degree Master of Science in Civil Engineering

Department of Civil Engineering

University of Moratuwa

Sri Lanka

February 2019

DECLARATION

I declare that this is my own work and this thesis does not incorporate without acknowledgement any material previously submitted for a Degree or Diploma in any other University or institute of higher learning and to the best of my knowledge and belief it does not contain any material previously published or written by another person except where the acknowledgement is made in the text.

Also, I hereby grant to University of Moratuwa the non-exclusive right to reproduce and distribute my thesis/dissertation, in whole or in part in print, electronic or other medium. I retain the right to use this content in whole or part in future works (such as articles or books).

Signature: ……. Date: …….

The above candidate has carried out research for the Master's thesis under my supervision.

Names of the supervisors: Dr. L.I.N. De Silva

Signature of the supervisor: …… Date: …….

Dr Y.W.R. Amarasinghe

Signature of the supervisor: …… Date: …….

ABSTRACT

This research focused on introducing a new mechanism to measure the effective earth pressure and total earth pressure in one degree of freedom sensor system. To identify the structural deformation with respect to the earth pressure (in other words sense the earth pressure) strain gauge based cross beam structure is introduced as the sensing structure. This study was focussed on measuring 150 kN/m^2 maximum earth pressure however, it is capable of customizing the system according to the measuring requirement. A novel mechanism is developed to measure the effective earth pressure directly by allowing infiltration of water into the sensor and there by cancelling the outside pore water pressure. Finite element analysis was carried out to identify and optimize the sensing cross-beam structure dimensions. Dimensions and the shape of the sensor were finalized after referring to the literature. Aluminium material was used to manufacture this sensor considering different geotechnical, mechanical and environmental factors. Precision marching methods were used to manufacture a high-quality sensor minimizing the manufacturing errors. For that CNC milling machine and CNC lathe machine in the Die and Mould laboratory were used. After that a complete data acquisition system was developed to collect, visualize and store the data. Cloud database based remote sensing mechanism was also introduced to monitor the earth pressure in real time via a web portal. Laboratory testing and validation were done using sand material. Sensitivity, zero load drift and thermal characteristic of the sensor was also identified. Finally using the developed sensor system, arching effect of sand was studied. Initially the active and passive arching effect behaviour of dry sand due to the settlement of clay soils was investigated. After that research was carried out to investigate the arching effect of dry sand and saturated sand with the known settlement. Special apparatus was developed to create a known settlement inside a sand fill .

ACKNOWLEDGEMENTS

I would like to express my sincere gratitude and admiration for the person who was behind me throughout the whole duration of this research, Dr. L.I.N. De Silva (senior lecturer, Department of Civil Engineering, University of Moratuwa) my research supervisor. Actually, this project might not have been a success without his priceless collaboration with valuable guidance.

I would also like to thank Dr. Y.W.R. Amarasinghe (senior lecturer, Department of Mechanical Engineering, University of Moratuwa) my co-research supervisor for his guidance, suggestions, and encouragement throughout this research for me to overcome the obstacles faced in the completion of the research and also for the knowledge that I gained by working under his guidance. As a multi-disciplinary topic, it wouldn't have become a success without your cooperation.

I would like to express my gratitude and special thanks to the head of the Department of Civil Engineering prof. J.M.S.J Bandra as well as the research coordinator Prof. Rangika U. Halwathura Department of Civil Engineering of University of Moratuwa. Special thanks go to all the academic and academic support staff of both the Department of Civil Engineering and Mechanical Engineering of University of Moratuwa

Finally, my heartiest gratitude is given to Prof. S.A.S.Kulatilaka, Dr U.P. Nawagamuwa and Dr. (Mrs.) Ashani Ranathunga from Geotechnical Engineering Division, as well as the non-academc staff of the Geotechnical Engineering Division Department of Civil Engineering, University of Moratuwa. My special thanks should go to my colleagues for the support and encouragement they gave throughout this research study.

Thank You,

A.M.D.C. Bandara

CONTENTS

LIST OF FIGURES

LIST OF TABLES

1 INTRODUCTION AND STRUCTURE OF THESIS

1.1 Research background

Identification of the load transmission through the soil skeleton and evaluation of pressure on planes due to applied forces is important. According to [1] there is a relationship among the three stresses in soil. Total stress is defined as the force acting per unit area due to soil mass in the normal direction on a plane. Pressure due to water filling in the voids, is named as pore water pressure. Stress on the plane due to soil skeleton is known as the effective stress. In addition, several internal and external factors influence the earth pressure. One of the prominent scenarios is the arching effect. When the part of support of the soil mass is going to yield while the remaining soil mass stay in the same position, relative movement occurs between the adjacent soil masses, which develops a shear resistance to keep the yielding soil mass stationary. Therefore, pressure transfers to the stationary soil mass from the yielding soil mass. Then pressure of stationary part increases. That mechanism is commonly called the arching effect.

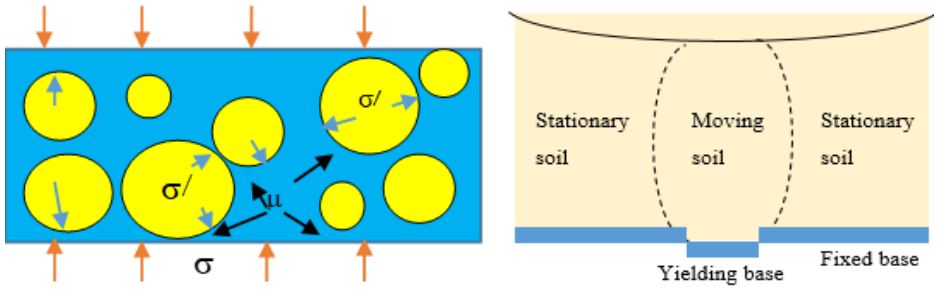

Figure 1: Pressure transfer in soil and arching effect

In Civil Engineering perspective, all kinds of structural loads ultimately get transferred to soil. These loads and loads due to the existing soil mass and water, create an earth pressure (total stress, effective stress) on a given point in a soil mass or an interface between structural elements and the soil mass. For the applications like dams, retaining walls, backfills, culverts, different types of abutments and foundations; measurement of soil pressure acting on different directions is an essential requirement. In addition, earth pressures will be affected by arching action (Ex: flexible pipe in the earth dam, culvert in the embankment) which highlights the

importance of measuring actual earth pressure on such locations. There are, three methods available to estimate the earth pressure. Those are constructive theories and mathematical models, computational and numerical techniques and field earth pressure measurements.

Earth pressure cell is kind of a force transducer which is designed to measure the normal stress in soil [2]. According to their usage, they can be divided into the two major categories [3] namely; embedment type earth pressure cells which will measure the pressure distribution inside the soil mass and magnitude of the soil pressure [4] and contact type earth pressure cells which is used to measure the earth pressure in the interface of soil mass and the structure [5].

Figure 2: Earth pressure cells [6]

Main task of the earth pressure cell is to obtain an actual representation of the real earth pressure. Accuracy and reliability of the sensor is important, which varies with several factors. Those are inclusion effects (aspect ratio, cross-sensitivity, proximity of structures and other stress cells, stress-strain behaviour of soil), cell/soil interaction (s-cell stiffness ratio, diaphragm deflection(arching), eccentric, non-uniform and point loads), placement effect and environmental effect, and dynamic response. Two types of earth pressure cells are available; hydraulic pressure cells and deflecting diaphragm type cells. Hydraulic pressure cell consists of two welded metal plates on their periphery, creating an intervening cavity which is filled with a thin layer of fluid [7]. Deflecting diaphragm cells have a readable electrical output due to attached strain gauges or vibrating wire strain gauges.

1.2 Research problem

Even though several constructive theories of geomaterial behaviour and computational techniques have been developed to estimate the earth pressure, verification of the developed theories is necessary to establish the basic principles [8]. In addition, direct use of constructive theories or use of numerical techniques for this purpose is questionable because of the several external and internal factors affecting the accuracy like arching effect and non-homogenous nature of soil. Hence, in practice, it's common to see engineering judgments taken with the aid of experience which leads to over estimation or under estimation. To overcome those problems, use of an earth pressure cell will be much useful.

Other than that, evaluation of arching effect is not an easy task via analytical or numerical methods. Finite element methods are applicable for small strains and deformations, but soil/pile systems usually accompany large deformations due to soil arching behaviour. We have to consider the finite deference method which is valid for large deformations. However, this approach is needed for a proper definition of interface mechanical model, however in the practical scenario it is very difficult to obtain a reliable soil/structural interface constructive model.

Based on the above discussion it can be concluded that devices like earth pressure cells, measuring systems and measuring instruments are available to estimate the directional earth pressure. However, in Sri Lankan context it is difficult to use these available devices due to the incompatibilities of requirement basically impractical power supply method ,difficulties and complexity of operations and unbearable cost. On the other hand most of the available systems are capable of measuring only the total earth pressure and it is needed to measure pore water pressure separately to estimate the effective earth pressure.

1.3 Objectives

The objective of the research work could be identified as follows. The scope of the research is bounded by the objectives.

• Develop a sensor system to measure the effective and total soil pressure both in laboratory conditions and under field conditions. This sensor system consists of two sensors which are capable of measuring pressure up to 150 kN/m^2.

• Develop a data acquisition system with the developed sensor system which is capable of collecting the real time data and transmit that data to cloud-based system. Furthermore, it will be able to store the collected data locally and display those in real time.

1.4 Limitations

The research work is bounded by following limitations which caused due to technical capacity and time frame constraints.

Upper limit of 150 kPa pressure level is used in the research work. This upper limit could be justified since the experienced effective earth pressure and total earth pressure values are within the chosen upper limit in most cases. Although the design was limited to the above upper limit it could be increased to higher values if there is such a requirement.

The embedded depth of one degree of freedom sensor system Is limited to 3 metre depth due to the length of the selected cable. it is justifiable to use at 3 metre depth in measuring the arching effect since the critical values of affective earth pressure and total earth pressure could be experienced within the depth of 3 metres. The design could be altered to reach higher depths if required. The sensing system is designed to correspond and measure pressure values to an accuracy of 1 kPa.

After the development of the sensor system it is required to calibrate. The research work was extended to calibrate the device for sandy soil. Due to the time constraints the calibration process was limited for sandy soil. Calibration should not depend on the soil type.

Testing of arching effect using this device could be validated only for sandy soils as the calibration was carried out using sandy soil in the research work. it could be extended to other types of soils in future work.

1.5 Methodology

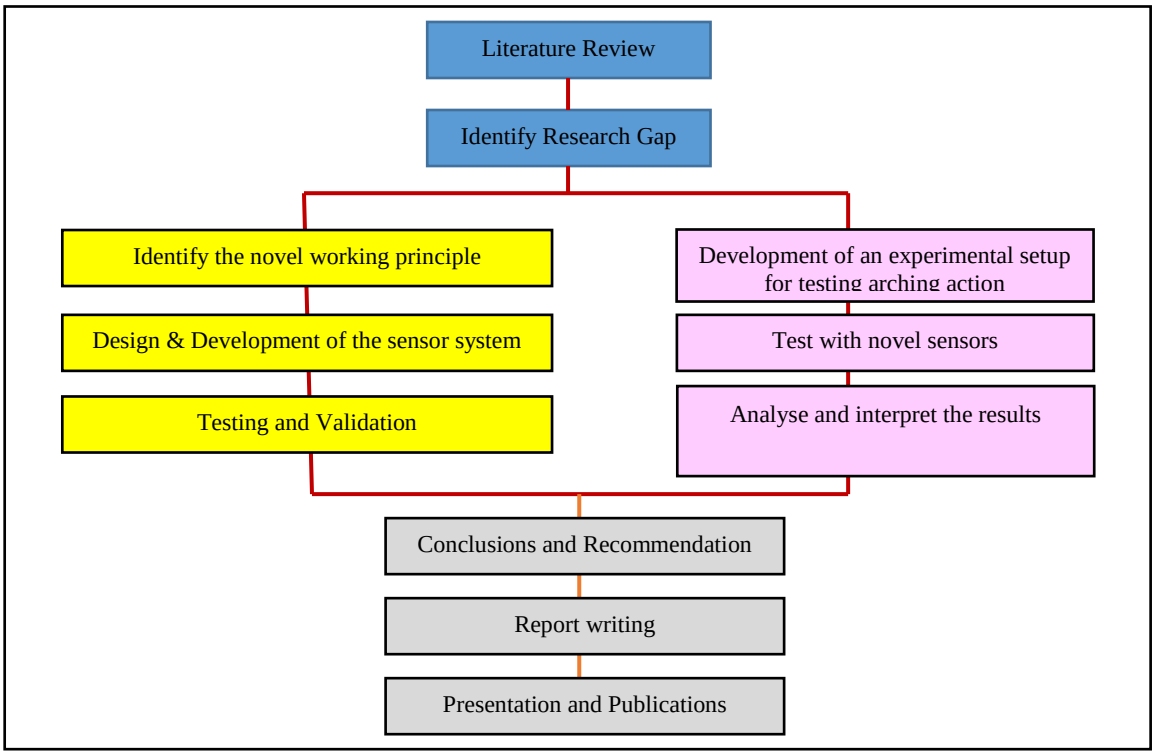

Figure 3: Methodology

The methodology of developing a new mechanism to measure the effective earth pressure and total earth pressure in one degree of freedom sensor system is structured as given in the Figure 3.

An in-depth literature survey is done to identify and study the available methods for measuring earth pressure and pore water pressure and the technologies available for load sensing systems. The literature survey initially evaluates the concept of earth pressure cells in which the whole ideas of the research is based upon. Later, different types of load cells which are used for measuring pressure are evaluated and compared. Measuring principles behind load cells, sensing method used in fiber optic sensors for earth pressure measurement, principles behind tactile sensors and piezoresistive cells are discussed in detail to understand the theory behind the research objectives.

Next the literature survey identifies factors affecting the earth pressure measurement and arching effect. Factor such as sensitivity of measuring equipment, effect due to stress-strain behavior of soils, Non-uniform load distribution, placement effects of earth pressure cells and environmental effects and dynamic response are evaluated

based on the available literature. It was possible to identify drawbacks in the existing methods and possible improvements which could be implemented in this research. Further requirement of calibration and methods of calibrating earth pressure cells are evaluated.

The latter part of the literature survey elaborates on the theory behind arching effect of soils. Starting from the background behind the arching effect of soils, it elaborates on different theories proposed on quantifying the arching effect. The literature survey concludes after elaborating on several experiments conducted to evaluate arching effect of soils which could be used in developing the proposed sensing equipment.

The methodology expands to the third chapter which explains the design and development of a new sensor and data acquisition system to measure the earth pressure including soil and pore water pressure. It starts with explaining the novelty behind the proposed methodology compared to the methods available in literature. The proposed method has two sensing units, one for measuring the total stress in the soil and the other one for measuring the effective earth pressure in the soil. The sensing mechanism is based on the deflecting diaphragm which deforms respect to the earth pressure. The next sections further elaborate on sensing techniques which are used in measuring the pressure values. The latter part of chapter 3 explains about the data acquisition system proposed in design and the development principle behind it.

The chapter 4 elaborate on structural development of sensing equipment. It discusses the methods used in developing sensing structures required in the sensing equipment. A finite element analysis is presented to understand the structural integrity of the sensing equipment which will contribute to precise measurements. The chapter 5 elaborates on methodology used in developing sensing elements and theory associated with the sensing architecture. Further it justifies the placement of sensing elements in the sensing equipment. The chapter 6 discusses on the fabrication and packaging of sensing equipment. Precision machining of sensing structure, main casing, pressure acting plates, load transfer rod and other fixing elements were discussed in detail. Further fixing of sensing elements to sensing structure and water filtering mechanism

is discussed at later stage. The chapter 7 focus on the methodology used on communicating the sensed measurements from the sensing equipment to data logger. communication methods of signal conditioning processes, amplification of signals, analogue to digital conversion are discussed in detail. The chapter 8 focus on the remote monitoring platform and data logging system embedded to the sensing device which make it a wholesome product to be used at industry level.

2 LITERATURE REVIEW

2.1 Earth pressure cell

2.1.1 Introduction

Earth pressure cells are used to measure accurate values of earth pressure. When considering the types of earth pressure cells, those can be separated according to the preposes, the basic mechanisms used to develop etc. Mainly earth pressure cells are designed to measure the earth pressure within the soil mass or in between a structural element and soil mass[3]. Normally embedded load cell is used to measure the magnitude and as well as distribution of the insitu stress in backfill material and embankment. Other than that, contact earth pressure cells are used to take the measurements of pressure in culverts, shallow foundations, culverts and retaining walls [9]. The Main purpose of using earth pressure cells are to measure the actual earth pressure to verify the design assumptions and get feedback to improve the future designs [10].

Behaviour of soil is very complicated because it is depending on the soil type, stress history, shear and normal stresses, drainage and boundary conditions, and several other environmental effects. Therefore, different researchers identified different factors to minimize the difference between actual stress and the shown value of the earth pressure. Factors like inclusion effects, cell/soil interaction, placement effect, environmental effects and dynamic responses are identified.

To overcome the above effects and focusing on the different requirements, various types of earth pressure cells have been developed. Mainly two types of mechanisms are used to sense the earth pressure namely; hydraulic pressure cells and deflecting diaphragm sensing cells [9]. Based on these mechanisms, several types of earth pressure cells are available including load cells, fiber optic sensors, tactile sensors and soil Pressure Mini-Sensor etc [10].

One of the most prominent techniques of the load cell is the strain gauge based deflecting diaphragm sensing cells. Other than the earth pressure measuring, in

modern days strain gauge-based load cells are developed for various purpose[11], [12]. Mainly the load cells applied in robotic research and haptic-based human-computer interaction is currently developed using this strain gauge based deflecting beam structures [13], [14]. Furthermore, these kinds of sensors are used to identify the foot forces in human legs as well [14], [15], [16]

2.1.2 Types of earth pressure cells

2.1.2.1 Load Cell

Load cell belongs to the transducer family which convert forces into an electrical output. When considering the load cells, various kinds of transducers are available considering the application requirement and installation procedure. Fairly high stiff plate or surface is provided in the load cell to carry the load transfer to the transducer. As an example, this plate's top surface is in contact with the soils. When load is applied on to the deformable face, the relevant signal transfers to the transducer and a readable output is given via the data acquisition system [10]. Load cells can be divided into different types according to the mechanisms of the output signals generated like hydraulic, pneumatic, electrical, etc.

Hydraulic pressure cell consists of two welded metal plates on their periphery, creating an intervening cavity which is filled with a thin layer of fluid [7]. The pressure from the soil transfer to the top piston pad and that is going to compress the hydraulic fluid which is filled in the middle diaphragm chamber as shown in Figure 4. This sensor is ideal for applying in the hazardous areas due to no electric components.

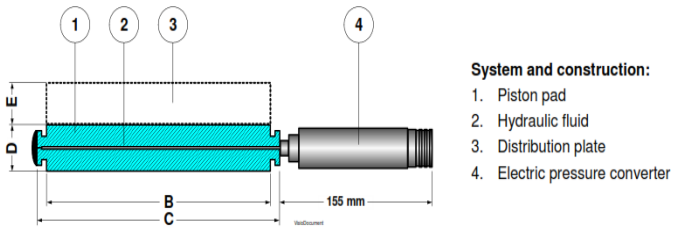

Figure 4: Hydraulic Pressure Cell [6]

Pneumatic load cell is also based on the force balancing method. In this case no fluids are in the middle of the diaphragm. These kinds of resonant wire type pressure cells (transducer) were introduced around 1970s ([17],[18]). In this wire, one end is

connected to the static element and other end is connected to the sensing diaphragm as shown in Figure 5. A circuit is included to make the wire to oscillate at its resonant frequency. When the deformation of the diaphragm varies due to pressure, wire is subjected to tension. That phenomena changes the resonant frequency of the wire. This frequency change can be identified very precisely. Therefore, this kind of a load cell can be used to measure the very low differential pressure values.

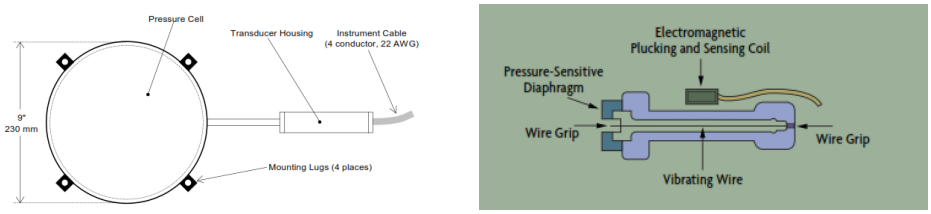

Figure 5: Transducer [17],[18]

Strain gauge-based load cells are widely used to measure the pressure, but not only the earth pressure. This research is also focused on developing an earth pressure cell. Mechanism of this load cell converts the loads into electrical signals via strain gauges. These strain gauges are connected to the structural element using the bonding agents. Purpose of that is to sense the deformation of the structural elements when a load is applied [9]. A typical strain gauge-based load cell is shown in Figure 6. In this case four strain gauges have been used to sensor the deformation of the structural members to make the Wheatstone bridge to obtain the maximum sensitivity and temperature compensation.

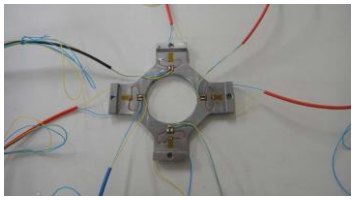

Figure 6: A typical strain gauge based load cell [15]

The null pressure cell was introduced by J. E. Jennings [19]. In that case they have used the pressure balancing method to measure the applied pressure. Chamber deformation due to the applied pressure on outside is measured and provide equivalent pressure to make the deflection zero. To maintain the chamber deformation in zero position, null point indicator which is kind of a linear differential transformer,

is used [19]. Null pressure concept-based load cell is initially developed and used to measure the soil pressure under road embankment by G. Margason and M. J. Irwin[20]. According to Figure 7 strain gauges are bonded to the structural sensing elements in an air pressurized steel chamber. When some membrane strain affects the sensing element due to external pressure, it is detected by strain gauges and air is pressurized until the membrane comes back to their original positions. M. Talesnick [21] used null pressure cell to measure the contact pressure on a buried structure.

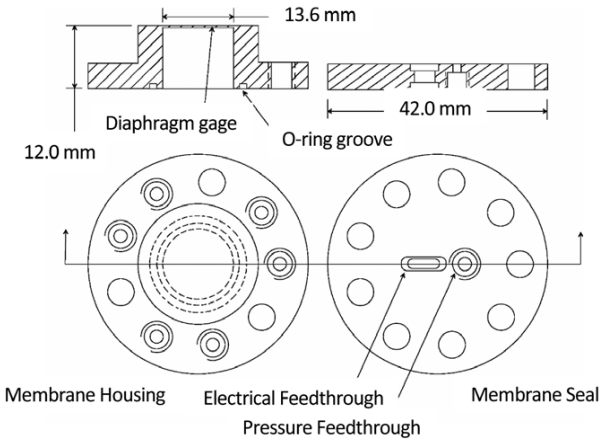

Figure 7: Schematic section of null pressure sensor [21]

According to the above discussion, it can be concluded that various kinds of load cells with various types of mechanisms are available for earth pressure measuring purposes. Most common type of load cell for earth pressure measurement is hydraulic pressure cells.

2.1.2.2 Fibre optic sensor (FOS)

Nowadays fibre optic sensors are widely used for different applications [22] including biomechanics [23], biomedicine [24], temperature [25], water and waste water treatment [26], navy applications (navigation) [27] etc. There are some parameters in the optical beam which are intensity, wavelength, polarization etc. have been used for the sensing principle. FOS became a commonly used sensor tool during late 1970's due to the advantages of immunity to electromagnetic interface, small size, large bandwidth, lightweight, high sensitivity and easy implementation [28].

Other than the pressure measurements, it is used for different purposes in civil engineering field includes bridges, dam and tunnels monitoring systems [29], moisture and chemical content of the soils [30], [31] and strain in the pipes [32].

When geotechnical applications are considered the most common types of FOS are Fabry Perot Sensors (FPI) and Fibre Bragg Grating Sensors (FBG), rather Distributed Brillouin/Raman Scattering Sensors that are used mainly for structural health monitoring systems [33]. The different between the FPI and FBG sensors are such that FBI has two mirrors reflectance which are separated by an air gap as shown in Figure 8 and FBG is made out by altering the optical fibre core via exposing to the Ultraviolet light as shown in Figure 9. As shown in Figure 10 Fibre Bragg Grating Sensors are manufactured to measure the effective and pore water pressure in soil application [34], [35].

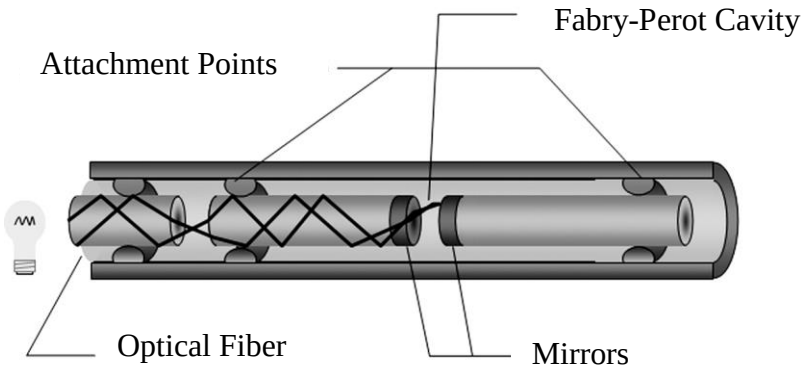

Figure 8: Operating principle or a Fabry-Pérot cavity sensor [33]

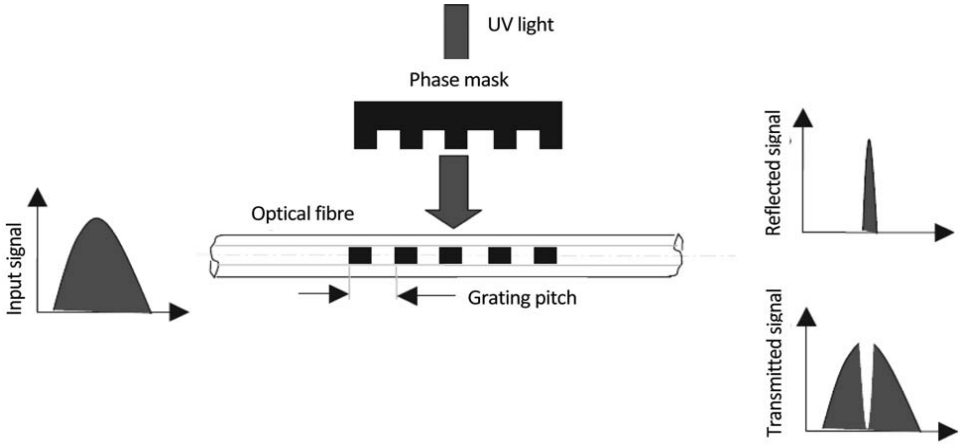

Figure 9: Operating principle or a Fibre Bragg Grating Sensors [10]

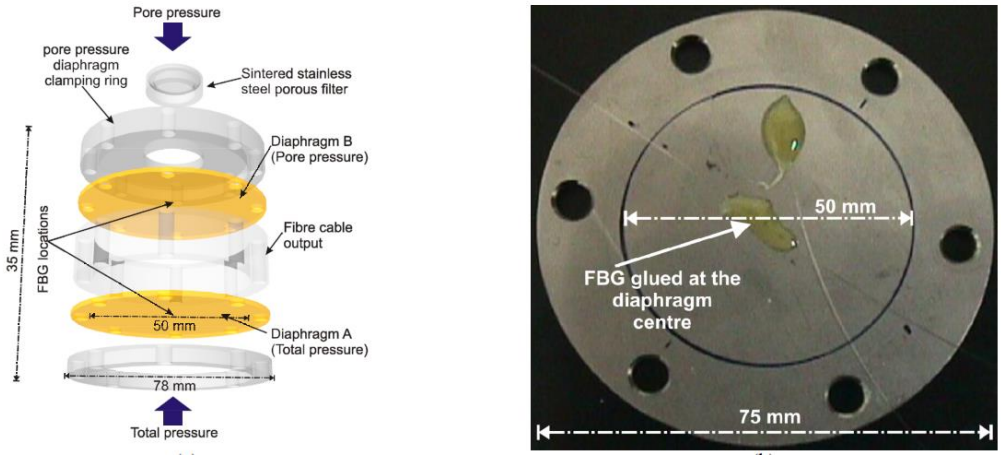

Figure 10: Schematic diagram of the effective pressure sensor (Left) and photograph of an FBG glued at the diaphragm centre (Right) [34]

2.1.2.3 Tactile sensors

Principle behind the tactile sensors is the change of electrical resistance with the pressure of a material placed between two electrodes or in touch with two electrodes placed at one side of the material [36]**.** Tactile sensors are widely used in different geotechnical applications to measure the soil pressure. Tactile sensors are used to measure the pressure distribution under rigid footing on sandy soil by S. G. Paikowsky[37]. And, they show a good relationship between theoretical values and measured value. Other than that tactile sensor is used to measure the rock fall pressure distribution on protection wall by S. Springman[38]. In addition to the previous examples, tactile sensors are used to measure the soil pressure on buried pipes in radial pressure [39],[40] to measure the lateral earth pressure on the pipe [41] as shown in Figure 11, and to measure the soil pressure on pipes due to cyclic loads [42].

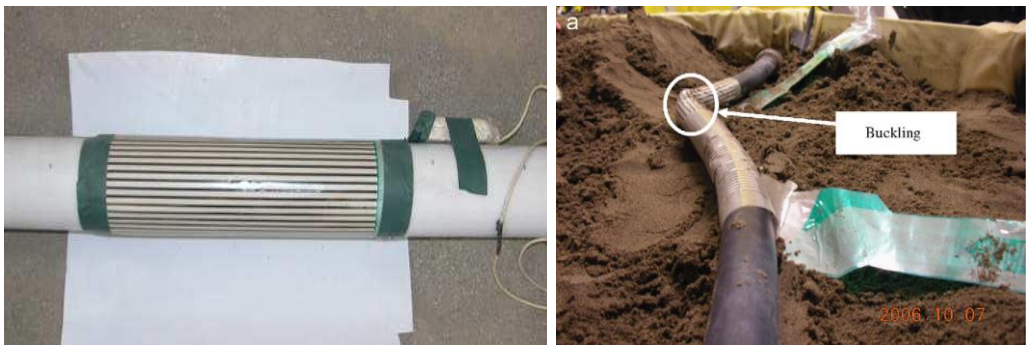

Figure 11: Tactile sensors are bonded to pipes [41], [39]

2.1.2.4 Piezoresistive Cells

This cell is based on the generation of electric current with some frequency when piezo-electric materials like polyvinylidene fluoride, mono-crystalline silicone are subject to the pressure. This material is generally laid on the flexible sensor to generate the current with respect to the applied pressure. Importance of the piezoresistive cells compared to tactile sensors is piezoresistive cells can be used to measure the dynamic load rather than static loads. Piezoresistive cell is used to measure the soil pressure under explosive loads [10].

In addition to the above, different types of sensors have been developed to measure the earth pressure. One of the examples is **Normal and Tangential Pressure Cells** to measure the earth pressure in vertical and horizontal directions. To measure the soil pressure, **Mini-sensor** which is used to measure the earth pressure, developed by Y. Xiao [43] can be used.

Nowadays lot of researchers are moving to develop the mems sensors rather than dealing with the conversional earth pressure cells.

Table 1: Comparison of Different Types of EPC

Technique of the earth pressure cell	Advantages	Disadvantages
Conventional load cells	• Are in use for more than 7 decades • Due to the wide usage, lot of technical problems and errors are identified • Commonly available. Because many suppliers are there • Familiar to use these load cells	• Most of the load cells are based on strain gauges, then limitations of stain gauges are common to load cells • There are some problems like aspect ratio due to the geometry • Can measure only one pressure at a located point

Fibre optic sensors	• No issues related to the electrical circuitry • Remote sensing method available for long distance • Capable to resist the water effects • Multiplexing feature is also available to connect several sensors to one wire	• Given value can get affected from the temperature • Small gauge length (around 25 mm) • Not much common because it is relatively new to the earth pressure measurements
Tactile sensors	• It is possible to measure the earth pressure distribution rather than observing the single point pressure value. • 3D soil pressure distribution can be visualized • Size of the sensor is very thin and flexible • Possible to customize different sizes and shapes according to the requirements like pipe diameter and curvature.	• Given output is based on the qualitative measurement rather than quantitative measurement • If quantitative value is required, extensive calibration should be needed.

2.1.3 Factors affecting the earth pressure measurement

2.1.3.1 Arching effect

One of the most important phenomena in the earth pressure is the arching effect. There are two situations namely active arching effect and passive arching effect. First one occurs when the modulus of the structural element is larger than the modulus of the soil medium at the measuring point. In such case the measuring stress of the earth pressure cell is larger than the actual stress at that point in the free condition. That phenomenon is called as "passive arcing" and due to that "over-registration" occurs by the cell. Second one occurs when the modulus of the structural element is less than the modulus of the soil medium at the measuring point. In such case the measuring stress of the earth pressure cell is less than the actual stress at that point in the free condition. That phenomena is called as "active arcing" [1] and due to that "under-registration" is happening by the cell. This is shown in Figure 12.

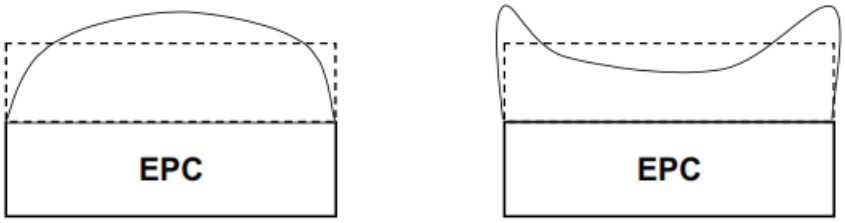

Figure 12: over-registration and under-registration [41]

Table 2: Factors affecting to Earth Pressure cell output results

Factors affecting the earth pressure cell out put	Explanation of the error	Suggested method for correction
Inclusion effects for earth pressure cell		
Aspect ratio (Cell thickness: Cell diameter)	Cell thickness is going to change the stress field around the cell	• Use of the relatively thin cells [9] • To maximize the accuracy of the earth pressure cell output, aspect ratio should be minimized as much as possible [46]
Error due to stress (improper stress distribution at cell)	This error occurred due to stress concentration in corner areas of the earth pressure cell. Due to that reason cell is going to over register.	• To avoid the effect, outer rim is provided which does not affect the input. In other words, it is called as an inactive outer rim. Sensitive area to whole area ratio (d^2 to D^2) might be less than 0.25 – 0.45 [4], [47] • Other (Outer) sensing area diameter called active diameter. The values of d to D_{50} which is the grain size ratio should be greater than 10 [48]

	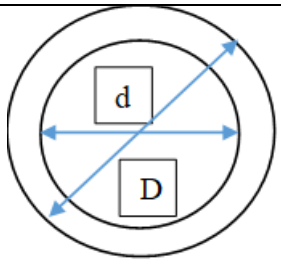	
Cross sensitivity of the Earth Pressure Cell	Cell can deform due to lateral pressure of soils..	• Solution is depending on the sensing mechanism • In strain gauge-based earth pressure cell, sensor can be added to outer ring [49]
Effect of the gap between structures and other earth pressure or stress cells	Other cells and structures influence on stress distributions.	To avoid and minimize the effect of other structures and cells, following gap should be maintained with the earth pressure cell. • Horizontal Distance – 1.5 x Diameter of sensor • Vertical Distance – 4 x Diameter of sensor • From face of structure to edge of cell Distance – 0.5 x Diameter of sensor [3]
Effect due to stress-strain behavior of soils	Confining conditions can affect the earth pressure cell results	To avoid that error, calibration of the earth pressure should be done in real condition.
Cell/soil interaction effects for earth pressure cell		
Stiffness of the soil and earth pressure cell ratio	If stiffness of the soil and cell are not compatible that may lead to nonlinear calibration	Ratio between the earth pressure cell stiffness and soil stiffness might be greater than or equal 0.5 [50]. To avoid this issue, stiff load cells should be used.

Arching effect due to the deflection of the diaphragm	Pressure distribution is going to change around the Earth pressure cell. This issue occurs due to excessive deflection of the load acting surface.	Ratio between the sensitive diameter of the earth pressure cell and the maximum deflection > 2000 – 5000 [51]
Non-uniform load distribution, Eccentricity of load and acting of point loads	One of the main reasons is the soil particle size. When grain size is too large compared to the cell size this can happen.	Sensitive diameter should be large (D/D_{50}>10 to 50) [4]
Placement effects of earth pressure cell		
Effects due to placement	When the Earth pressure cell is going to get placed, disturbance can happen to soil structure.	This is a kind of a random error
Stresses variations	Sometimes this is occurring due to the soil compaction.	
Environmental effects and dynamic response		
Temperature effects	Effects due to temperature variations inside the soil.	Earth pressure cell should be calibrated at that specific temperature or result adjustment should be done according to the temperature variation

Dynamic stress effect to the EPC measurements	Response time of the EPC, natural frequency of the EPC and inertia of the EPC may cause some error	When EPC is calibrated, dynamic effect should consider (dynamic calibration)
Corrosion and moisture effects	This may lead to breakdown or failure of the earth pressure cell	According to the situation proper action should be taken

2.1.4 Calibration of the Earth pressure cells

The calibration of the earth pressure cells is the investigation and identification of the specific relationship between the earth pressure cell output result and the applied load [52]. Calibration is focused on identifying the calibration factor to convert the EPC output voltage value which is related to pressure value provided by the EPC, to stress (kPa). Whole idea of the developed earth pressure cell properties and expressions of the design is provided by the calibration experiments [3]. It is better to do a higher number of testing under various condition, because it helps to get accurate output when it is used in the field with unknown loading histories [53]. Mainly there are two ways to calibrate the earth pressure cells namely; known fluid pressure applied method and using a soil pressure applied method. When these two methods are compared, unlike a fluid calibration, earth pressure calibration shows non-liner behaviour between the applied load and the output voltage due to arching effect in the soil [54], [55].

The relationship between the applied load and EPC measured value was described by the CAF concept in other words Cell Action Factor concept as shown in Eq. 1. Mainly this concept is introduced to countify the error of the measurement. Actually, this factor is the ratio between the normal pressure which is measured by the earth pressure and pressure of that point when EPC in the absence [55].

$$CAF = {P_{measured}}/{P_{Applied}} \qquad \text{…….. Eq. 1}$$

2.1.5 Strain gauge based deflecting diaphragm sensors for different purposes

2.1.5.1 A novel self-decoupled four degree-of-freedom wrist force/torque sensor

A novel 4 DOF wrist force/torque sensor has been developed in the past which is suitable for HapHCI as shown in Figure 13[13]. When Fx force is applied to the elastic body in X- direction OA and OC are floating on the two vertical beams AA' and CC' which act as compliant beams. Similar to that when Fy is applied in Y direction OB and OD become a freely supported beam with two vertical beams BB' and DD' acting as rigid beams.

When Fx force is applied on the elastic body in X- direction OA and OC are floating to the two vertical beams AA' and CC' which act as compliant beams. Similar to that when Fy is applied in Y direction OB and OD become a freely supported beam with two vertical beams BB' and DD' acting as rigid beams. Z direction also act in a similar way. When applying the Mz movement to four horizontal beams OA, OB, OC, OD, they are identically deformed.

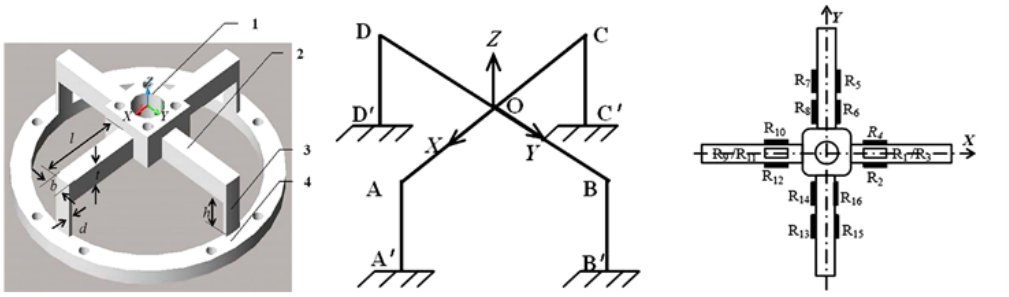

Figure 13: Sensing structure of 4DOF force/torque sensor [13]

(Song et al., 2007) developed this sensor system in the measurement range of the forces/torque as FX = ±20 N, Fy = ±20 N, Fz = ±20 N, Mz = ±20 · 4.5 N mm, respectively. Song et al., (2007) has used only 16 strain gages.

2.1.5.2 A novel three degree-of-freedom force sensor

During 2009 Chen & Song has targeted to introduce new a three degree of freedom force sensor for Haptic based human-computer interaction[56]. A spoke-type elastic body is used for sensing of the forces as shown in Figure 14. The applied force is transferred to the elastic beam through the axle which is fixed in the center support.

Hilton bridge circuit is used to place the 12 strain gages to measure three orthogonal forces with low couple interference. When applying Fx force in x-direction to the centre OA and OC become compression and tensile members while OB and OD bend and act as simply supported beams. Then strain gauges which are connected to the OB and OD can be used to measure Fx. Fy can be also measured in a similar way.

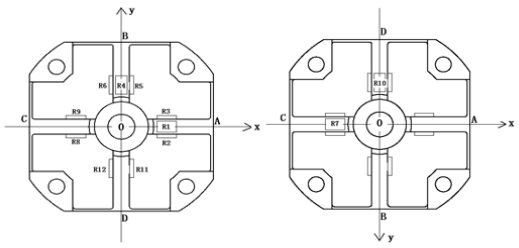

Figure 14: Sensing structure and 12 strain gauge distribution [56]

When applying Fx force in x-direction of the centre OA and OC become compression and tensile members, respectively while OB and OD bend and act as simply supported beams. Then strain gages which are connected to the OB and OD can be used to measure Fx. Fy can be also measured in a similar way. When applying Fz force in z-direction AOC and BOD beams act as simply supported beams with center joint. Fz can be measured by Hilton Bridge Circuit which composes of strain gauges on both front and back surfaces of cross beams OB and OD. The sensing element which is used for the generation and amplification of force signals contains the sensitive section, Hilton bridge circuit and the amplifying circuit, while the sampling circuit consists of the circuit with USB interface mainly.

2.1.5.3 A three degree of freedom force/torque sensor to measure foot forces

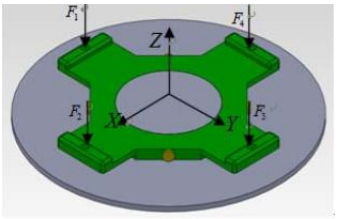

Figure 15: Symmetric sensing structure [15]

A 3 degree of freedom force/torque sensor has been introduced to measure foot forces [15]. For that a strain gauge attached cantilever system is used as shown in Figure 15.

Main three components, base plate which is touching the ground, upper plate which is connected to the foot and the sensor element which is placed in between that plate, are used to make the sensor platform with a 10mm overall thickness. Sensor element which is made out of 17-4PH stainless steel, consists of four chains of cantilevers. Because it is needed to identify the vertical force and horizontal components (fx, fy and fz) for simulating the motion of human or legged robots. This sensor is designed for a maximum 2000N vertical load and 500N lateral loads considering human weights. Other than that microprocessor-based data acquisition system is designed to handle the data. [15]has tried to develop a very simple and thin structure with a capability of supporting a large force and a low-cost sensor system.

2.2 Arching effect

2.2.1 Background of the arching effect

The beginning of the arching effect findings are dated back to late 1800s. During early 1900s drainage engineers observed some structural failures in conduits (Buried pipelines) which are placed in underground due to soil loadings[57]. Then they started to evaluate different soil loading action on the underground pipelines [57]. The concept was based on a soil column which is above the buried pipelines, transferred their (soil column) weight to the adjacent soil walls due to arching action. Therefore, finally due to the result of that phenomena transferred overlying soil loads on the pipe will be reduced. To quantify that effect, different empirical relationships were introduced. Some developed relationships which are used up to now [58]. According to K. Terzaghi [1], arching effect in soils which occurs in the field and laboratory conditions is a universal phenomenon. Terzaghi used these phenomena to describe the soil overburden pressure on yielding foundation types and different type of voids which are created due to differential settlements. In 1985, the shape of the catenary concept for soil arching was proposed by Handy. Handy proposed that the shape of the arched soil is a catenary. He proposed that the major or the minor principal stresses take the shape of a catenary; if the arch is fully self-supporting, as is the case of a lintel, the catenary represents the direction of the major principal stress, and, if the arch is only partially supporting, the catenary is inverted and describes the path of the minor principal stress [59].

Early 1970's computer technology-based techniques were introduced to study different types arching problems. In the beginning, (Getzler,et. al., 1970) carried out some analysis for arching pressure in ideal elastic soil model using finite difference method. In 1982 L. C. Rude was going to identify the behavior of an installed culvert in the laboratory tank via linear FEA (Finite Element Analysis) program [60]. Other than that, several FEM models are presented by different researches [61], [62] and [63]. The main limitation of finite element method (FEM) is, it can be applied only for small strains and small deformations [64]. Other than the FEMs, Finite Difference Method (FDM) was also widely used [65]. The limitation in this FDM is, it is valid mostly for large deformations. Researchers have moved to the use of discrete element methods recently [64].

After Terzaghi's findings (1936) regarding the arching effect in trap door test lot of researchers continue research in this field. As examples [66], [67], [68], [69] and [70]. Centrifuge modeling was used to identify the scaling issues and study about the arching effects in geomaterials by G. Lglesia [71]. Other than that photogrammetric method was used to measure and identify the stress distribution by T. Yoshida [72]. Tactile sensing method was used to investigate the stress distribution.

2.2.2 Definition of the Arching

"When a specific part of a soil mass support is going to yield while another part of the soil mass support remains same at the same position, then adjacent stationary soil masses try to hold yielding part soil in the original position. Shear resistance generates within stationary and yielding masses due to relative movement of them. Since the shearing resistance tries to keep the yielding mass in its original location, the pressure acting on the yielding part is reduced and the soil pressure on the stationary part of the support is increased." [1] as shown in Figure 16.

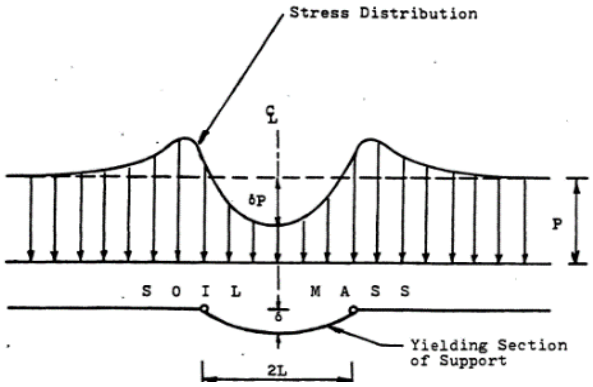

Figure 16: Stress Distribution of the soil above the yielding part of the support[73]

2.2.3 Arching theories

2.2.3.1 Marston and Anderson Theory (1913)

This concept is based on the load in the soil column which is above in the buried pipe is changed by the arching action via transmitting the soil column load to the adjacent prisms in column sides as shown in Figure 17. Due to that reason the load acting on the pipe is reduced. mason and Anderson introduced following expression (Eq. 2) to calculate the load acting on the pipe.

$$W = \frac{\varepsilon^{1-\frac{1}{2K_{\mu'}\frac{H}{B}}}}{2K_{\mu'}} wB^2 \ldots\ldots\ldots\ldots\ldots\ldots \text{Eq. 2}$$

Please double check the accuracy of this eq. It does not look right.

Where

W= total weight on pipe, per unit of length

V= the average intensity of vertical pressure at the top of pipe, per unit of area

w= the weight of ditch filling, per unit volume.

B= breadth of ditch a little below the top of pipe

H= height of ditch filling, above the top of pipe

μ= the coefficient of internal friction

K= the ratio of lateral to vertical earth pressure

μ'= the coefficient of friction of ditch filling against the sides of the ditch

ε= the base of Napierian logarithms

C= a coefficient of loads on pipe ditches.

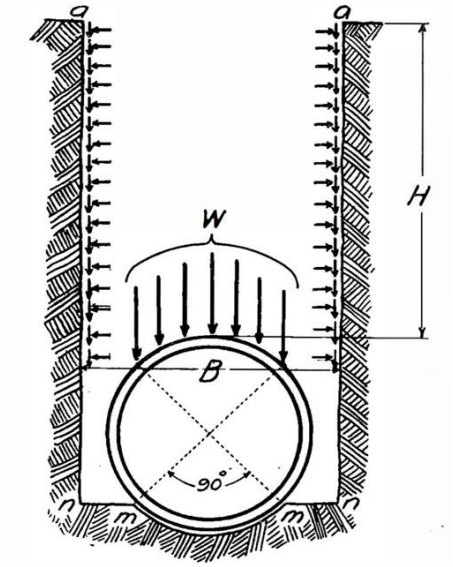

Figure 17: Load Acting on the pipe[57]

2.2.3.2 Terzaghi Theory (1948)

Terzaghi explained the arching effect by distributing the pressure among the yielding part of soil mass and the stationary part soil masses. According to his theory, this load transfer happens due to shear resistance which is due to relative movement among the contact area between the yielding soil mass and stationary soil mass.

According to the real scenario, Terzaghi observed that sliding surfaces' behaviour is curved shaped and spacing of soil surfaces is greater than the yield strip width. As shown in the following Fig yield strip named as "ab" and the real curved sliding surfaces are named as curve "ac" and curve "bd". Following assumptions which is based on experimental observations, are made in arching theories.

- The sliding surface were vertical (which is shown as ae and bf in Fig 18)
- Pressure acting on the yield strip (ab) is equal to difference of the weight of the sand in vertical strip (area among the ae and bf lines) and vertical section shear resistance.
- Across the horizontal section, normal stress is uniformed
- Lateral stress coefficient (K) is constant
- Along the sliding surfaces, cohesion is (c)

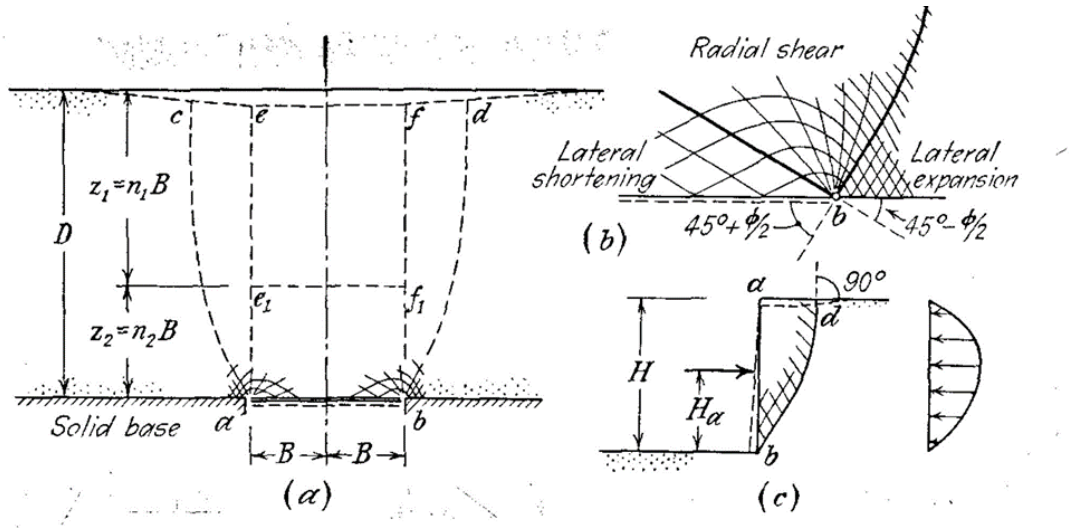

Figure 18: Terzaghi's arching effect models[1]

Considering the free body vertical equilibrium as shown in Figure 19 the Eq. 3 was derived.

$$2B\gamma dz = 2B(\sigma_v + d\sigma_v) - 2B\sigma_v + 2cdz + 2\sigma_h dz \tan\emptyset \ldots\ldots \text{Eq. 3}$$

Where

2B = Yield strip width,
z = Depth to the support,
γ = Unit weight of soil,
σ_v = Stress in vertical direction,
σ_h = Stress in horizontal direction,
K= Lateral stress coefficient,
c = Cohesion,
∅ = Friction angle.

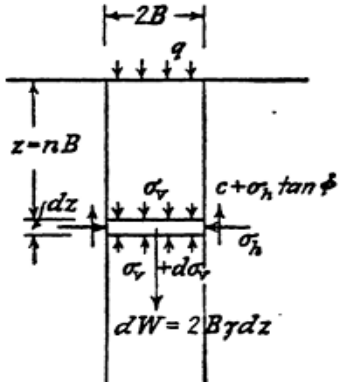

Figure 19: Free body diagram [1]

Then considering the boundary conditions, (σ_v = q (surcharge) and z = 0 level) Eq. 4 was obtained.

$$\sigma_v = \frac{B\left(\gamma - {}^{C}/_{B}\right)}{K\ tan\emptyset}\left(1 - \ e^{-Ktan\emptyset\frac{z}{B}}\right) + q.e^{-Ktan\emptyset\frac{z}{B}} \ldots\ldots\ldots\ldots \text{Eq. 4}$$

According to the Terzaghi assumptions shear resistance is active on the lower part of "ae" and "bf" boundaries. Let z_1 = n1B which is part of the prism act as the surcharge and z_2 = n2B which is a part of the prism act as shear resistance as in Eq. 5.

$$\sigma_v = \frac{B\left(\gamma - {}^{C}/_{B}\right)}{K\ tan\emptyset}\left(1 - \ e^{-Kn2tan\emptyset}\right) + Bn1.e^{-Kn2tan\emptyset} \ldots\ldots\ldots \text{Eq. 5}$$

Where q = γn1B and z = n2B.

The aforementioned theory is applied to a tunnel by Terzaghi. Stress distribution of the tunnel is the same as the stress distribution on the yield part strip. During the construction period, tunnel laterally yields toward the direction of the tunnel. As shown in the Figure 20 active earth pressure creates yield zone with an inclination of (45^o +∅/2). Assuming yield prism $e_1b_1b_1e_1$ and consider yield zone as side walls.

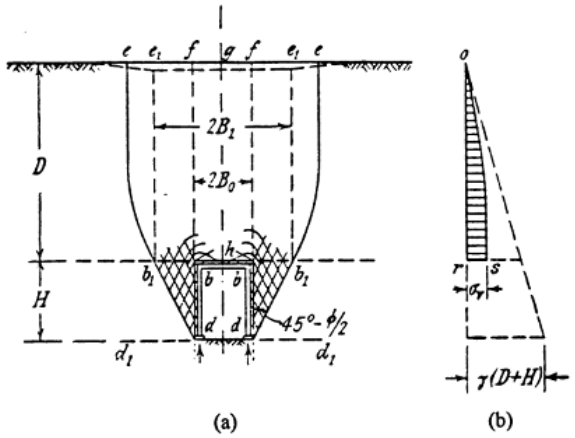

Figure 20: Arching effect in a tunnel [1]

Considering the depth of the tunnel is D from the ground, then the vertical stress of the tunnel roof is following Eq. 6;

$$\sigma_v = \frac{B\left(\gamma - {}^{C}/_{B_1}\right)}{K\ tan\emptyset}\left(1 - \ e^{-Ktan\emptyset\frac{D}{B_1}}\right) \ldots\ldots\ldots\ldots\ldots \text{Eq. 6}$$

After a certain limit (certain depth from the top surface D_1 of the tunnel as shown in the following Figure 21), arching effect not extend furthermore, we can estimate the D_1 distance using the Eq. 7 [59].

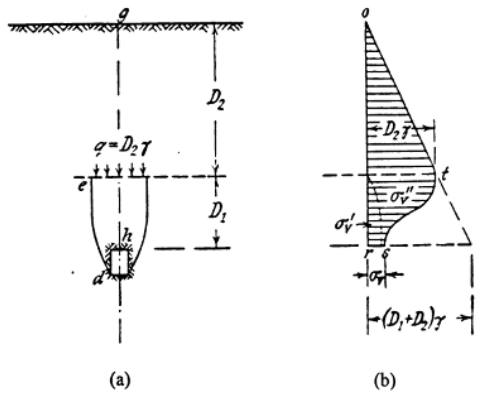

Figure 21: Depth of the arching action effected [1]

$$\sigma_v = \frac{B_1\left(\gamma - {}^{c}/_{B_1}\right)}{K\tan\emptyset}\left(1 - e^{-K\tan\emptyset {}^{D_1}/_{B_1}}\right) + \gamma D_2 e^{-K\tan\emptyset {}^{D_1}/_{B_1}} \ldots\ldots \text{Eq. 7}$$

2.2.3.3 Handy Theory (1985)

The summation of vertical forces for the catenary representation of the soil arch is similar to that of the classical representation with the only arching difference being the lateral earth pressure coefficient (not clear). In the classical model, the coefficient which relates horizontal stress to vertical stress is Rankine's active earth pressure coefficient (Ka) shown in part (a) of Figure 21. Handy developed a similar earth pressure coefficient that proposes that the shape of the inverted arch describes the path of the minor principal stress, as shown in Figure 22 as Kw [59].

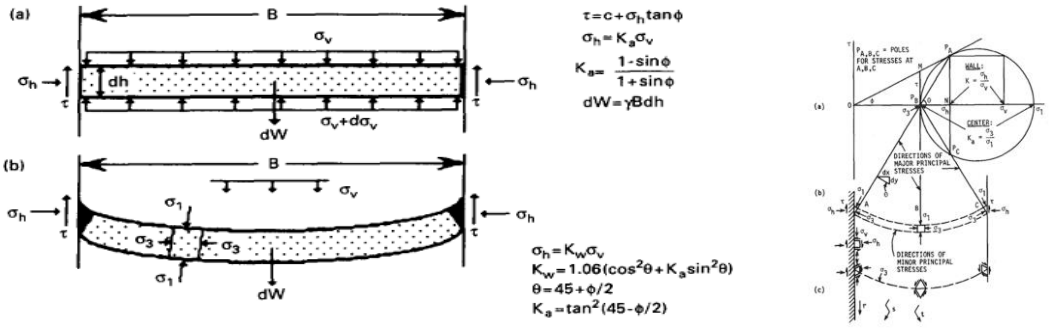

Figure 22: Handy arching effect model [59]

$$V = \gamma B^2 \frac{1-e^{(-2K_w \mu \frac{h}{B})}}{2K_w \mu} \text{..... Eq. 8}$$

V = Total vertical accumulated load,

h = Depth,

γ = Unit weight of soil,

B = Trench width

μ = tan Φ

2.2.3.4 Silo Theory

To find the vertical force on the silo base, let's take "dh" as a differential element, diameter B and depth of h as in Figure 23. The vertical force which is acting top surface on the element "V" , is in a downward direction and in the bottom surface (V + dV) it's in an upward direction. Self-weight of the considered element W = $\gamma \sigma B^2 dh/4$ as shown in the following fig. Let's consider the lateral stress $\sigma_h = 4KV/\pi B^2$ which is symmetric about to the centreline of the silo.

Two assumptions are made on silo theory

1. In all depths lateral stress coefficient (K) constant
2. Shear stress developed over full depth via sufficiently settling the material w.r.t to side walls.

By considering those assumptions, when the element tries to move in a downward direction upwards shear stress is developed as in Eq. 9;

$$\tau = \frac{4KV tan\emptyset'}{\pi B^2} \text{..... Eq. 9}$$

Taking the friction coefficient between the granular material and silo wall to be tanØ ; Eq. 10 was derived.

$$V = \frac{\gamma \pi B^3}{16 K tan\emptyset'} \left(1 - e^{-4K tan\emptyset' \frac{h}{B}}\right) \text{.....Eq. 10}$$

When h replaces with full height H, the force acting on the base can be obtained

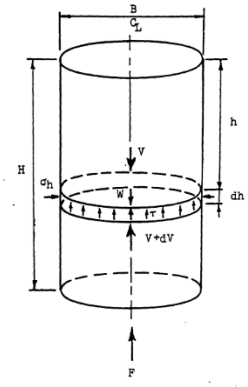

Figure 23: Free body diagram of silo theory [73]

2.2.4 Different types of trap-door setups used to identify the arching effect

Table 3: Different trap-door experiments

Experiment details	Arching setup and experimental figures
Experiment by McNulty, (1983) This experimental setup consists of a circular trap-door in the bottom of a cylindrical soil chamber. Using this set up McNulty studied both active and passive arching concepts. In Figure 24 P_B, Ps,δ, H and B indicate the measuring pressure, surface pressure average displacement, effective overburden depth and door diameter respectively	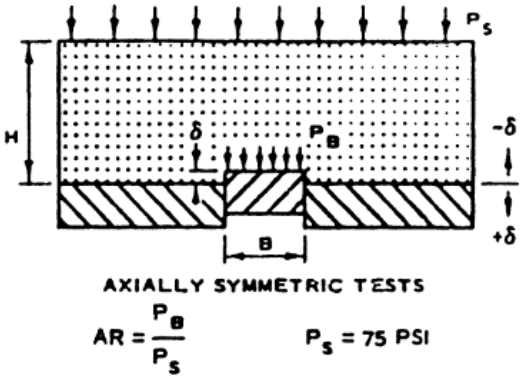 Figure 24: Experimental setup layout of [66]

Experiment by Ladanyi & Hoyaux, (1969) This was done based on the granular mass laying on the trap-door setup in plane strain condition. According to the Figure 25 and Figure 26 100cm high and 200cm wide Aluminum rod paced on the U-shaped steel frame.	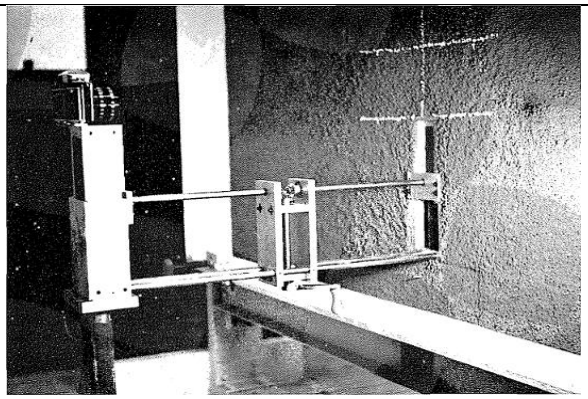 Figure 25:Apparatus of [67] 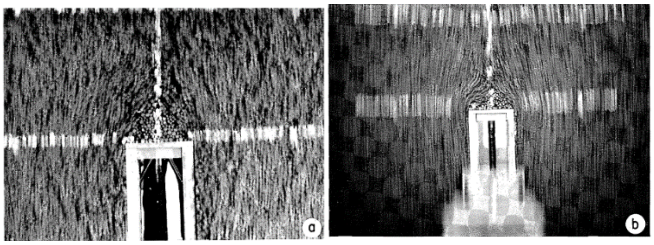 Figure 26: Displacement of trajectories [67]
Experiment by Harris, (1974) This experiment was focused on simulating the stress redistribution in the long wall. The set-up has a parallelly connected series of trap-doors which can independently move to simulate the advancing face. Pressure measuring cells are placed in each trap-door as shown in Figure 27.	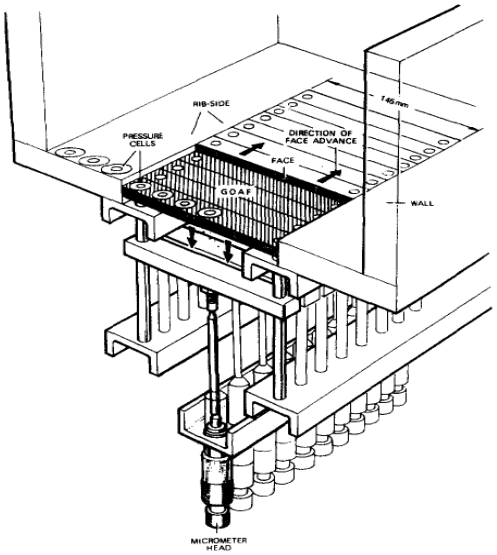 Figure 27:Experimental setup used in [68]

Experiment By EVANS, (1984)

This first setup which is in Figure 28 was initially developed to verify the accuracy of the diaphragm type pressure transducers for arching effect scenarios. In addition, Figure 29 shows the Evans rectangular shape main trap-door setup for his primary experiments in plane strain condition. His setup also consists of series of trap-door to simulate the advancing tunnel. This instrumentation set up is similar to trap-door set used by Terzaghi in 1936. In this experiment diaphragm type transducers were used to get more accurate pressure reading on trap-doors and bottom part of the testing box.

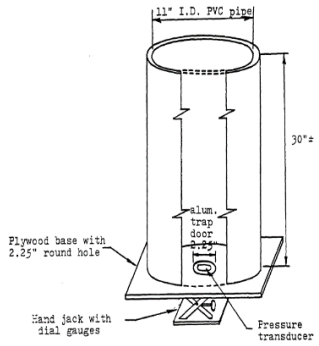

Figure 28: Experimental setup with circular trap door [70]

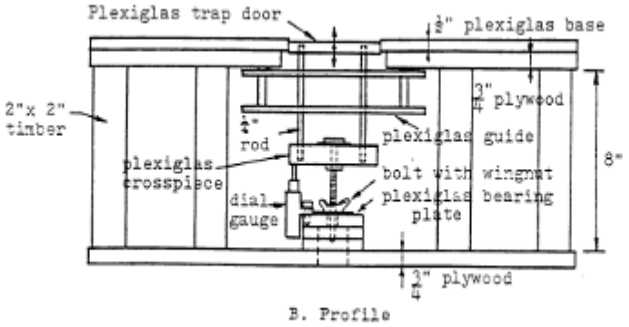

Figure 29: Experimental setup with rectangular trap door [70]

Experiment by Iglesia, Herbert, & Robert, (1990) This trap door setup is also similar to the previously discussed experimental setup. In this case as shown in Figure 30, a real trap-door is utilized for the centrifuge model. In this experimental setup, whole raw mass inside the system can be moved under gravity by lowering the trap-door. In addition, force measurements can be taken on the trap-door corresponding to it's displacement.	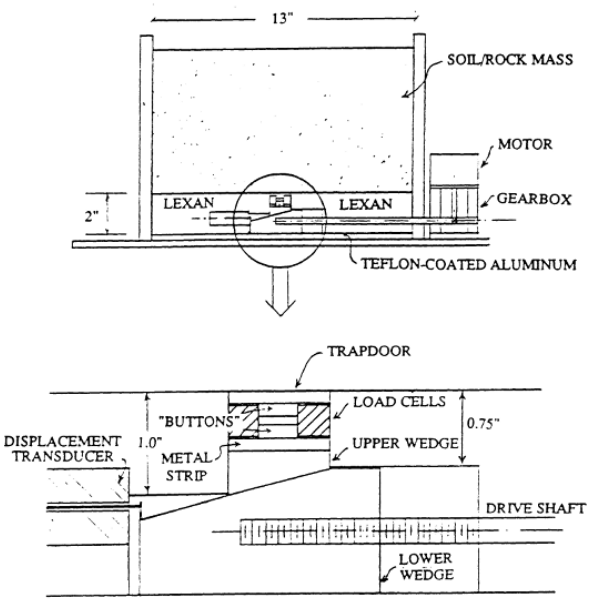 Figure 30: Centrifuge trap-door experimental setup[74]
Experiment by Vardoulakis, (1981) This is a kind of a small-scale simple trap-door setup based on the Terzaghi's in 1936 setup as shown in Figure 31.	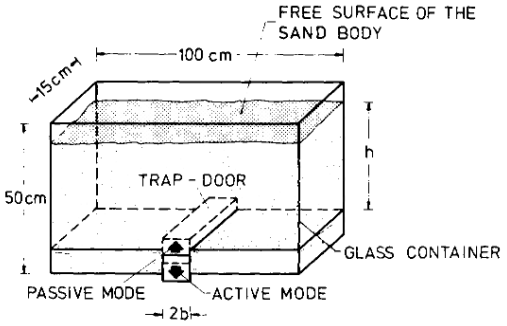 Figure 31: Trap door setup by [69]

Experiment by Sadrekarimi & Abbasnejad, (2010)

The experimental setup as shown in Figure 32 also consists of circular trap-door in the bottom of the sand container which has 0.358m^3 volume, 60cm height and 98 cm diameter. Specialty of this setup is that, it consists of 3 different dimensional circular trap-doors.

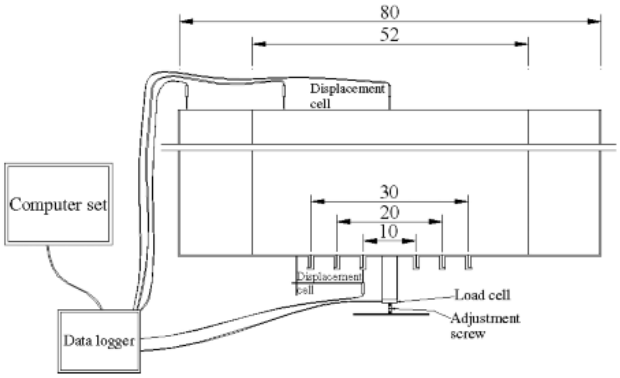

Figure 32: Experimental setup by [75]

Experiment by R. Rui, A. F. Van Tol, Y. Y. Xia, S. J. M. Van Eekelen, and G. Hu [76]

This experimental setup consists of two main compartments as shown in Figure 33 and Figure 34: First one is a sand chamber and the other one is a moving section. Length, height and width are 1200mm, 800mm and 300mm, respectively. This experimental setup consists of 16 movable steel beams to control the trap-door.

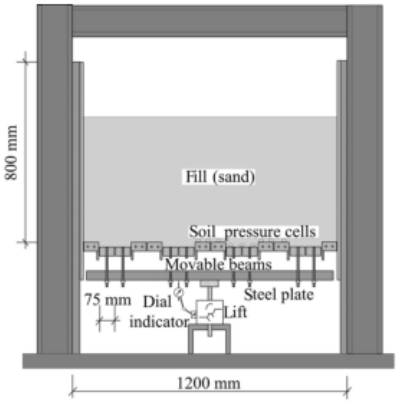

Figure 33: Cross sectional view [76]

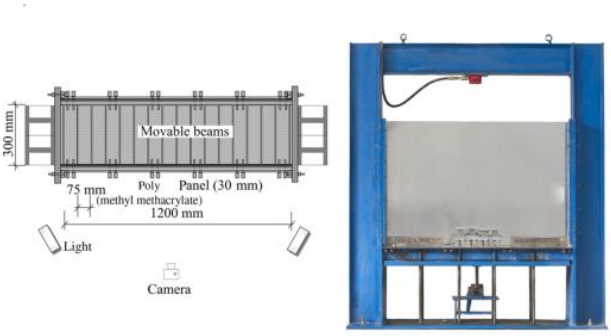

Figure 34: Setup plane view and photo[76]

3 WORKING PRINCIPLE OF SENSOR SYSTEM

3.1 Introduction

Different earth pressure cells which work under different principles and methods, to measure the earth pressure in different directions. In this research, a strain gauge-based earth pressure measuring, and monitoring system is developed. Measurement of the total earth pressure, effective earth pressure and pore water pressure using a single sensor system is a novel approach. The working principles of the sensor system is shown in Figure 35.

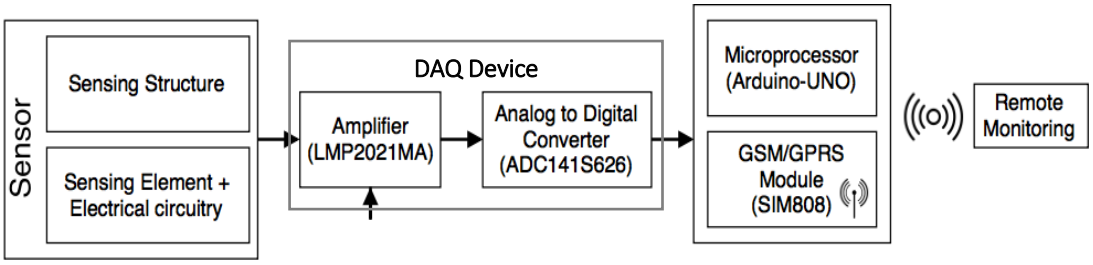

Figure 35: Proposed sensor system with remote data logging and monitoring system

This system includes two sensing units, one for measuring the total stress in the soil and the other one for measuring the effective earth pressure in the soil. Working principle of sensing units is discussed in the following sections. These two values given by the sensor can be used to find the pore water pressure in the located point. The sensing mechanism is based on the deflecting diaphragm which deforms respect to the earth pressure. Strain-gauges were used to detect the deformation of the structure with respect to the applied earth pressure. In addition, it is needed to develop the signal conditioning system to amplify the output voltage given by the Wheatstone's bridge electrical circuit. Analog to Digital conversion (ADC) method is used for obtaining the readable outputs. After that the data acquisition system was developed to collect the data and visualize the data with remote monitoring facility. The microcontroller was used for the processing purposes.

3.2 Proposed Novel Sensing System

This novel sensor was developed to measure the soil pressure which is acting perpendicular to the instrument. But according to the requirement, this can be used to

measure the pressure acting in vertical and horizontal planes by placing the instrument correctly according to requirements.

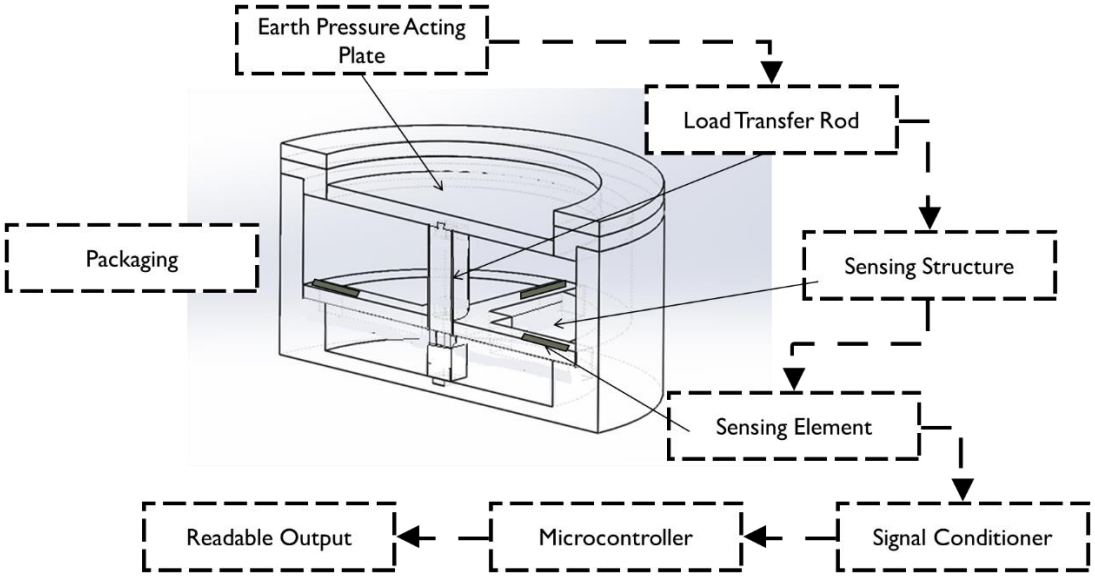

Figure 36: Schematic view of proposed sensor

This sensor can be used as an embedded type earth pressure cell than a contact type one. When earth pressure cell is placed inside the soil mass, the earth pressure, which is acting on the plate as shown in Figure 36, and it slightly moves only in the vertical direction on which the pressure is applied. Then that acting pressure is transferred to the sensing structure through an intermediate rod which is called in above Figure 36 as Load Transfer Rod. The top end of that load transfer rod is connected to the earth pressure acting plate and the bottom end of the load transfer rod is connected to the sensing structure. That Sensing Structure consists of four beams and those four beams can deform with respect to the acting pressure on the top plate. Sensing elements are bonded to the sensing structure according to the structural analysis which is discussed in the next chapter. Then sensing elements detect the deformation of the sensing structure and get the output values with respect to the acting pressure from this sensing elements. This sensing structure is connected to the outer package using bolts.

To measure the total pressure, effective pressure and the pore water pressure, two sensors were developed. One sensor directly measures the total stress and the other one can measure the effective stress directly.

3.3 Total Stress Measuring Technique

Working principle of the load transferring mechanism is as same as mentioned above. This sensor unit is developed to measure the total stress of the soil mass on the placed point. For that, this sensor allows transferring of the soil pressure as well as the pore water pressure acting on the same plate which the total earth pressure on to the sensing structure via load transfer rod.

To achieve the above objective, the entire sensor unit should be water-tight. The only place of the structure where water can get leaked into the sensor is the gap between the earth pressure acting plate and the outer plate. To avoid that leak two modifications were proposed. One is to apply greasy material and the other one is providing a water sealant rubber ring as shown in Figure 37.

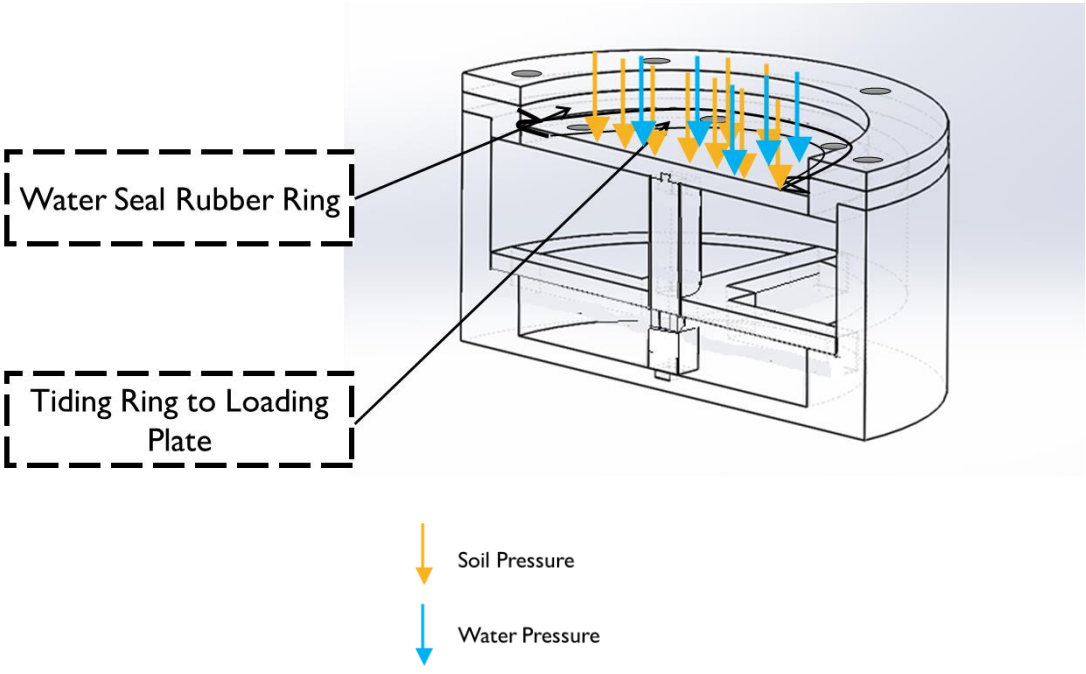

Figure 37: Mechanism to measure the total Stress

3.4 Effective Stress Measuring Technique

This sensor unit is focused on measuring the effective earth pressure at the point of which the sensor is placed. The specialty of this sensor unit is that the effective earth pressure can be measured directly without measuring pore water pressure. To achieve the objective a new earth pressure sensor was developed as shown in Figure 39. In this apparatus, the sensing mechanism is designed to cancel out the pore water pressure effect by itself. In this sensor, water is allowed to go inside through the provided holes. These holes were covered using a geotextile to prevent the soil moving into the sensor. Then water fills the inside of the sensor and with time it reaches the equilibrium with outside water pressure. Then that water pressure is applied to the bottom part of the earth pressure acting plate and cancel out the effect of pore water pressure acting on the top part of the earth pressure acting plate.

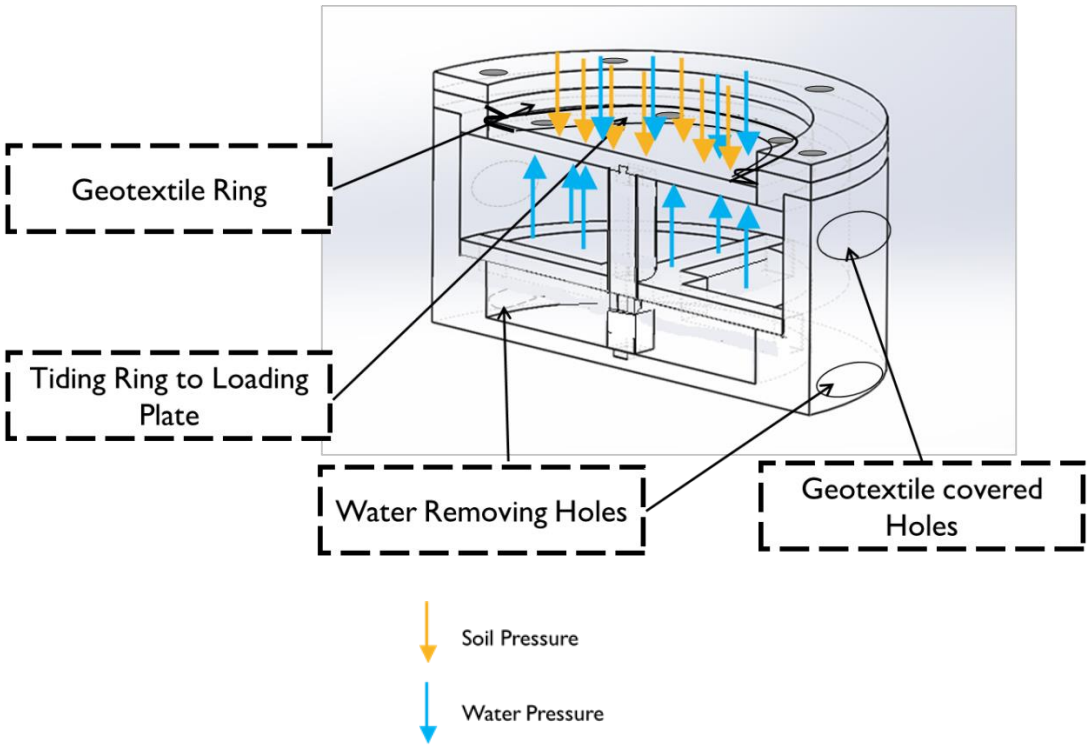

Figure 38: Effective stress sensing mechanism

In this sensor, some holes were placed below the sensing structure to remove the water inside when the water level gets lowered compared to the point which the sensor is placed as shown in the above figure.

3.5 Remote Data Logging and Monitoring System

One of the most important part of this sensing system is the data acquisition system. After processing through the microprocessor data, three ways were introduced to get the output values. First one was the real-time visualization, in that case, an LED is display was attached to the main controlling unit. The second method was storing the data to a storage unit inside the main controlling unit. Finally, data were sent to a remote cloud-based data storage through a GSM/GPRS module in real time. Then earth pressure can be monitored using a web-based platform.

4 STRUCTURAL DESIGN

4.1 Cross beam structure

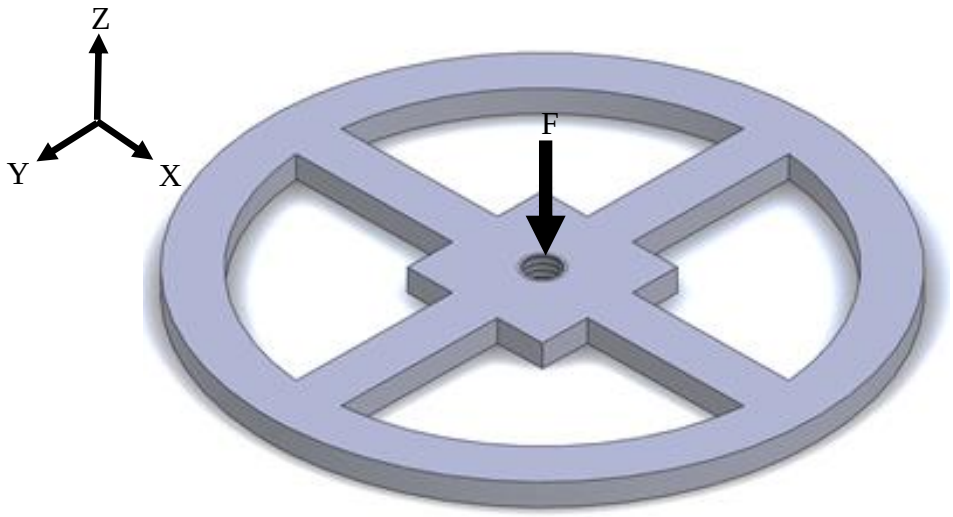

Figure 39: Proposed cross-beam structure with connected outer ring

To obtain the soil pressure acting on the sensor, the deformation of the diaphragm was used. This sensor system was developed to measure the normal stress. As a diaphragm, the cantilever cross beam structure was used to deform with respect to the force acting on the sensor in the normal direction. Sensing elements (strain gauges) were placed to identify the strains which occur in X- direction and Y- direction due to the force acting in the Z- direction on the middle square island according to Figure 39. Therefore, this sensor has a single degree of freedom.

Symmetrical load distribution among the cantilever four cross beams is very important to create the symmetrical deformation of the structure if not it is difficult to place the sensing element symmetrically. To distribute the load symmetrically around the structure, four cantilever beams with fixed end conditions were used. Middle island for the cross beams was provided to transfer the forces equally to the surrounding cantilever beams.

4.2 Specifications of Cross-Beam Structure

One of the prominent considerations of the earth pressure cell is the dimensions of the sensor. Final dimension of the sensor unit depends on the dimensions of the cantilever system. Apart from that movement of the loading plate depends on the deformation of the cross-beam structure. But it can be neglected, to avoid the occurrence of an arching effect while measuring the earth pressure. According to the literature normally its preferred that the ratio between the sensitive cell diameter and the maximum deflection of the earth pressure acting plate (δ_{max}) be in the range of 2000–5000 [51]. Then considering the above factors, it is necessary to come up with proper height, width and the length of the beam to reduce the deflection and maintain the overall dimensions of the sensor units.

Dimensions in Table 4 are used to fabricate the sensing cross beam structure after doing a thorough structural analysis.

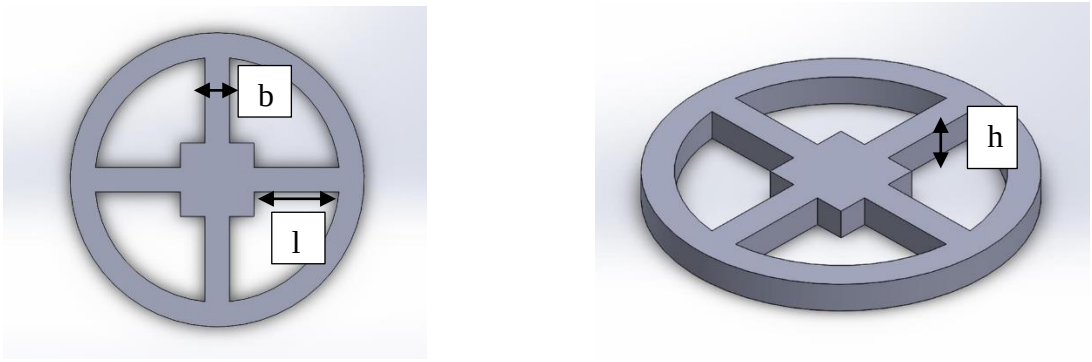

Figure 40: Cross-beam structure model

Table 4: Dimensions of Cross-beam structure

Item	Symbol	Dimensions (mm)
Height	h	5
Width	b	10
Length	l	35
Middle island is 30mm x 30mm		

4.3 Modeling and Simulation of Cross-Beam Structure.

To analyze the cross-beam structure, the following assumptions were made.

•The end conditions of the four beams were assumed to be perfectly fixed ends in the finite element model considering monolithic fabrication of four beams and rim.

The ends of the beams were restrained against rotations and translations about any axes, as the monolithically constructed rims prevent such actions. Hence, it was satisfactory to restrain all 6 degrees of freedom of the beam ends using a fixed boundary condition as shown in Figure 41.

Figure 41: Fixed end condition

•As the load is transferred to the middle island through a rod passing through a hole in the middle, the load was modeled as a point load without eccentricity as shown in Figure 42.

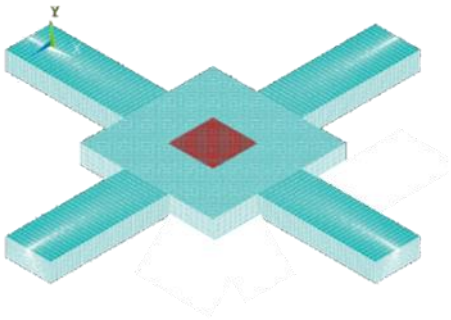

Figure 42: Applied load

This idealization was made assuming a fabrication of the equipment with good workmanship ensuring that the rod can pass through the middle with negligible offsets. Hence, it can be assumed that there isn't any eccentricity in the load transfer mechanism and thus the moment created are negligible.

4.4 Model of the elastic body for finite element simulation.

Here, ANSYS finite element analysis software was used to analyse the deformation of the cross-beam structure for different dimensions. The SOLID185 element was used which is a high precision element available in ANSYS. SOILD185 is a 3D brick type 8 node element having 3 degrees of freedom which has plasticity, large deflection, and high strain capabilities. Use of solid elements provide a high-fidelity model of the actual structure and capture stresses throughout the beam. Furthermore, a control mesh was placed near to the end of middle region where the strain gauges are being mounted. This was done to optimize the computation capabilities and to get values with high accuracy as shown in Figure 43. The Ansys finite element model consisted of 378000 elements and 400861 element nodes after mesh generation as shown in Figure 44.

In this model, aluminium was used as the elastic body material which has Young's Modulus of 69000 MPa, Poisson's Ratio 0.334[77] and density 2.78x103 kg/m^3.

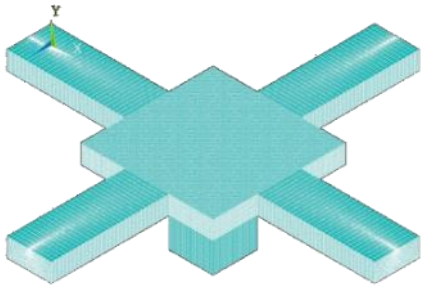

Figure 43: Control mesh of stress and strain analysis

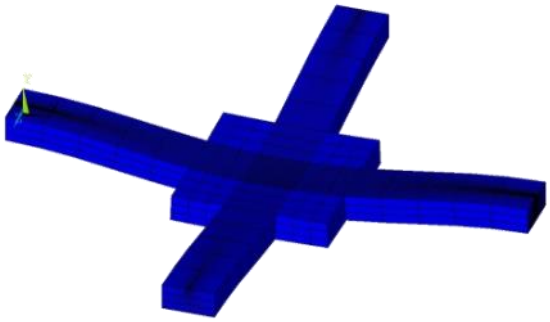

Figure 44: Deformed control mesh of stress and strain analysis

4.5 Simulation Results and Discussion

To simulate the model, the pressure is applied to the middle part of the structure (middle island) P_Z = 1180N/mm^2 on a 100mm^2 area. That value comes from the maximum design load of this sensor system. This sensor unit was designed to measure up to 150 kN/m^2 soil pressure. When that value was converted into the force using the 100mm diameter loading plate area, the single force acting on the sensing structure is F_Z= 1180N.

4.5.1 Results of the strain analysis

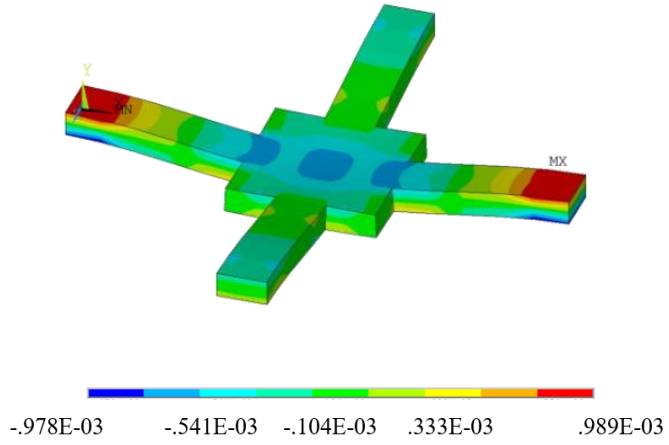

Figure 45: Strain contour in x-direction

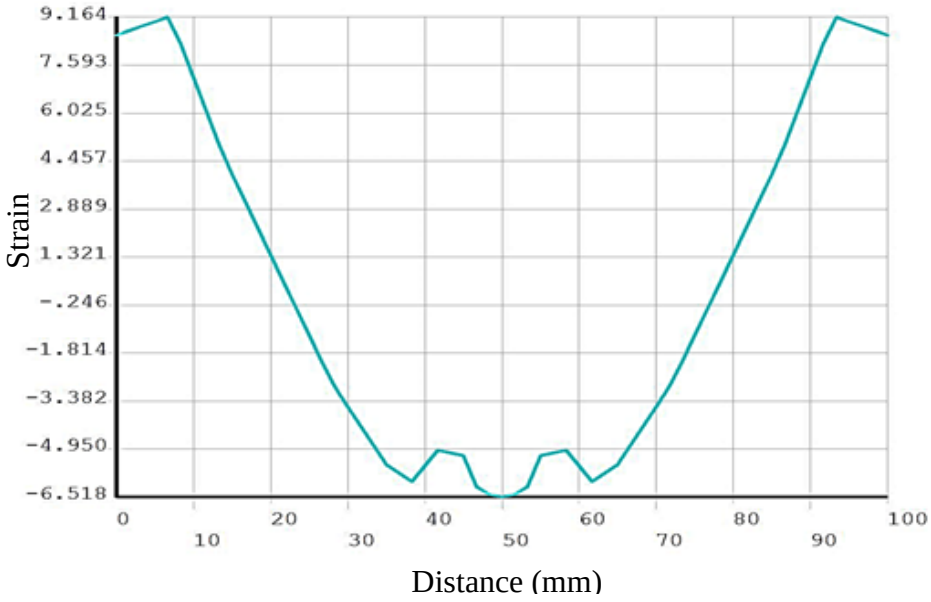

Figure 46: Strain variation on top and bottom surface of single beam in x-direction

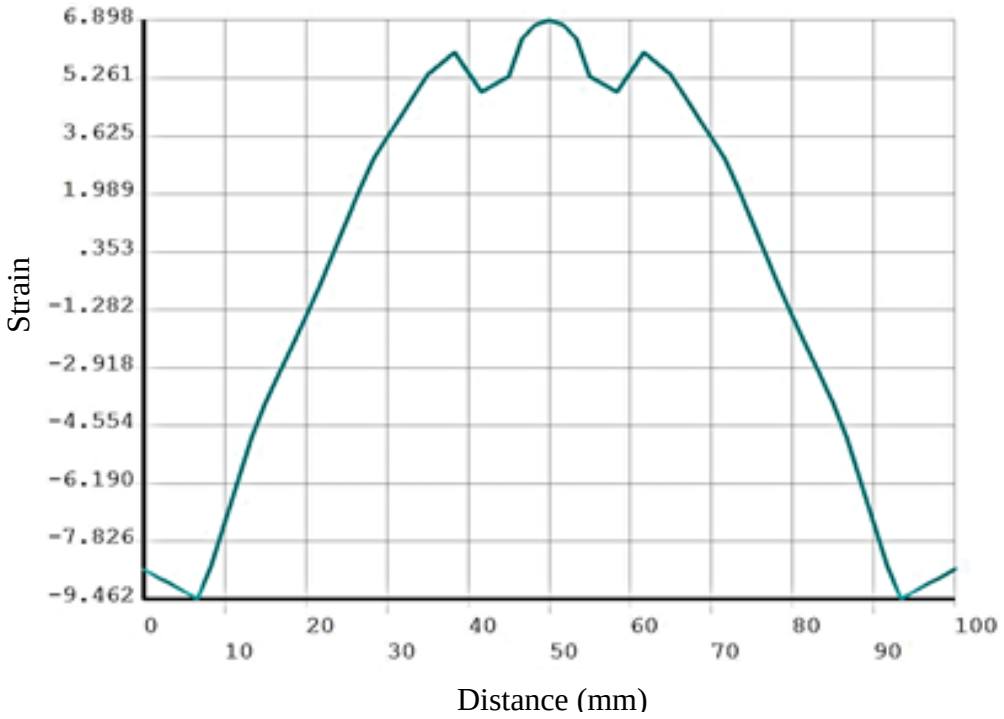

Figure 47: Strain variation on the bottom surface of a single beam in x-direction

According to the symmetric behavior of the cross-beam structure strain along the x-direction and y-direction are similar. Therefore, strain variation graph with the distance shown above is only for the x- direction. In addition, it is needed to find the maximum and minimum strain values. Because to get the optimum output values from Wheatstone's bridge circuitry, strain gauges should be bonded to those two places. Therefore, it is needed to analyze the top surface and the bottom surface of the cross-beam structure. Considering the symmetric behavior of the cross-beam structure, strain gauges should be located on the centre median line of the beam. Therefore, the analysis was carried out for the middle line of the beam as shown in Figure 45. According to the finite element simulation result given in Figure 46 and Figure 47, it can be clearly seen that maximum strain varies between 9.16×10^{-4} and -6.52×10^{-4} at the top surface and maximum strain varies from 9.46×10^{-4} to -6.9×10^{-4} at the bottom surface. Strain variation along the top and bottom surfaces of the beam are more or less similar. Hence, it is easy to locate the strain gauges along the beam to make the full bridge circuit. In this analysis, it was possible to see a maximum positive strain

and a negative strain varying near to the fixed end and on the island as well as at both ends of the single beam.

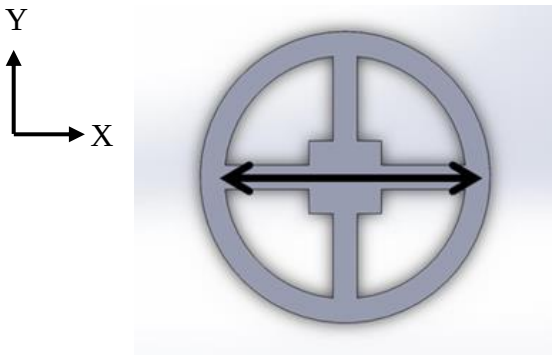

Figure 48: x-y coordinates

4.5.2 Results of Stress Analysis

Similar to the strain analysis; stress analysis was also done on the X-direction of the cross-beam structure due to the symmetric behavior of it. According to the finite element analysis shown in Figure 49, highest stress was concentrated to the fix ends and central area of the middle island region but the highest strain was concentrated in a bit away region from the fix end and the middle region. According to Figure 50 and Figure 51, maximum stresses of the top surface varies from 63.64 kN/m^2 of tensile stress to 67.19 kN/m^2 of compressive stress. On the bottom surface maximum stresses varies from 65.25 kN/m^2 of tensile stress to 65.35 kN/m^2.

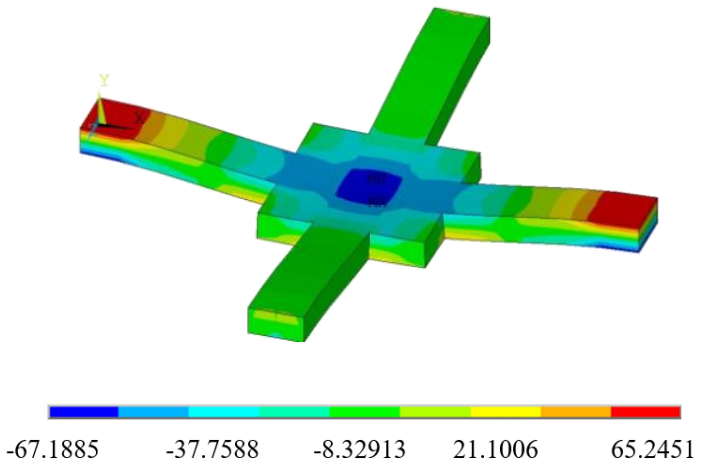

Figure 49: Stress contour in x-direction

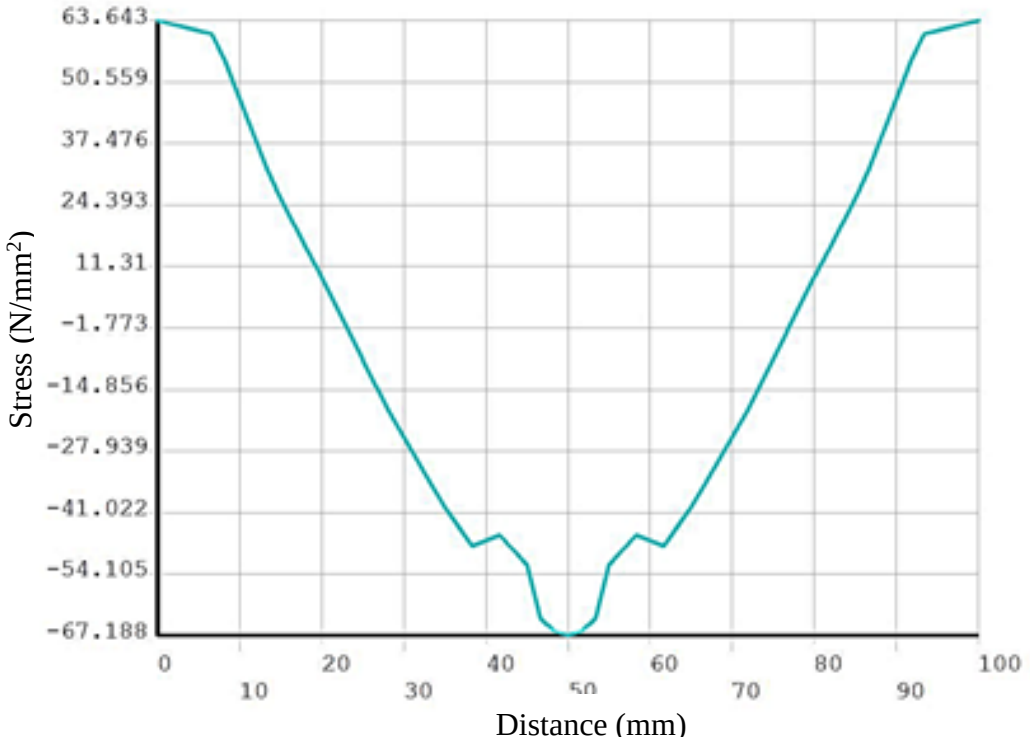

Figure 50: Stress variation on the top surface of a single beam in x-direction

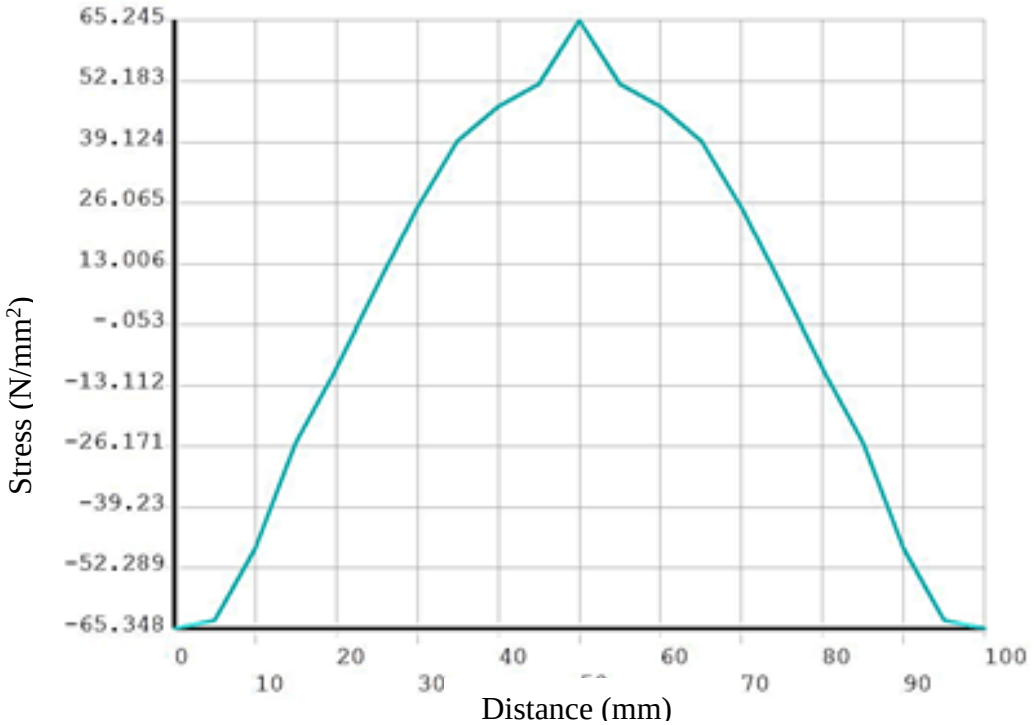

Figure 51: Stress variation on the bottom surface of a single beam in x-direction

4.5.3 Discussion

According to the finite element values, maximum strain of the cross-beam structure is 946 micro strain for the maximum applied pressure of 150 kN/m^2. This 946 micro strain value is less than the 2000 micro strain or 0.2% off set yield strain as shown in Figure 52. Beyond that 0.2% strain, cross beam structure goes to the plastic range. Now it is in the elastic range. The nominal yield strength of the aluminum is 250 MPa but in the current case that value is not exceeded.

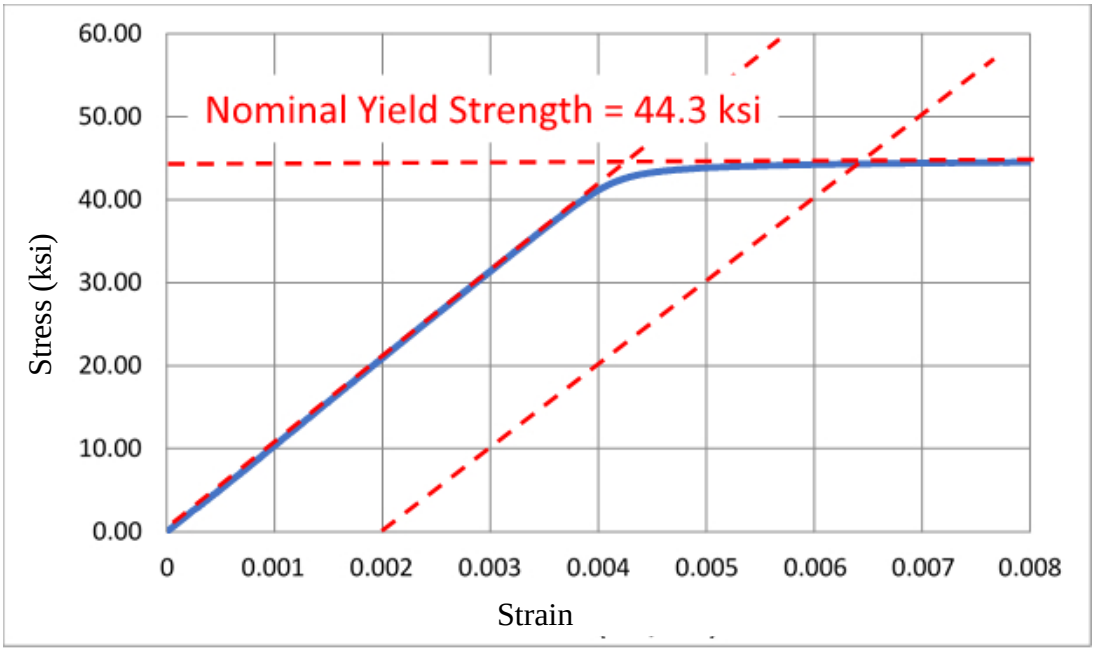

Figure 52: Definition of yield

5 SENSING ELEMENTS

5.1 Strain sensing principle

As mentioned previously, strain gauges are used to measure the strain in the sensing structure. The effect of soil pressure and the effect of pore water pressure transferred to the cross-beam structure makes the cantilevers bend. Hence, strain gauges show some variation of the resistance due to tension and compression according to the Eq. 11. Then the voltage output corresponding to resistance can be measured through the full-bridge circuit.

$$\epsilon x = \frac{6(l-x)F}{4Ebh\text{^}2} \quad \text{..... Eq. 11}$$

Eq. 11 above gives the relationship between the strain generated in the given direction and applied force F on to the cantilever structure. When one of the cantilever beams is considered, only one-fourth of the total force acts upon it, and the dimensions of the rectangular section of the cantilever of width 'b' and height 'h' are made with a material, which has Young's modulus of 'E'. 'x' is the measuring distance to the strain gauge from the fixed end of the cantilever.

According to the Eq.11 above, the strain is proportional to the force. Then using Eq. 12, the force acting on the sensor can be found through a full-bridge circuit.

$$F = \frac{4Ebh^2UA}{3Ss\ UE\ (l-x)} \text{ ..... Eq. 12}$$

Eq. 12 is used to identify the relationship between force and the output voltage of the bridge. In this Eq. 12, U_E is the known input voltage and S_s is the gauge constant. Then it can clearly be seen that 'F' force acting on the sensor is directly proportional to the output voltage 'U_A'. Hence using Eq. 12 above, the force acting on the sensor can be obtained [8].

5.2 Selection of the strain gauges

In this sensor strain gauges called FLA-5-350-23-3LJB model was selected as the sensing element which is manufactured by TML, Japan. This strain gauge is crafted using Cu-Ni alloy foil for the grid and special design plastic for backing. One of the special features of this strain gauge is this can be used for a wide range of operating temperature as shown in the following Table 5 and Table 6 as shown in Figure 53.

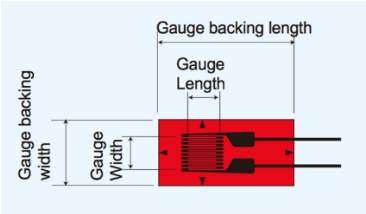

Figure 53: Strain gauge details

Table 5: Strain gauge dimensions

Gauge length	5mm
Gauge width	1.5mm
Aluminum	23ppm/°C
Resistance	350Ω

Table 6: Strain gauge characteristics

Applicable specimen	Metal, Glass, Ceramics	Backing	Special plastics
Operational temperature(°C)	-196 ~ +150°C	Element	Cu-Ni
Temperature compensation range(°C)	+10 ~ +100°C	Strain limit	5% (50000×10^{-6} strain)
Applicable adhesive	CN, P-2, EB-2	Fatigue life at room temperature	1×10^{6} ($\pm1500\times10^{-6}$ strain

5.3 Strain Gauge Placement

The ratio between the output voltage and input voltage can be derived; as shown in Eq. 13

$$\frac{U_A}{U_E} = \frac{R_1}{R_{1+}R_2} - \frac{R_4}{R_{3+}R_4} = \frac{R_1.R_3 - R_2R_4}{(R_1+R_2)*(R_3+R_4)} \text{..... Eq. 13}$$

If $U_A/U_E = 0$, $R_1=R_2=R_3=R_4=0$ or $R_1:R_2=R_3:R_4$, to get the balance bridge condition it is important to arrange strain gauges with very less deviations of resistivity among strain gauges or satisfy one of the above two conditions mentioned in beginning of this paragraph. Then sensing structure is equipped with balancing elements.

It is vital to locate the strain gauges in proper places to get the optimum output from the Wheatstone bridge. To optimize the bridge output those places were selected according to the following Eq. 14.

$$\frac{U_A}{U_E} = \frac{1}{4}\left(\frac{\Delta R_1}{R_1} - \frac{\Delta R_2}{R_2} + \frac{\Delta R_3}{R_3} - \frac{\Delta R_4}{R_4}\right) \text{ ..... Eq. 14}$$

In the above Eq. 13 and 14 R_1 to R_4 are four resistors of the Wheatstone bridge four arms. As same in Eq. 12 U_E is the excitation voltage (input voltage) of the bridge and U_A is bridge output voltage as shown in Figure 56. The term ΔRi denotes the resistance variation in each resistor. In this case, strain gauges were used as resistors which vary resistivity with strain variation of the sensing element with respect to the earth pressure. To get the maximum voltage output from the Wheatstone bridge, resistance variation should be high. To increase the resistance variations, strain gauges should be placed in the maximum strain points. Using structural analysis result, the exact location was found using the graph in the Figure 54. The maximum positive strain was developed near the fixed end (7mm away from the fixed end) on the top surface of this cross-beam structure. Another negative strain is developed at the bottom beam corresponding to R1 and R3. According to the above data, the strain gauges are placed 17 mm inwards from the outer circle of the ring as shown in Fig. 9.

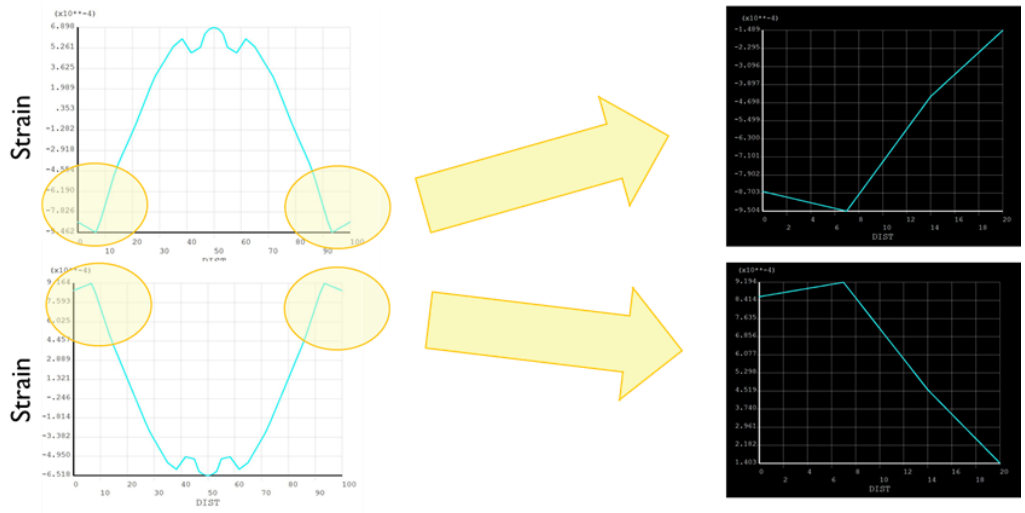

Figure 54:Sensing element bonding location

When the top surface of one beam in the sensing structure is considered, a strain occurred in X-direction $\epsilon_1 = {}^{\sigma}/_{E}$ due to tensile force. On the bottom surface of the same beam it become compressive force in X-direction $\epsilon_2 = {}^{\sigma}/_{E}$. Similarly, ϵ_3 and ϵ_4 are tensile strain and compressive strain respectively which are identical as ϵ_1 and ϵ_2 . Locations of $\epsilon_1, \epsilon_2, \epsilon_3$ and ϵ_4 in the sensing structure are shown in Figure 55.

Tensile strain becomes positive for the resistive value and compressive strain values become negative. Then according to the Eq. 14, three (-) value turn to (+) value and gives accurate output. A similar arrangement is used in other cross beams to place the strain gauges.

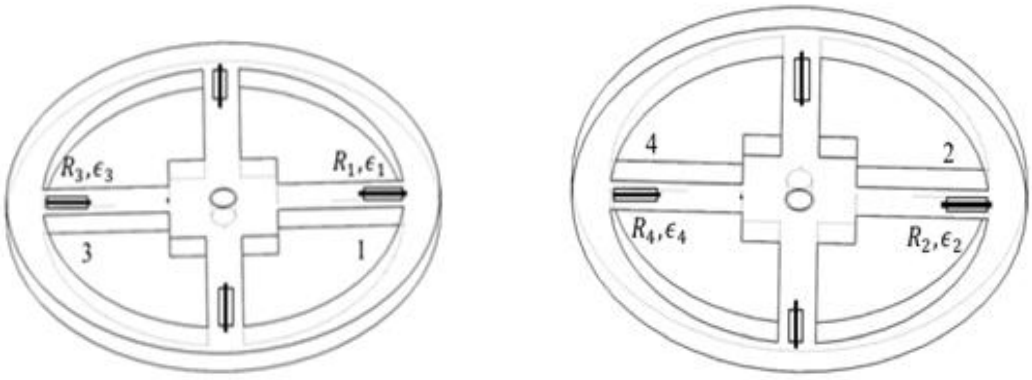

Figure 55: Sensing element locations in top and bottom surface.

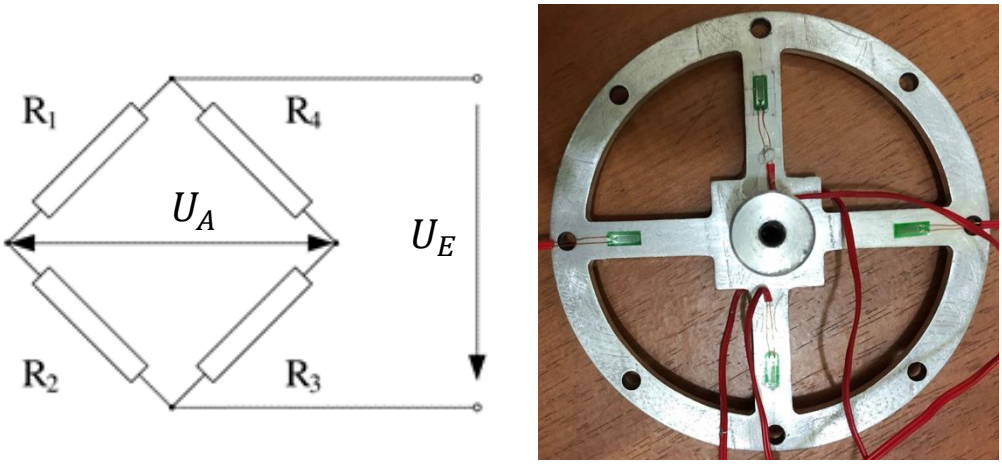

Figure 56: Wheatstone bridge and sensing element on cross beam structure

6 FABRICATION OF SENSING STRUCTURE AND SENSOR PACKAGING

6.1 Material

To develop the earth pressure cell aluminum metal was used. The main reason to select Aluminium is the surrounding environment inside soil. Due to the moisture in the soil other commonly used metals will corrode rapidly.
In addition, it has a lesser weight and a lower cost compared to stainless steel. Precision machining is also easier with Aluminium. After selecting the raw materials, 150 mm aluminium rods are used for main casings and 6mm, 4mm, 2mm aluminum plates are used for other parts.

6.2 Precision Machining

One of the main concerns of the sensor fabrication is the precision machining. In this research, very high precision machines were used which are available in the Die & Mould Centre at University of Moratuwa. CNC milling machine as shown in Figure 57 was used to prepare the cross-beam structure, main cup water penetration holes, load transfer plate and tiding rings. CNC lathe machine was used to make the main casing (main cup and load transfer rod).

Figure 57: CNC milling Machine

6.3 Fabrication of different parts

6.3.1 Sensing structure

One of the main components of this sensor is the sensing structure which is discussed in the previous section in detail. CNC milling machine is used for precision machining of this part as shown in Figure 58.

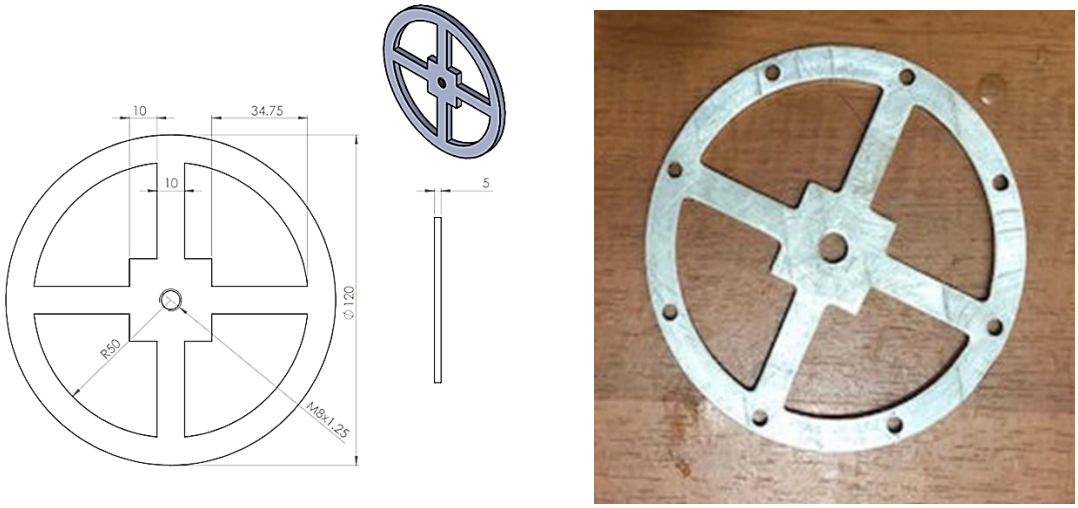

Figure 58: Cross Beam Structure

6.3.2 Main Casing

CNC lathe machine was used to fabricate the two main casings. One casing was for the total stress measuring sensor and the other one was for effective stress measuring. Difference between these two was effective stress measuring sensor casing consists of some holes as shown in Figure 59.

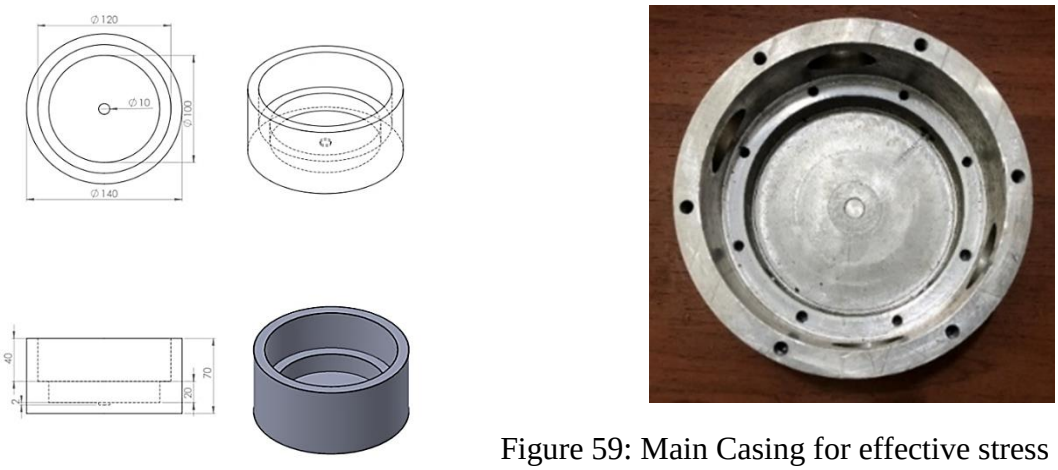

Figure 59: Main Casing for effective stress measurement

6.3.3 Pressure acting plate

5mm thick aluminum plate was used to fabricate this load acting plate as shown in Figure 60. CNC milling machine is used for fabrication.

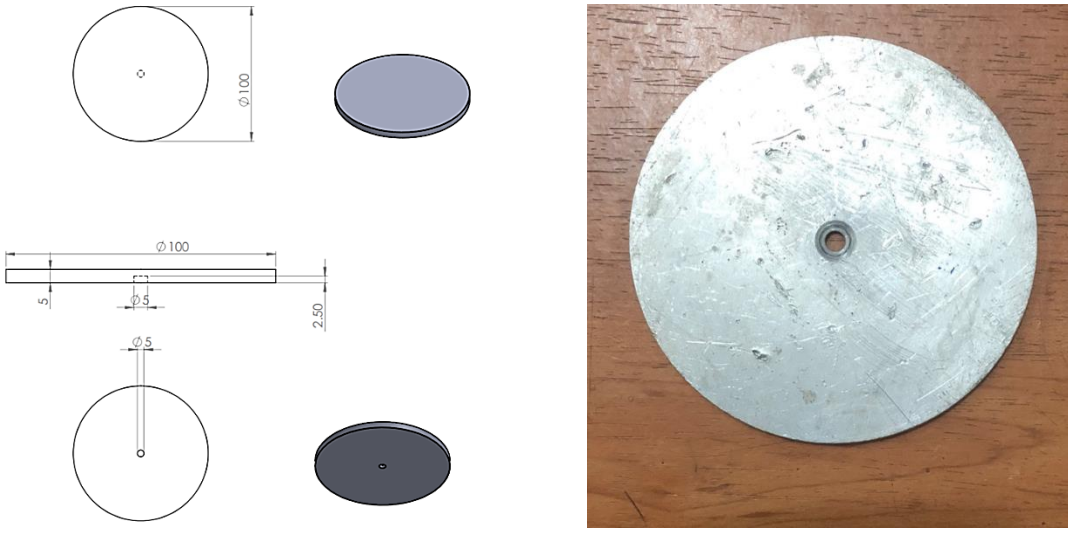

Figure 60: Load acting plate

6.3.4 Load transfer rod

Rod which is transferring soil loads from load acting plate to sensing the structure was fabricated using CNC lathe machine as shown in Figure 61.

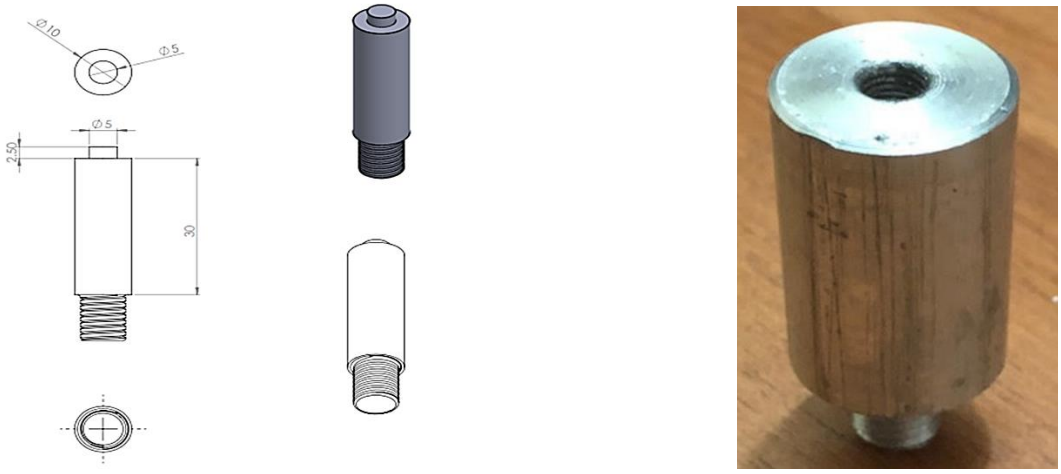

Figure 61: Load transfer rod

6.3.5 Tiding rings

Tiding rigs are used as guider to moving load acting plate as shown in Figure 62. On the another hand this act as an inactive ring to the top surface. Tiding ring was fabricated using a milling machine.

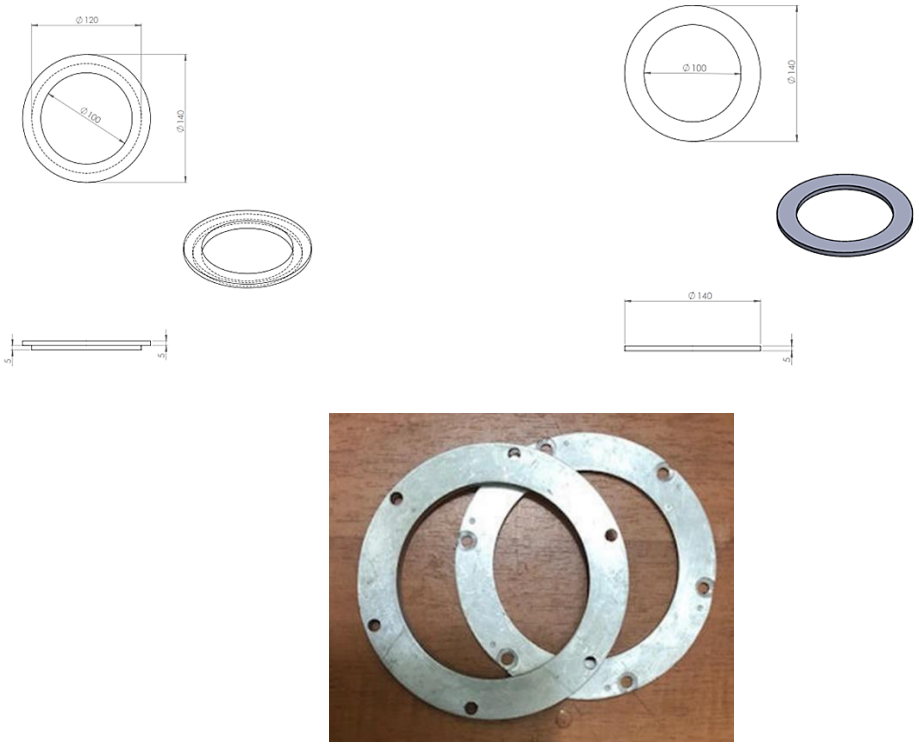

Figure 62: Tiding ring

6.3.6 Other parts

Some other small parts are fabricated in the Workshop at the Department of Civil engineering. Those were the outer rings of water infiltration holes and cable tiding rings as shown in Figure 63.

Figure 63: Water infiltration holes outer rings and cable tiding rings

6.4 Strain gauges bonding

According to the suppliers guidelines following steps were carried out.

- Initially, all kinds of moisture, rust, paint, etc was removed. After that, grinding is needed. For Aluminum it's suggested that 240 to 320 grade abrasive paper to be used to abrade an area which is larger than the strain gauge.
- The second step was cleaning the surface. To clean the surface propyl alcohol was used with cotton wool. Surface was cleaned until cotton wool comes away cleaned as shown in Figure 64.

Figure 64: Cotton wool, alcohol and 320-grade abrasive paper

- After that exact position of the strain gauges was selected, it was marked carefully using a 4H pencil as shown in the Figure 65.

Figure 65: Marking the position

- The third step is masking. In that case, cellophane tape was used to cover an area slightly larger than the strain gauge. This tape covering was used to prevent the spreading of the adhesive outside the installation area as shown in Figure 66.

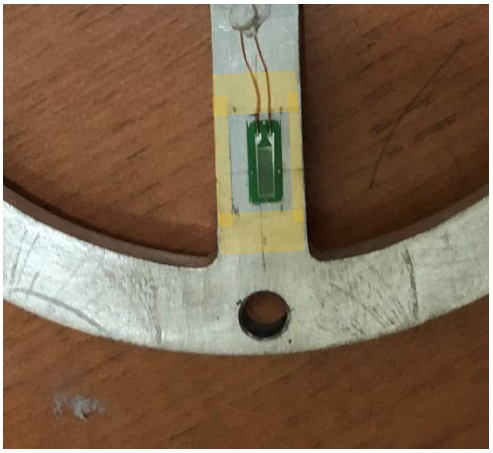

Figure 66: Masking

- The fourth step is dropping. According to the strain gauge suppliers, it has been suggested the use of CN adhesive. Initially one drop should be put on the back of the strain gauge. Normally the number of drops depends on the size of the strain gauge. In this case, two to three drops were used according to the requirement.
- The fifth step is spreading. After that using CN adhesive tube nozzle, spreading of the adhesive uniformly throughout the strain gauge was done as shown in the Figure 67.

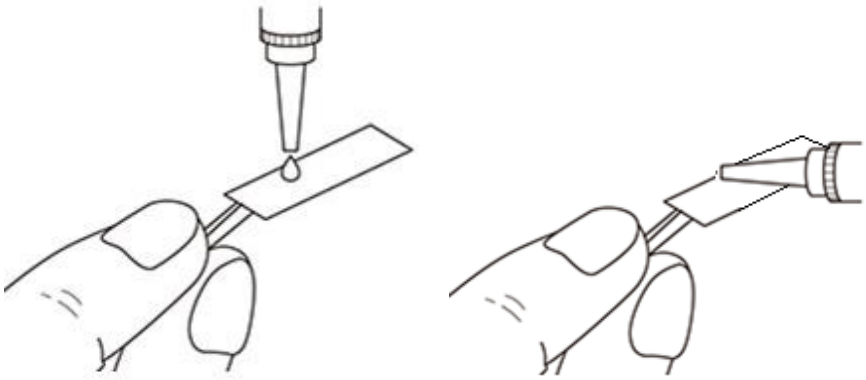

Figure 67: CN adhesive dropping and spreading

- The sixth step is Appling pressure. Strain gauges were located carefully on the pencil marks. In that case strain gauge should be held in the pre-attached lead wire. After that a polyethylene sheet was placed on the strain gauge and pressure was applied to the strain gauge with thumbs. Figure 68 shows that polyethylene sheet.
- Finally, the applied pressure was kept for 20-60 seconds.

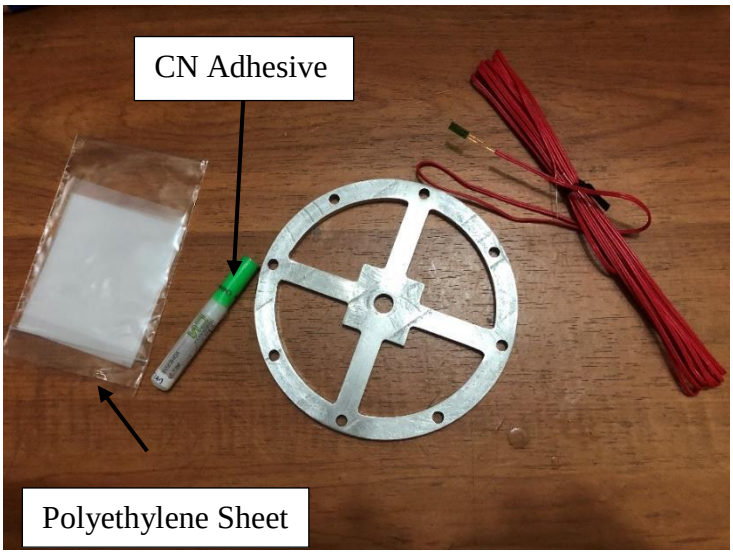

Figure 68: CN adhesive and polyethylene sheet

6.5 Water Proofing of Staring Gauges

The effective stress measuring sensor allows water to infiltrate. Therefore, strain gauges should be waterproof. SB tape was used as a coating product for waterproofing requirement as shown in Figure 69. It is a Moisture- and water-proofing coating for laboratory and field requirements

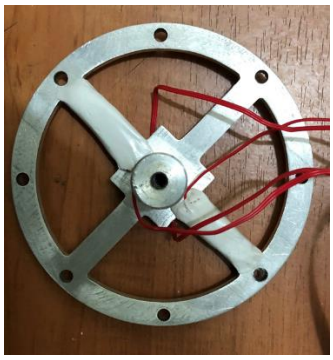

Figure 69: SB tape covered strain gauges

6.6 Water filtering mechanism

As we discussed earlier one sensor unit was designed for measuring the effective stress. In that case, the pore water balancing method was used. To allow the infiltration of water, 4 large holes are placed in the top part of the main casing. Other three holes are in the bottom part of the main casing. These three-holes were designed to remove the water inside the sensor when the water table goes down below the sensor. To prevent the soil particles from going inside, a geotextile was placed over the holes as shown in the Figure 70.

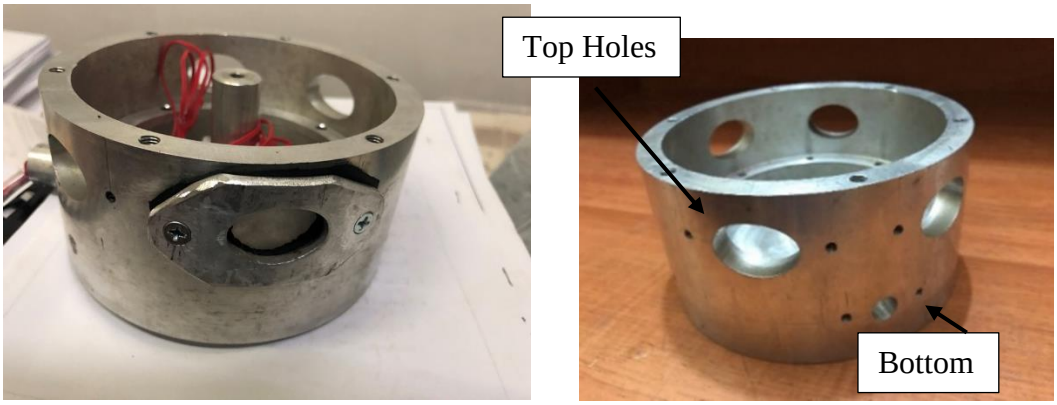

Figure 70: Water infiltration holes

7 SIGNAL CONDITIONING AND DATA ACQUISITION (DAQ)

7.1 Overall view

This chapter is focused on the electrical and electronic developments of the earth pressure measurement sensor system. The data acquisition system can be divided into three main categories as shown in Figure 71.

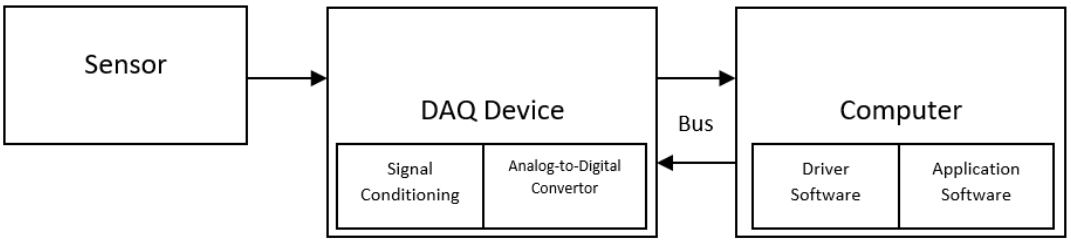

Figure 71: Data Acquisition System

In chapter 3, it was discussed about the working mechanism of the sensor. Chapter 4 and 5 were about the detail description of the sensing structures and sensing element. In this chapter, main focus is on the signal conditioning and the analogue-to-digital conversion. Other than that, a discussion about the development of the application solution, data logging and data visualization will be done in the next chapters. This signal conditioning part and the analog to digital conversion part are kind of an intermediate interface between the computation processing and sensor output. Results will be inaccurate if the signals coming from the sensor are measured since the outside noises can influence the sensor output signals. Therefore, to avoid that situation, a signal conditioning method should be used. Other than that, signal conditioning circuitry manipulates the sensor output form which is a favourable ADC signal. Other than the amplification of the filtering, attenuation and isolation are also done by the signal conditioning circuitry. It is a must to convert the analogue signal to a digital signal before it reaches the digital tools like computers. The primary function of the ADC is digitizing the incoming analogue signal and transmitting it to the controlling and processing device as a readable input. ADC chip is capable of giving the digital representation of the analogue signal rapidly.

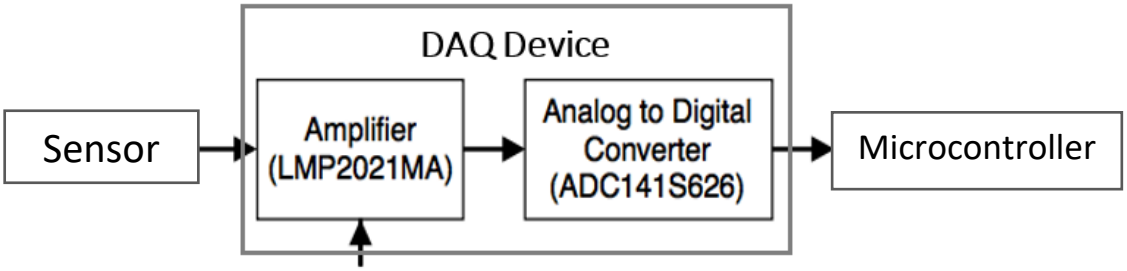

Figure 72: DAQ device components

In this sensor system, separate modules for amplifier and Analog to Digital converter were used as shown in Figure 72. When the real ground condition is considered, a lot of power lines, generators, motors, arc welders etc are located around the construction sites and some normal places as well. Therefore, a lot of noises can be added to the output signal of the earth pressure cell. Sometimes it is required to place the earth pressure cell so far away from the data receiver, in those situations, it is needed to provide a long wire, due to that reason lot of noises and resistance can affect the output signals of the earth pressure cell. Therefore, LMP2021MA industrial type bridge instrumentation amplifier evaluation board was selected as a signal conditioner. Further discussion is carried out about this amplifier in the next topic in this chapter

When considering about the Analog to Digital converter in this sensor system, it is needed to provide a highly accurate one. Because the signal variation range of the electrical circuitry of the sensor is very small. Therefore, it is needed to provide the highly accurate and highly precise Analog to digital converter. When considering the ADC in a selected Arduino, it is a 10 bit one. It has a lesser accuracy. Therefore, it is not enough to use as the ADC in this application. Though HX711 is a 24-bit ADC, its accuracy is not up to the expected level.

7.2 Amplifier

In this sensor system, LMP2021MAEVAL instrumentation amplifier evaluation board was used for signal conditioning which is shown in Figure 73. It is configured as a differential-in, differential-out using LMP2021 chip. Especially it includes the precision reference. Other than that, it consists of a buffer to drive a bridge sensor. In this amplifier, it was provided with the precision 5V reference as an excitation voltage.

The output of the amplifier is compatible with the (pin to pin compatible to) ADC141S626EB evaluation board which is used as an Analog to Digital converter in our sensor system.

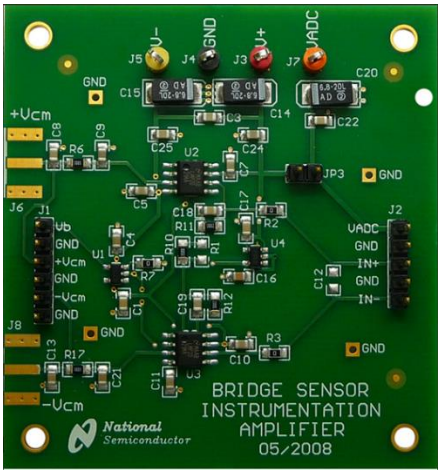

Figure 73: LMP2021MAEVAL instrumentation amplifier evaluation board

The gain of this amplifier depends on the R1 resistor which can be placed according to the requirement. The gain of this amplifier depends on the following Eq.15 given in ADC141S626EB evaluation board data sheet.

$$1 + {}^{2R11}\Big/_{\frac{R1R10}{R1+R10}} = Gain \qquad \text{..... Eq. 15}$$

In this Eq. 15, R10 and R11 are already embedded resistors which are 150Ω and 10kΩ respectively. In this case, the output voltage of the bridge circuit varies with the constant excitation voltage of 5V according to the following Eq. 16 based on Figure 88 experiment data chart.

$$Y = 0.0199X + 1.2846 \text{..... Eq. 16}$$

In this Eq. 16, X is an earth pressure value in kg and Y is the output voltage of the bridge circuit. This Eq. 16 is further discussed in the next chapters.

According to that Eq. 16, when we take 200kg as the maximum load on the sensor output is around 5V

7.3 Analog to Digital converter

Figure 74: ADC141s626eb evaluation board

The ADC141S626EB/RoHS Design Kit is designed and manufactured by National Semiconductor and ADC141S626 differential input, micro power converter is designed and manufactured by the Texas Instruments which is shown in Figure 74. ADC141S626 is a 14-bit Analog to Digital Converter. This ADC's operating speed is in the range of 50kSPS to 250 kSPS. The operating temperature of ADC module is in the range of -40 ^{0}C to +85 ^{0}C. Other than that, it has the following features,

- True differential inputs
- It has an external reference
- It has Track mode with zero-power
- It has a serial interface which is compatible with MICROWIRE / SPI^{TM} / DSP/ QSPI^{TM}

ADC141S626 can be operated with digital input/output (V_{IO}) and independent analogue (V_A) supplies. Those can be set independent to each other. It can be used in the range of 2.7V to 5.5V both V_A and V_{OI}.

One of the main advantages of this ADC evaluation board is, it has two operating modes one is Stand-Alone mode and the other one is Computer mode. Stand-Along mode is suitable for our equipment because we can customize, as we want.

8 DEVELOPMENT OF REMOTE MONITORING AND DATA LOGGING SYSTEM

8.1 Overview

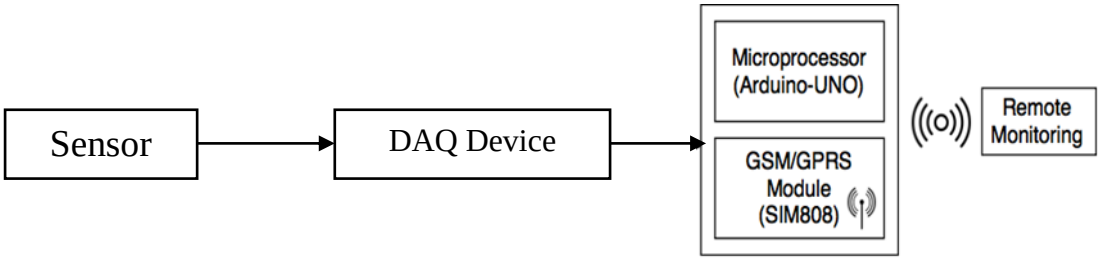

Figure 75: Processing and computation unit

In this chapter, last part of the data acquisition system is discussed as shown in the Figure 75 above. Most of the sensor systems were failed due to the complexity of receiving the output. In the case of the geotechnical applications, it is very difficult to reach the location regularly and collect the data. On the other hand it is important and necessary to access the real-time data especially in the monitoring systems for landslides. In most of the cases labors are involved in placing the sensor system, collect the data and so on. Due to that reason sensor handling and data collecting method should be easy. Considering all kind of issues and considering requirements, it was proposed to have a new data collecting, data logging and remote monitoring system.

The micro-controller-based processing system is used to handle the whole data acquisition system and three ways were provided to gather the data. First one displays the real-time sensor values, the second one stores the data into a memory inside the DAQ device and controller device and finally, store the data in a cloud-based database and in an online server-based web platform. Other than that, this system consists of the GPS facility also, from that feature the exact location where the sensors are placed can be identified. For this system, a rechargeable battery system is introduced as the power source. But according to the future requirements, there is a provision to develop the solar-power power supply system. Figure 76 shows a simple explanation of the overall mechanism of the data acquisition system.

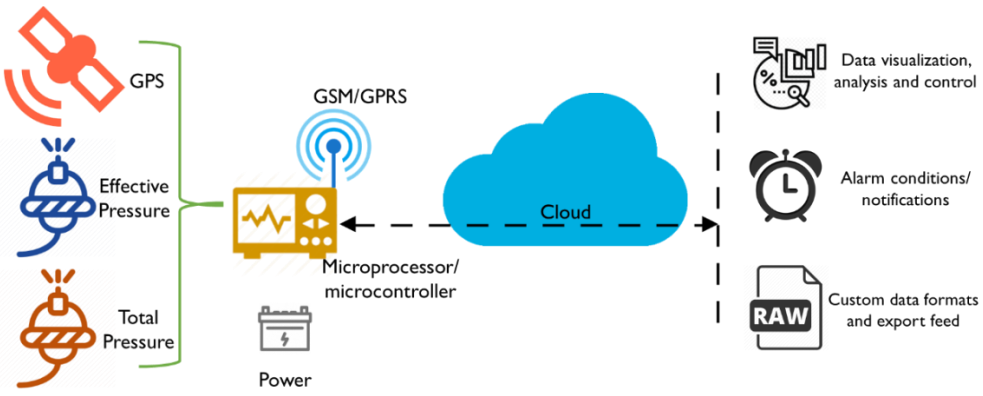

Figure 76: Total Data Acquisition system.

8.2 Microcontroller and another electronic circuitry

In the earth pressure measuring system, Arduino Mega 2560 microcontroller which is shown in Figure 77 was used to do the processing and computations. It has ATmega2560 processor with 16 MHz CPU speed. The following table shows the features summary of the Arduino Mega. Operating voltage of this Arduino is 5V, but its input voltage can be 6-20V. It has a 54 number of digital input/output pins and 16 number of analogue pins. A 128kB flash memory and 4kB are used to the bootloader.

Microcontroller (Arduino) gets the readable input from the sensor by amplifying the signals and converting analogue signals into digital signals from ADC. Suitable Arduino library was developed to get the readings from ADC. After that, SIM808 GSM/GPRS/GPS module was connected to the Arduino and through that real-time data was sent to the cloud database via a 2G network. It collects the GPS locations as well. This module is capable of operating with 2G network system as mentioned earlier. Therefore, this can operate in very remote areas as well.

Figure 77: SIM808 GSM/GPRS/GPS module and Arduino Mega

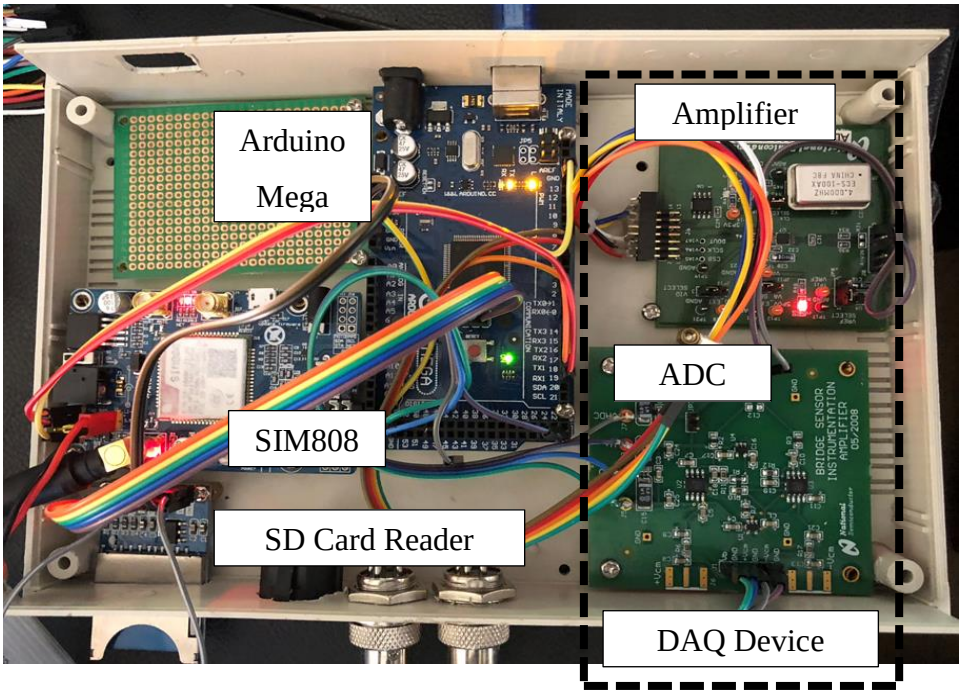

Figure 78: Main Control unit

8.3 The local data logging system

A SD card was selected to store the sensor output in the main controller. If some connection failure or some network error occurred cloud-based data storage system is going down. Therefore, it is needed to provide a way to store the data in the main controller itself. SD card-based system was implemented mainly due to simplicity and reality of that. The SD card module was connected to the microcontroller (Arduino Mega) as shown in the Figure 78 above. According to the following calculations 6 thousand files (6667 files) can save to 8GB SD card.

ADC 14Bit

Data range >> -9999 to 9999

Max data samples for single test >> 100000

approximately size of one file = 100000 * (5 byte + 7byte) = 1.2 MB

using 8 GB SD Card = 8GB/1.2MB = 6667 files

8.4 Remote monitoring system

As discussed earlier, it is very important to provide a remote monitoring system to access and monitor the data. The Figure 79 explains the mechanism which is implemented in this sensor system.

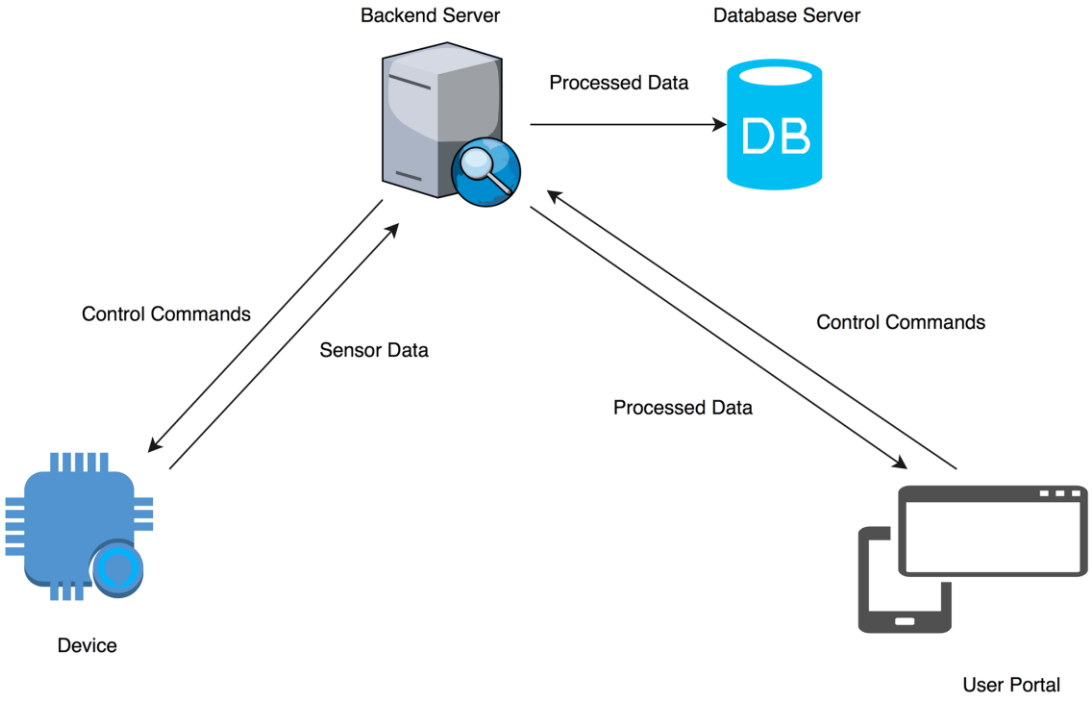

Figure 79: Remote monitoring system

After getting readable output from sensors to the microcontroller, it is sent to the back-end server as a response to the control commands. As a host server, Godaddy.com was used. After processing data in a backend server, they are sent to the database server for storage. After that web portal was developed for the access, monitoring and downloading of that data.

The frontend web portal was developed using PHP and REST protocol was used for communication purpose. There are basically two types of communications in the system.

1. Device to server and vice-versa
2. User portal to server

Each type is handled by two processing units of the server making it decoupled based on the purpose of use.

Host Service: Godaddy.com

Language: php / javascripts

Database: mysql

8.4.1 Development of the Soil Pressure Sensor Portal

The device data can be accessed by an online web portal. Each device has a unique key which is used for communication and processing purpose. Following used cases are supported by the online web portal.

1. User account creation (One can create accounts for others)

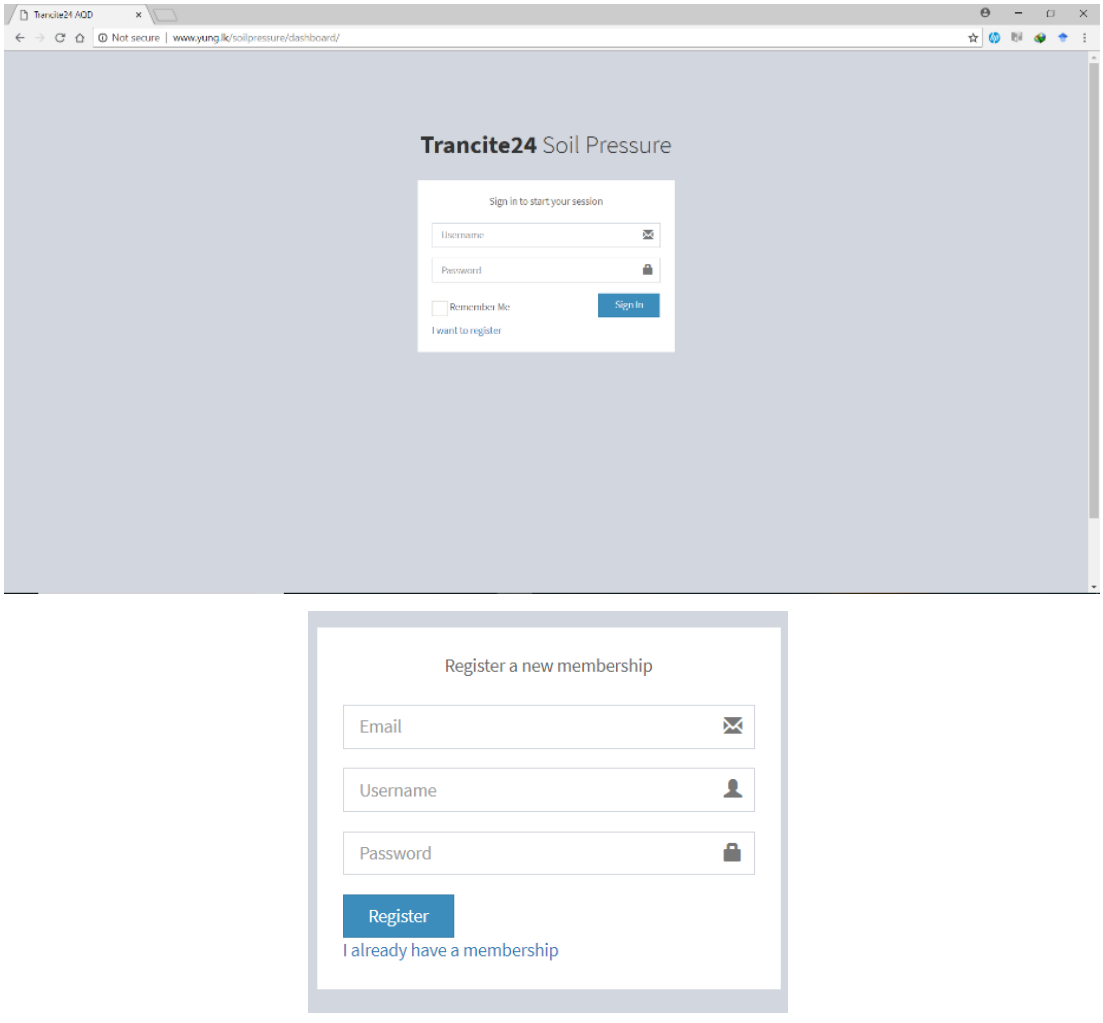

Figure 80: User logging and user registration

Initially, the user should create an account using his/her email account. After that, created account, username and password can be used for every login as shown in Figure 80.

2. Register a given device with a user

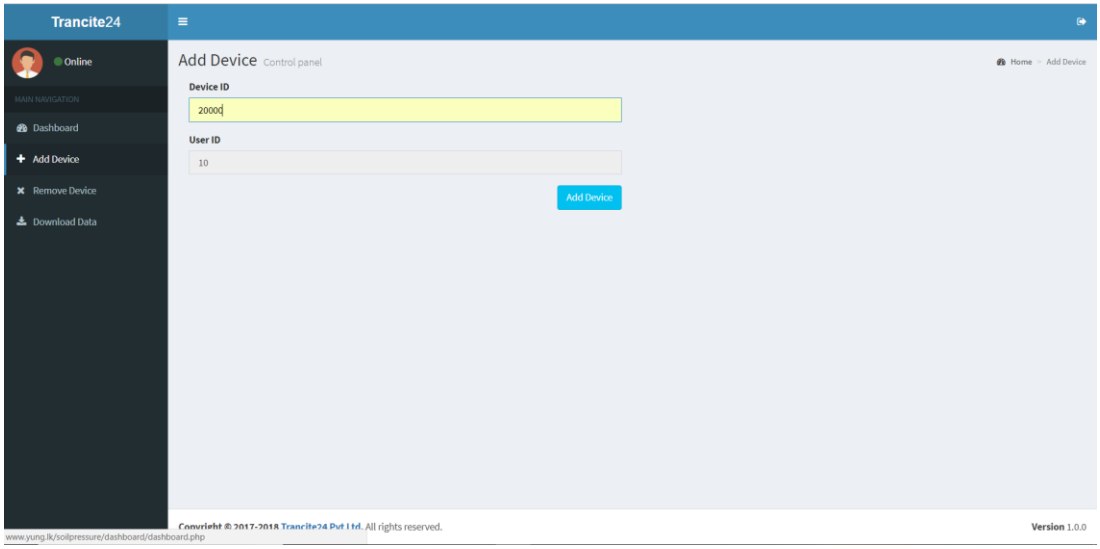

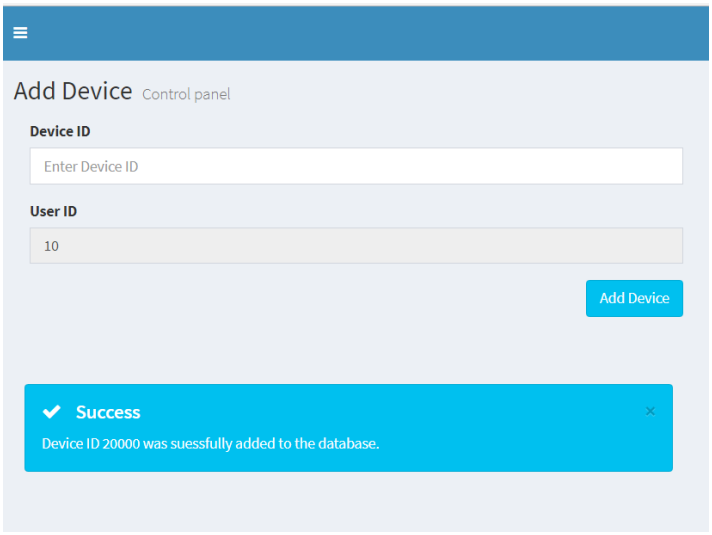

Figure 81: Add device

All sensors have unique identification numbers. According to that number, users should add the device into their account according to the Figure 81. Users can add any number of devices to their account. Earth pressure monitoring systems have many numbers of EPC. Therefore, in this system, all EPCs can be monitored simultaneously.

3. Unregister a given device from a user

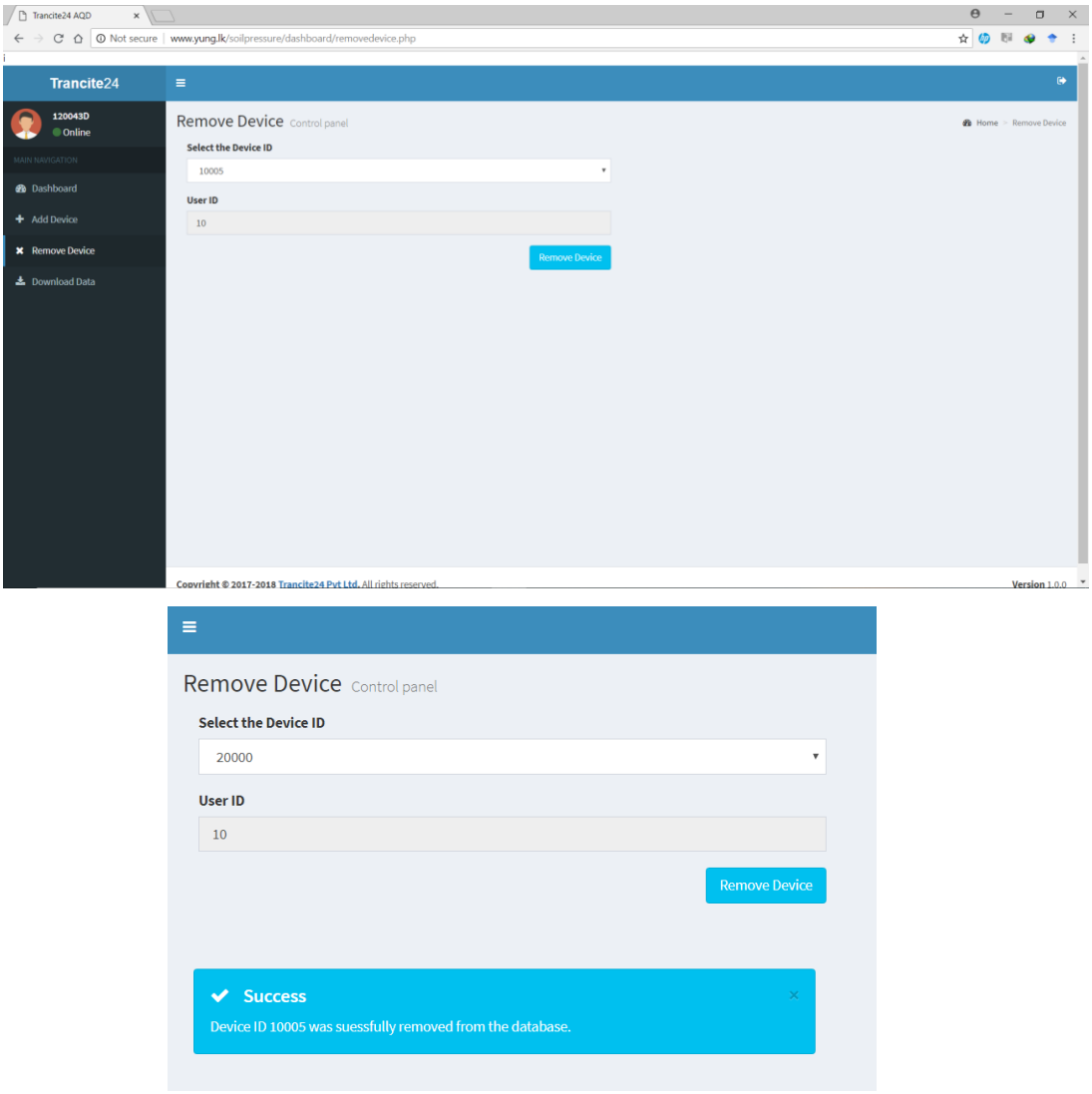

Figure 82: Remove Device

As similar to previously showed add devices, any device can be removed from your account at any time as shown in Figure 82.

4. View graphical illustrations of the data flow and view statistics of the data

In this web portal, a graphical illustration of the sensor data flowchart and static data are showed. In that chart, total Pressure and effective pressure are shown simultaneously. Therefore, the user can get a quick idea about the variations of the TEP and EEP as shown in the following Figure 83.

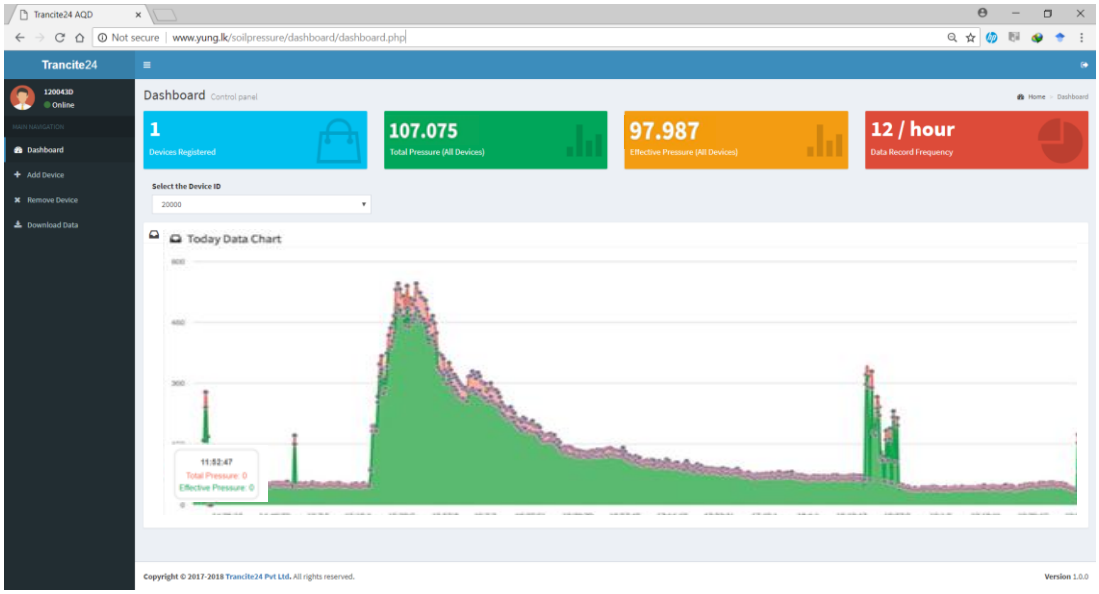

Figure 83: View of graphical illustrations of the data flow and View of Statistics of the data

5. Download raw data and View raw data

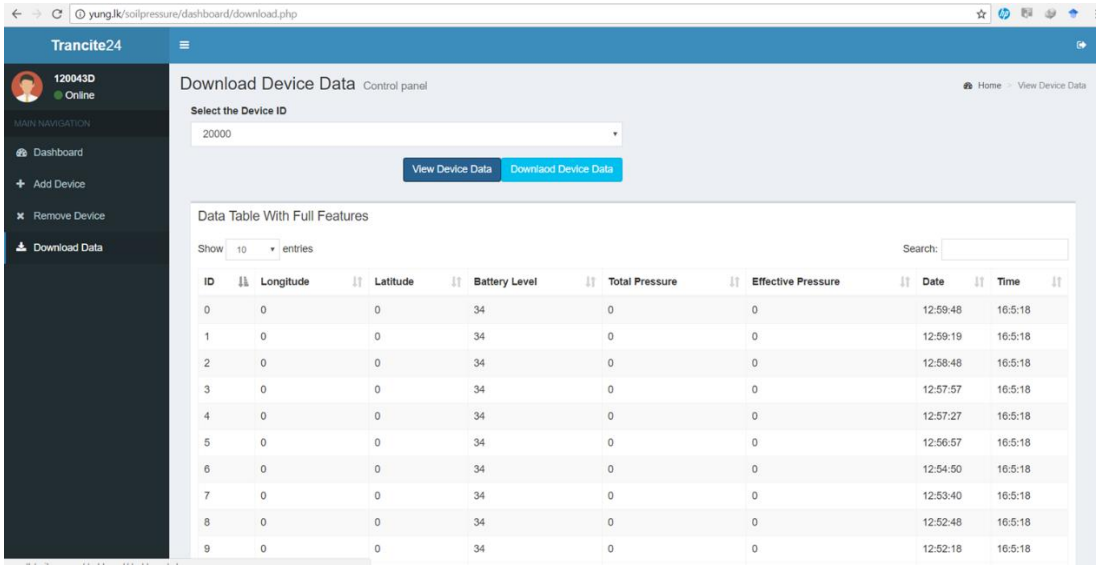

Figure 84: Download and view raw data

In this web portal, user can download all the data which is included in a GPS location, total pressure, effective pressure, date and time. All of these data can be downloaded in CSV format. Other than the download feature, the user can view all the raw data as shown in the Figure 84 above.

8.5 Display View

As mention in earlier, the user can visualize and see the sensor output values in embedded display in the main controller as shown in the following Figure 85.

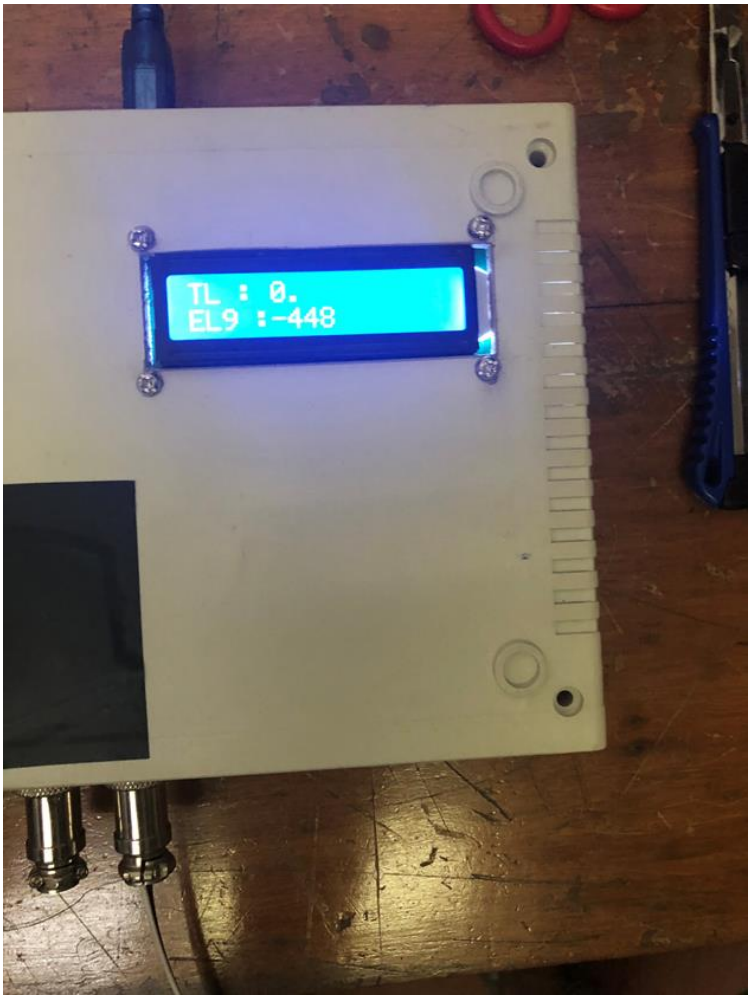

Figure 85: Display view

9 TESTING AND VALIDATION

9.1 The sensitivity of the sensor

To calibrate this sensor, known loadings were used. During this process steps of loads from 100 g to 60 kg were used to measure the corresponding signal as shown in the Figure 86. Output voltage was measured using a 6 1⁄2 desktop multi-meter with the accuracy of 0.0001 mV.

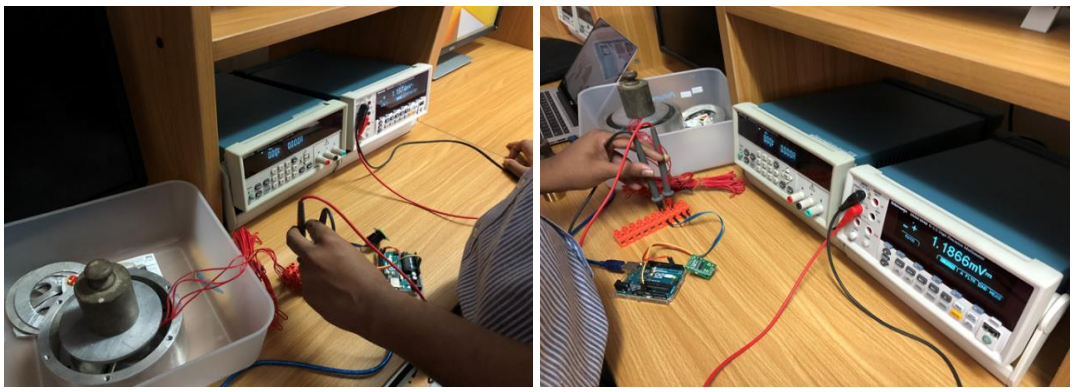

Figure 86: Laboratory testing for estimate the sensitivity

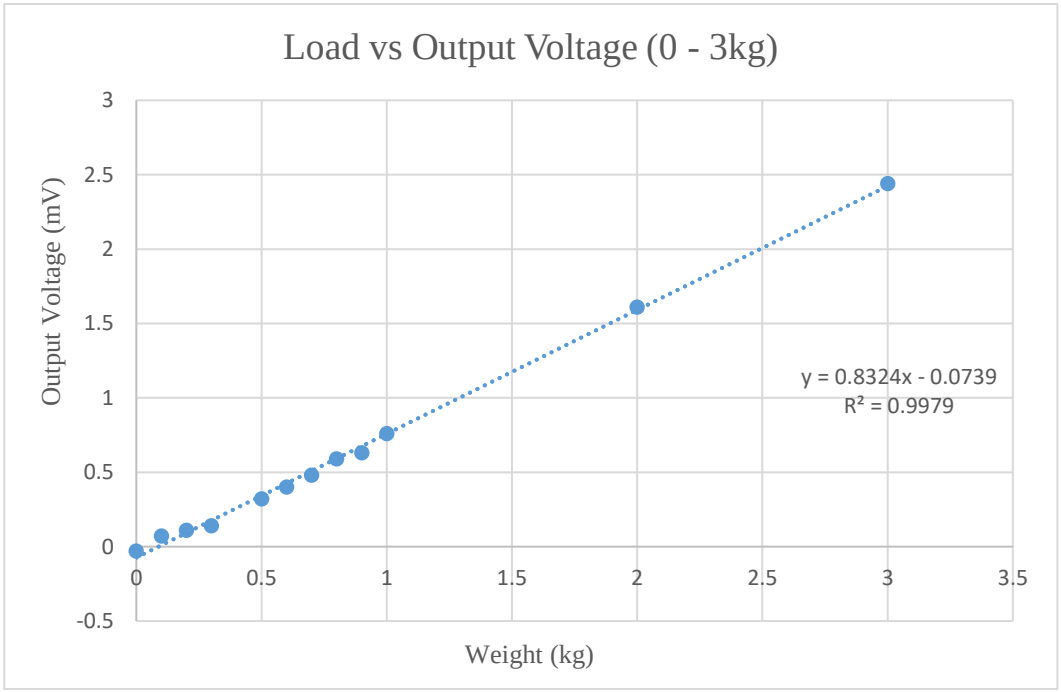

Figure 87: Sensitivity graph of the sensor (0 – 3 kg)

R-squared value is 99.79%. It shows that the response of the sensor is adequate to measure small loads as shown in the above Figure 87.

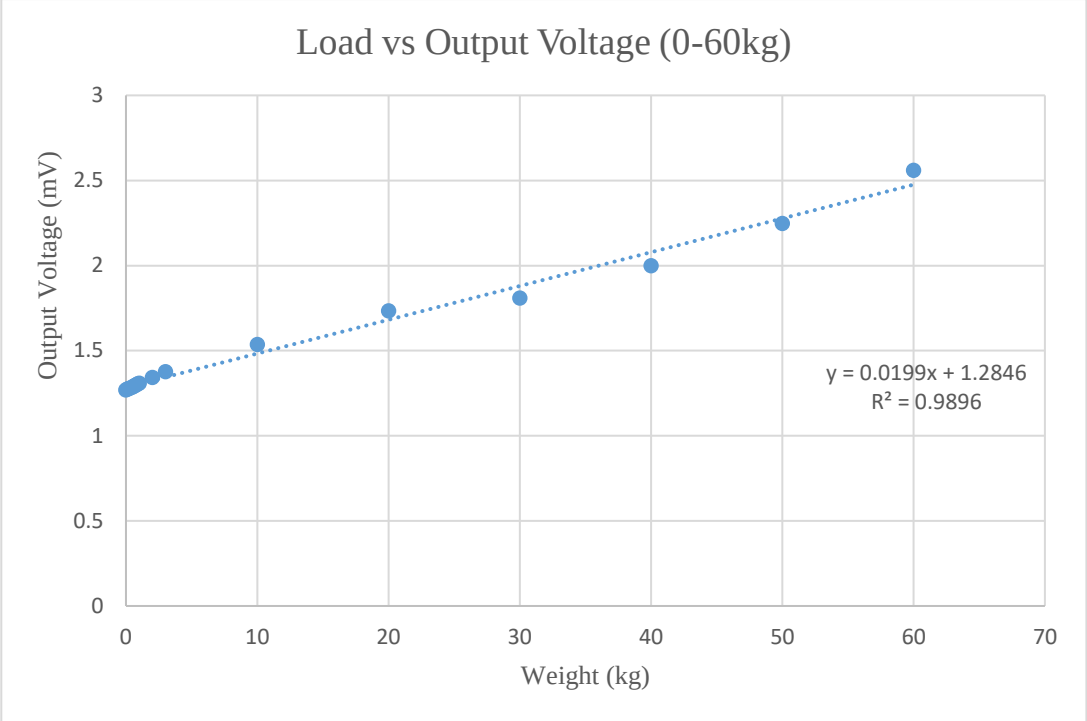

Figure 88: Sensitivity graph of the sensor (0 – 60 kg)

When the load is increased up to 60 kg, it shows an R-squared value of 98.96% as shown in Figure 88.

In the whetstone bridge, the solved resistance is 350Ω to excitation voltage because the strain gauges resistance is 350Ω, according to the specification of the selected strain gauges permissible current should be less than 30mA for metallic specimens. Therefore, according to the calculation 5V excitation voltage should be maintained. The sensitivity of the sensor is 1.63 mV/V per kPa.

9.2 Temperature Characteristics

In the test, it was aimed at identifying the load drift with respect to the temperature variation. For that purpose, temperature sensor was embedded in the sensor to measure the temperature variation as shown in Figure 89. In this case, temperature increase is only up to 50^0C. Because according to the research (76) temperature variation of the earth surface is not expected to be more than 40^0C.

Figure 89: Setups for measuring temperature characteristics

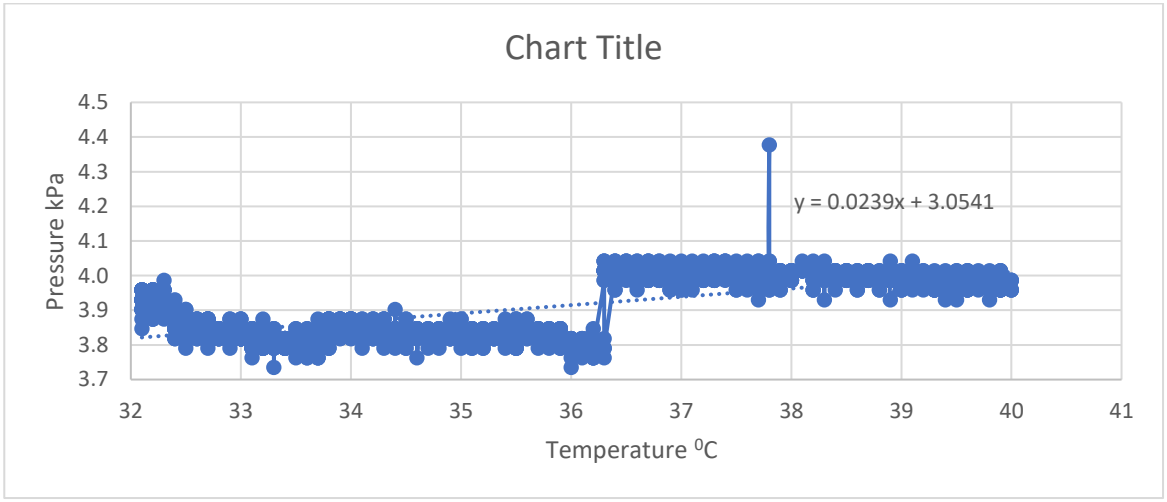

Figure 90: Temperature vs Pressure variation from 32^{0}C to 40 ^{0}C

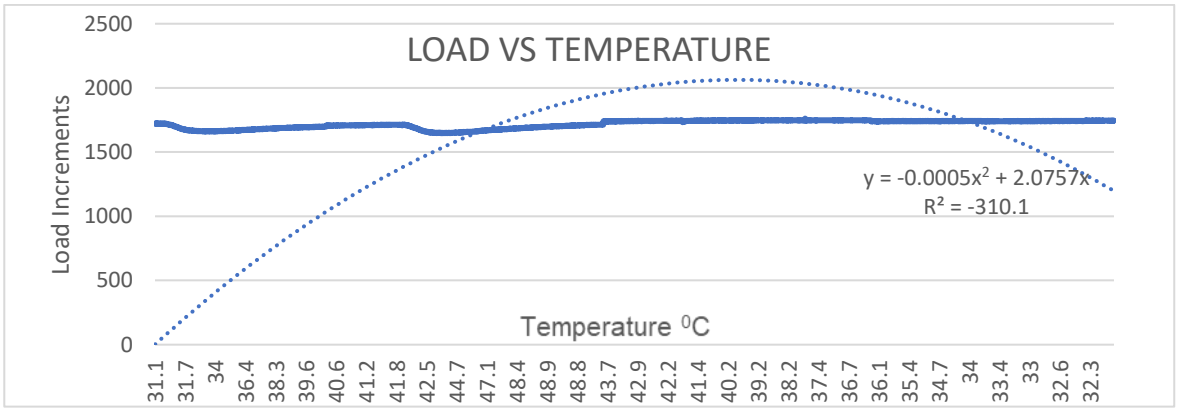

Figure 91: Temperature vs Output variation from 31^{0}C to 50^{0}C and 50^{0}C to 32^{0}C

According to the above Figure 90 and Figure 91, the variation of the load due to temperature variation would be within 1 kPa.

What is the unit of the load increment axis in Figure 91

9.3 Zero Drift

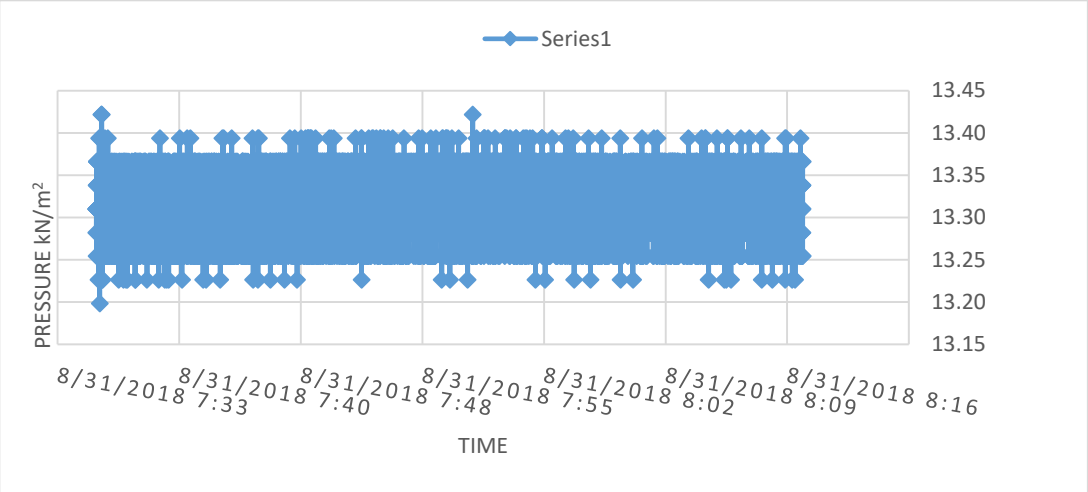

Figure 92: Sensor output variation with time for 10.5 kg load

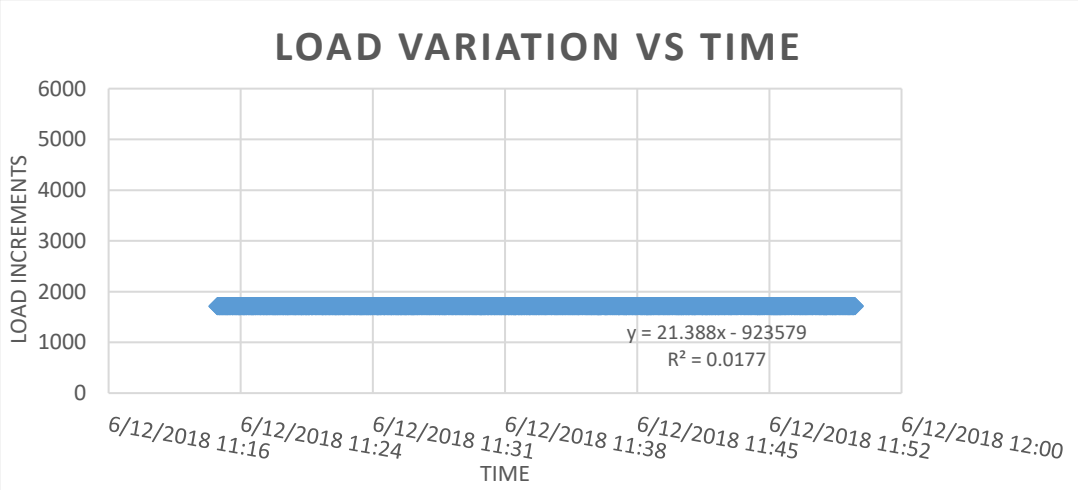

Figure 93: Sensor output vs time

Figure 92 shows the 12hr pressure output value with respect to the 10.5kg load. The load variation within this period as only between the 13.20kPa to 13.45kPa.

According to Figure 92 and Figure 93, the maximum variation of the sensor output value varies within the 0.5kPa. Therefore, this sensor satisfies the minimum measuring accuracy.

9.4 Hysteresis

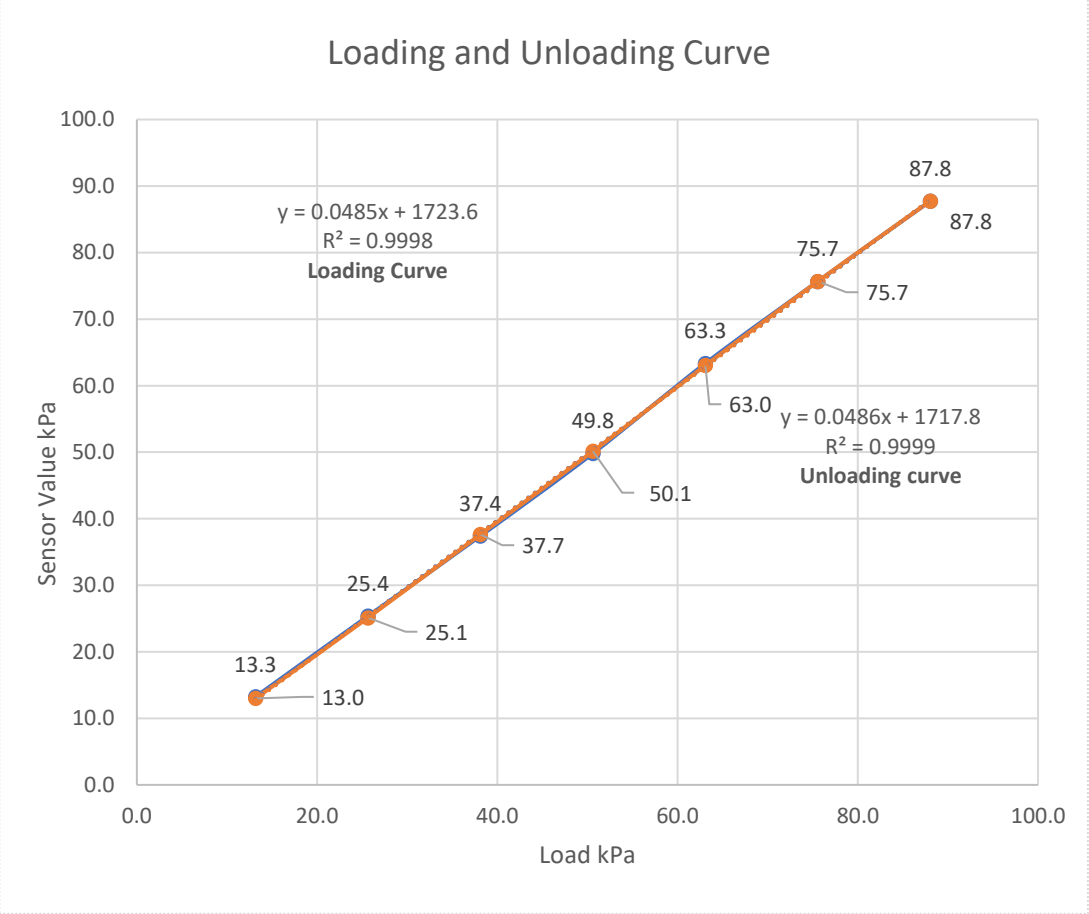

Figure 94: Hysteresis Curve

The hysteresis error interprets the maximum difference of the earth pressure cell output value at any specific measuring point while increasing and decreasing the earth pressure value within the specified range of the sensor.

In this sensor, hysteresis error is limited to around 0.4 kPa. Therefore, the minimum measuring value of 1kPa can be obtained from this sensor as shown in Figure 94.

9.5 Characteristic of effective pressure sensor

It is important to get an idea about the time that it takes to fill the water inside the sensor and reach equilibrium. For that a separate testing was carried out to for the effective pressure sensor as following figures.

Figure 95: Characteristics of earth pressure cell identification setup

First of all, the sensor was placed inside the bucket and filled with sand and kept for certain time period, after that, it was filled with water as shown in Figure 95.

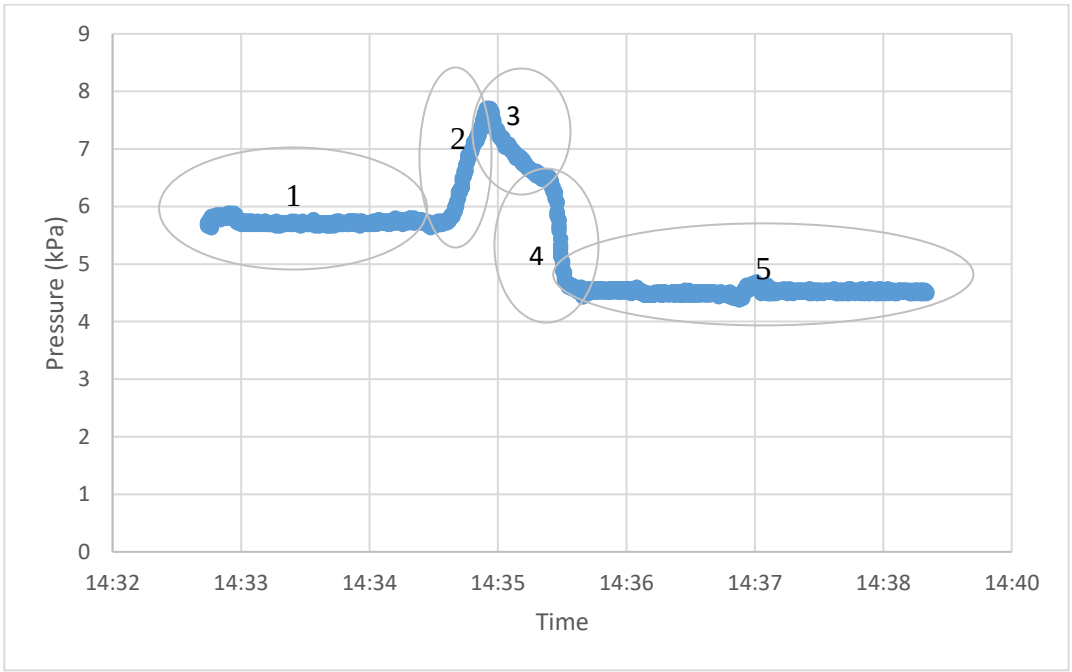

Figure 96: Saturated time curve for an effective sensor

In this experiment, the sand layer thickness was around 37 cm and water were also filled up to that level. Using that data following calculation can be done to verify the given result by the effective sensor.

Calculated pressure value at the sensor level before filling the water as shown in region 1 in the Figure 96,

$$P = \gamma_{dry}\, x\, h$$

$$P = 16kN/m^3 x 0.37m$$

$$P = 5.92\ kPa$$

After filling with water as shown in region 5 in the Figure 96,

$$P = (\gamma_{sat} - 9.81) x\, h$$

$$P = (22 - 9.81)kN/m^3 x 0.37m$$

$$P = 4.51\ kPa$$

Then, according to the results of the above calculation, Figure 96 can be justified. Therefore, referring to the above graph, it is indicated that it takes only around 1 min to saturate the sensor and become equilibrium in sand. In the above Figure, region 2 clearly shows that total load increases after adding water. Water pressure get reduced with time because of water infiltration to the inside of the sensor and balance with outside water pressure as shown in region 3 and 4. This density values were found out from measuring the weight of sand with and without water with known volume.

9.6 Characteristic of sand used for experiments

Sand was used for the EPC testing, validation test and arching effect experiments. Initially the particle size distribution of sand was identified from dry sieve analysis following guidelines in the ASTM D422 standards. According to the test results coefficient of curvature of this sand is 0.78 and coefficient of uniformity of this sand is 2.45. Test results are shown in Figure 97. This selected sand can be categorized as poorly graded sand following the Unified Soil Classification System.

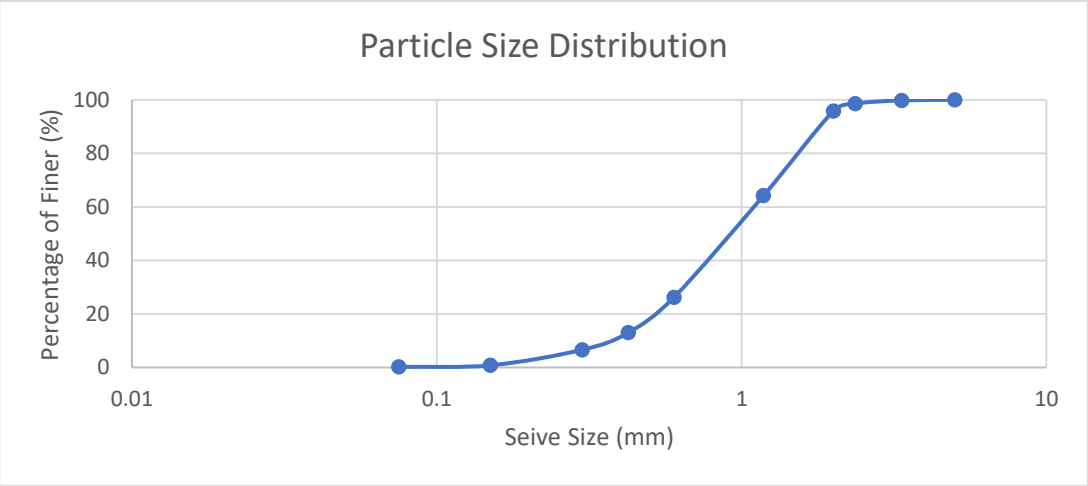

Figure 97: Particle size distribution of selected sand

According to the direct shear test in ASTM D3080, friction angle of this selected sand is 34^0. Test results are shown in Figure 98 and Figure 99.

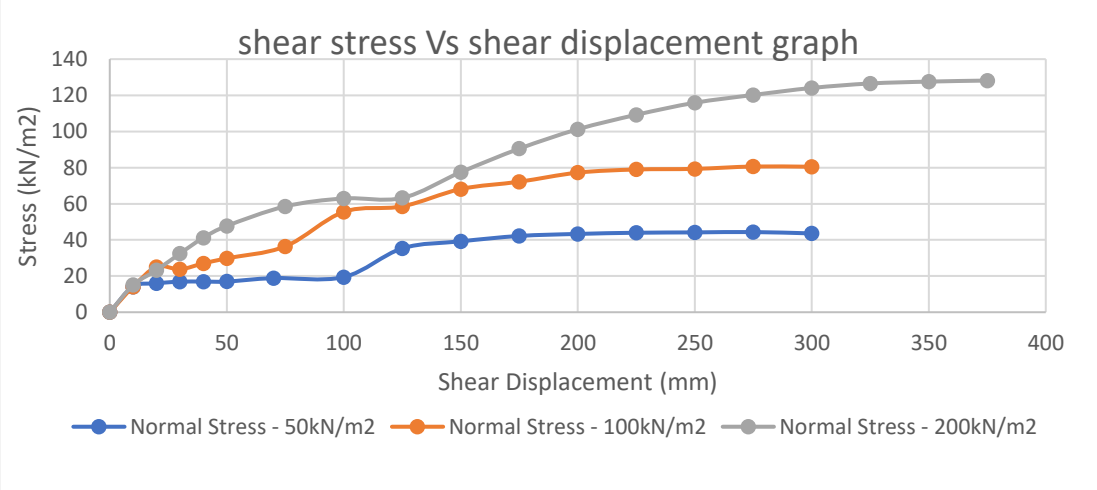

Figure 98: Shear Stress vs shear displacement

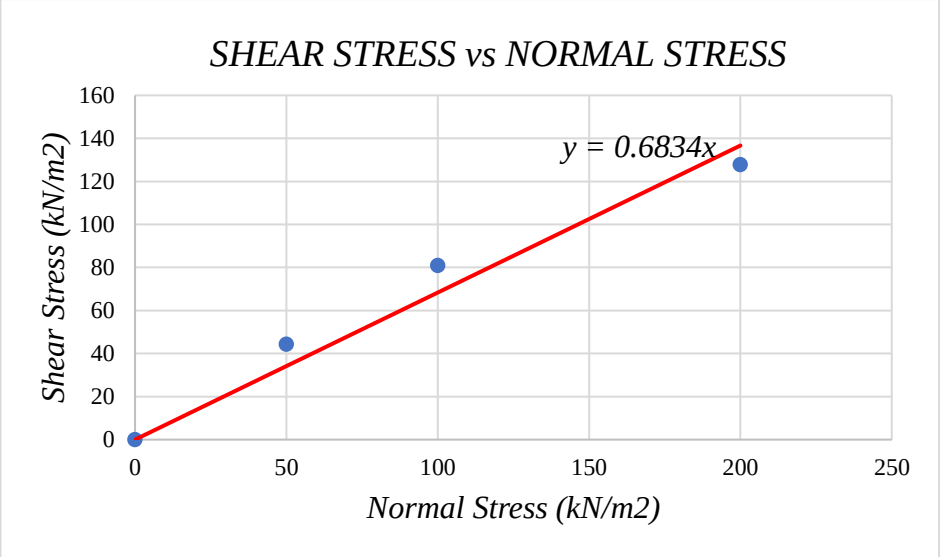

Figure 99: Shear Stress vs normal stress

10 EVALUATION OF ARCHING EFFECT USING DEVELOPED SENSOR SYSTEM

10.1 Validation of the arching test results

For this experiment a bucket with a 0.8m diameter and a 0.7m height, was used. Then the sensor was placed on a rigid base and covered with a 0.4m sand layer. A sand layer of thickness 8cm was used as a flexible layer with respect to the rigid base. After that the 25.5 cm square rigid steel plate was placed and the force was applied on to that via a hydraulic jacking system as shown in the Figure 100.

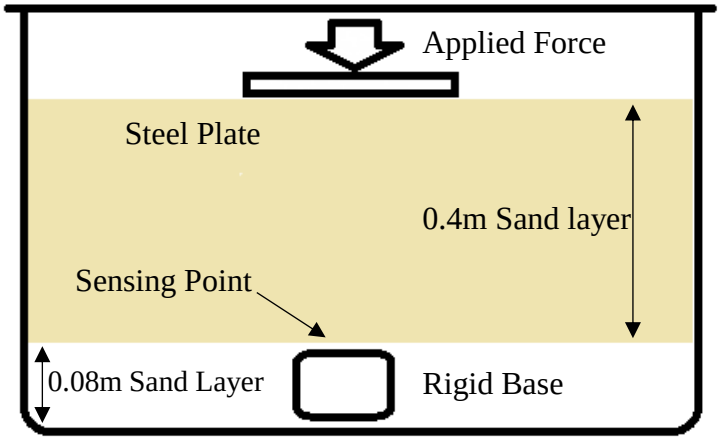

Figure 100: Details of the arching effect test setup

Figure 101: Laboratory experiment setup

A proving ring was used to measure the applied load using a hydraulic jack as shown in the above Figure 101. In this test, the load was increased according to the 1st column of the following Table 7 and sensor output values were recorded

Initially, to verify and validate the arching action, pressure results in given by sensor were compared with Terzaghi's arching effect theory. Considering boundary conditions and other factors, Eq. 17 was used.

$$\sigma_v = \frac{B(\gamma - {}^{c}/_{B})}{K\ tan\emptyset}\left(1 - e^{-Ktan\emptyset\frac{z}{B}}\right) + q.e^{-Ktan\emptyset\frac{z}{B}} \text{..... Eq. 17}$$

In the above Eq. 17, yield strip width(B) is 0.255m and depth to the support(z) is 0.4m. The selected sand has a unit weight(γ) of 16 kN/m^3. Cohesion of this sandy soil is taken as 0 and friction angle ($\emptyset$) is taken as 34^0 based on the results of the direct shear test. The stress which is acting in the vertical direction is denoted by σ_v. Lateral earth pressure coefficient (K) was calculated using Eq. 18.

$$K_a = \frac{1-\sin(\emptyset)}{1+\sin(\emptyset)} \text{..... Eq. 18}$$

According to the above calculation, K_a is 0.278. Using these values Table 7 was prepared. First column of the following table shows the load applied using hydraulic jack system. Second column includes $\frac{B(\gamma - {}^{c}/_{B})}{K\ tan\emptyset}\left(1 - e^{-Ktan\emptyset\frac{z}{B}}\right)$ component of the Eq. 17 and third column consists with $q.e^{-Ktan\emptyset\frac{z}{B}}$ component of the Eq. 17. Forth column and fifth column include pressure value at sensor level according to the Terzaghi's method.

Table 7: Terzaghi's Theoretical values vs Experimental values

Applied Stress (kN/m^2)	$B(\gamma - c/B)/(K\tan\emptyset) * (1-e^{-K\tan\emptyset * z/B})$	$q * e^{-K\tan\emptyset * z/B}$	$\sigma_v (kN/m^2)$	Sensor Value (kN/m^2)
14.87	5.5	34.4	40	33
15.21	5.5	35.7	41	35
16.17	5.5	39.6	45	36
16.82	5.5	42.2	48	38
17.13	5.5	43.5	49	41
17.46	5.5	44.9	50	41
17.94	5.5	46.8	52	45
18.28	5.5	48.2	54	45
18.42	5.5	48.7	54	45
19.88	5.5	54.7	60	53
20.84	5.5	58.5	64	56
21.63	5.5	61.7	67	60
22.28	5.5	64.4	70	64
23.74	5.5	70.3	76	70
24.87	5.5	74.9	80	75
25.82	5.5	78.7	84	79
26.95	5.5	83.3	89	85
28.08	5.5	87.9	93	89
29.37	5.5	93.1	99	94
30.33	5.5	97.0	103	98
31.29	5.5	100.9	106	103
32.58	5.5	106.1	112	106
33.23	5.5	108.8	114	107
33.88	5.5	111.4	117	108
34.35	5.5	113.3	119	111
34.66	5.5	114.6	120	113

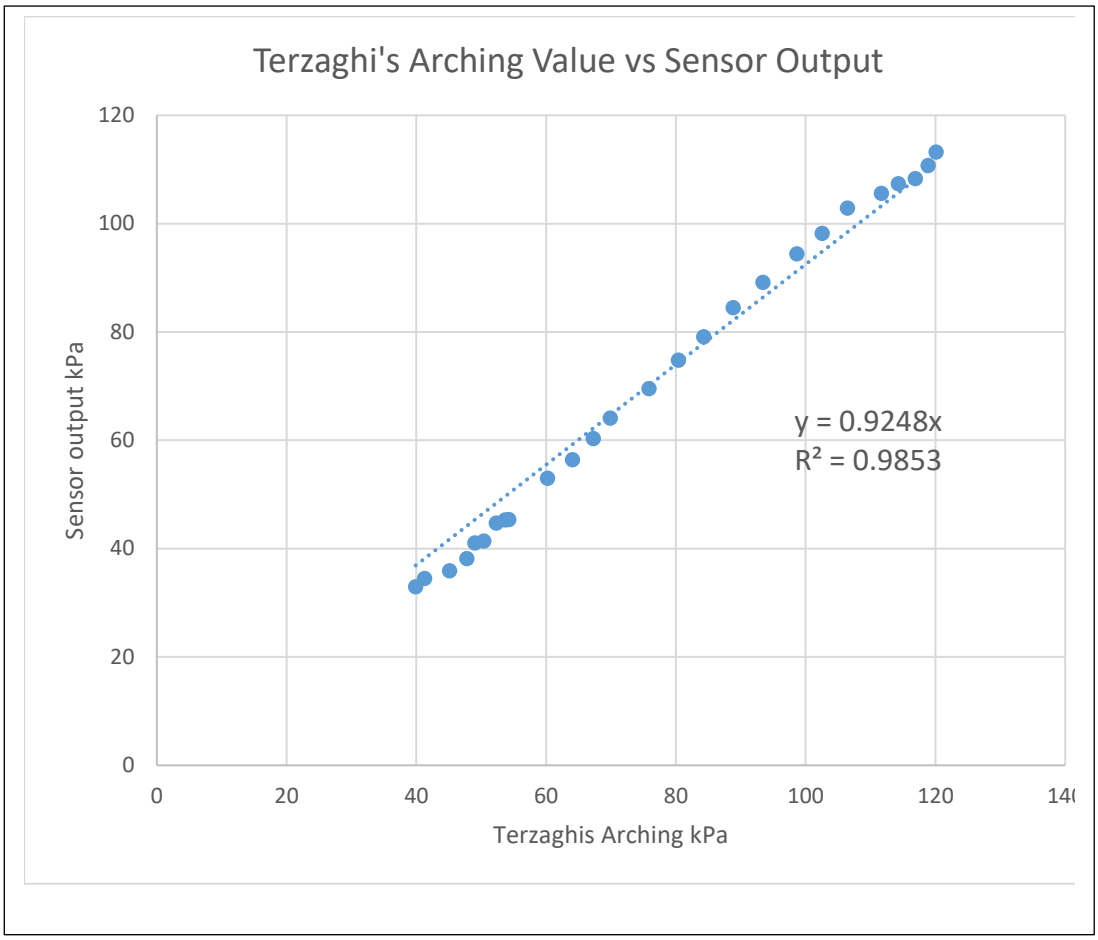

Figure 102: Terzaghi's Arching Value vs Sensor Output graph

In the above graph x axis is the applied pressure at sensor level according to the Terzaghi's equation and y axis is sensor output. Figure 102 clearly indicates that Terzaghi's theory of arching and sensor results varies with y=mx linearly. Other than that, the gradient of the trend line is also reasonably near to the value 1. Therefore, it can be concluded this sensor system can be used to measure the arching effect of the soil.

10.2 The active arching effect in dry sand due to the settlement of clay medium

To do this experiment, the same set of items were used. To make the active arching effect in the sand medium, a clayey cube was used as following Figure 103. Then the sensor was placed on the top of that clayey cube. After that the load was applied using a hydraulic jack system.

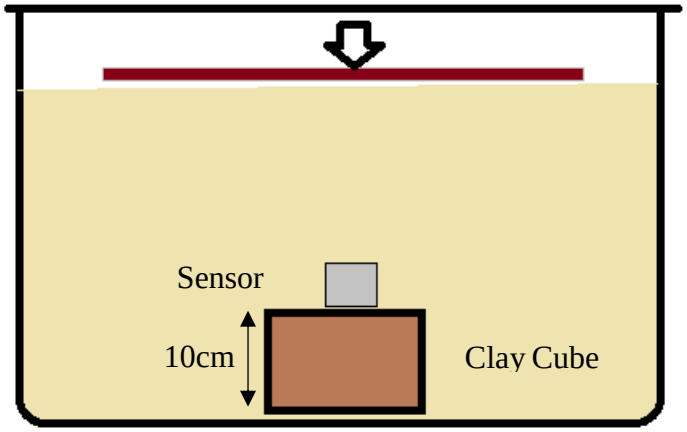

Figure 103: Experimental setup for evaluating the active arching due to the settlement of clayey soil

To prepare soil medium with a uniform density, sand was poured in the bucket with a constant height and a rate as in Figure 104. To avoid the frictional effect of the bucket wall, oil was applied.

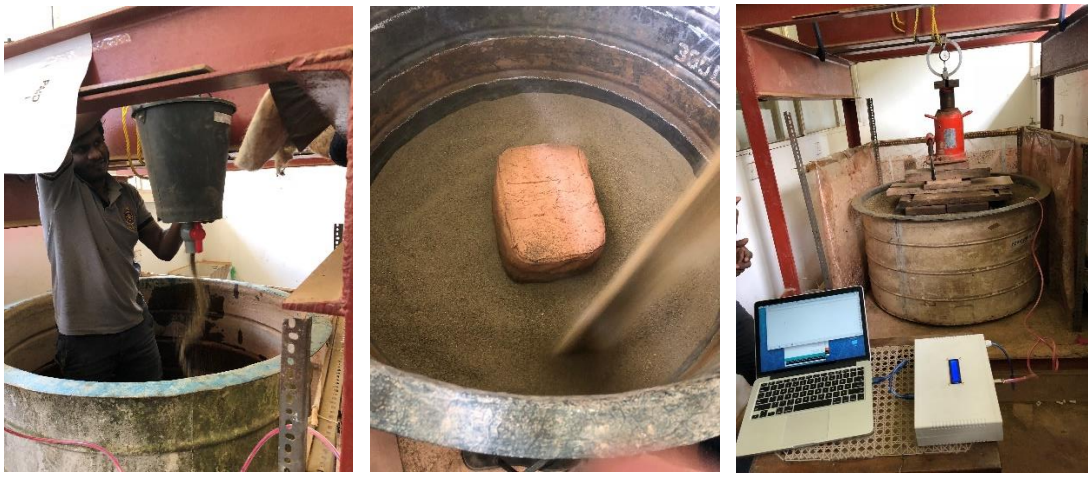

Figure 104: Sand filling (Left), clayey cube (Middle), whole setup (Right)

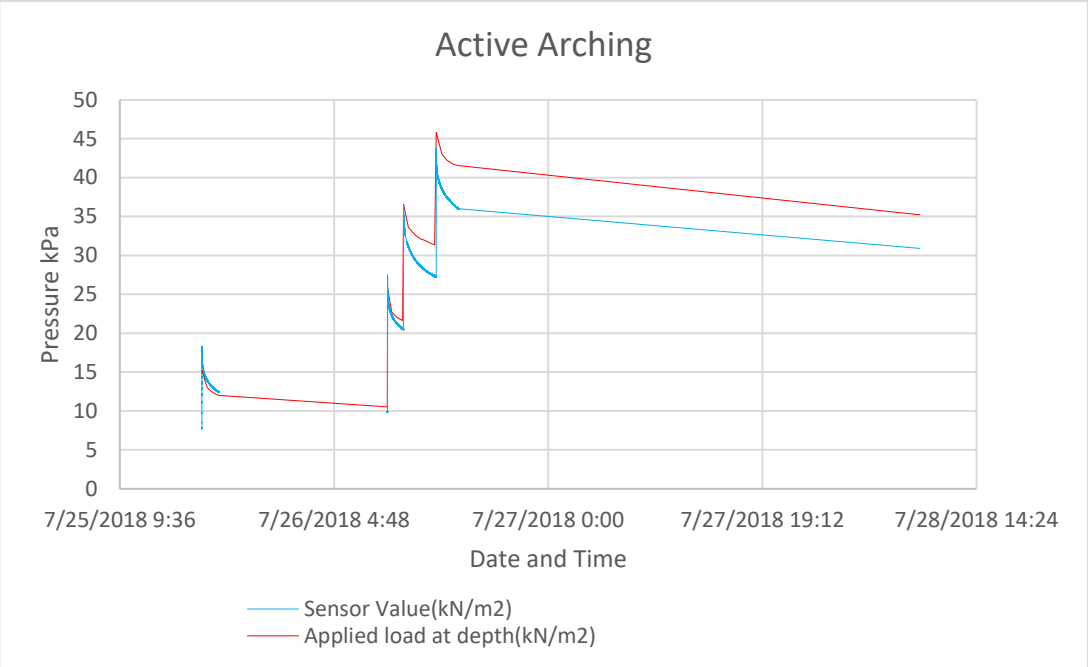

Figure 105: Active arching in the clayey medium (if possible please change the x axis to hrs)

In the above graph in Figure 105, x-axis of this graph is date and time of this experiment and y- axis of this graph is the sensor output value as a pressure in kPa at that sensor level. The blue line indicates the sensor output value and red line indicates the applied pressure which should be at sensor level according to the pressure calculations. Initially, sensor value and calculated stress values are behaving in an identical manner but when the load is increased, sensor values decreased with respect to the applied pressure. It clearly indicates that active arching happened due to the settlement of the clayey cube relative to the sand. On the other hand, more pressure reduction was observed for higher loads.

10.3 The passive arching effect in dry sand due to the settlement of clay medium

This experiment methodology is also similar to the previous one. To make the passive arching effect in the sand medium, a clayey doughnut shape fill was used as shown in Figure 106 and Figure 107. The sensor was placed on the concrete cube in the middle

of that clayey doughnut as a rigid base. After that the load was applied using a hydraulic jack system.

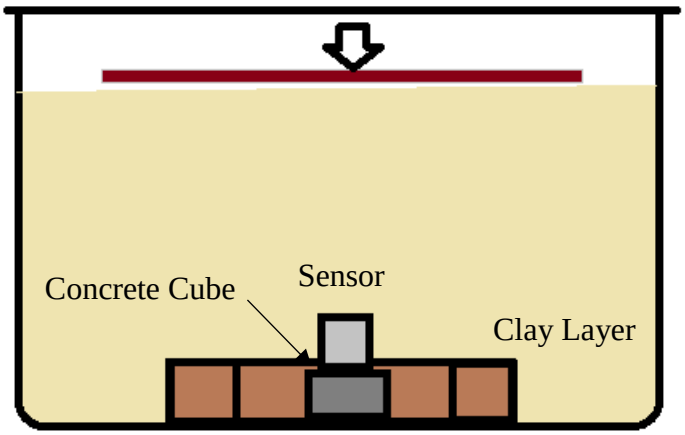

Figure 106: Experimental setup to evaluate the passive arching due to settlement of clayey soil

Objective of this setup is to model the passive arching effect by settling the surrounding area while keeping the sensor on a rigid base. To neglect the end effects oil was applied to the surrounding wall in this setup as well. Other than that it was attempted to maintain that clayey layer under fully saturated condition.

Figure 107: Doughnut shape clayey fill

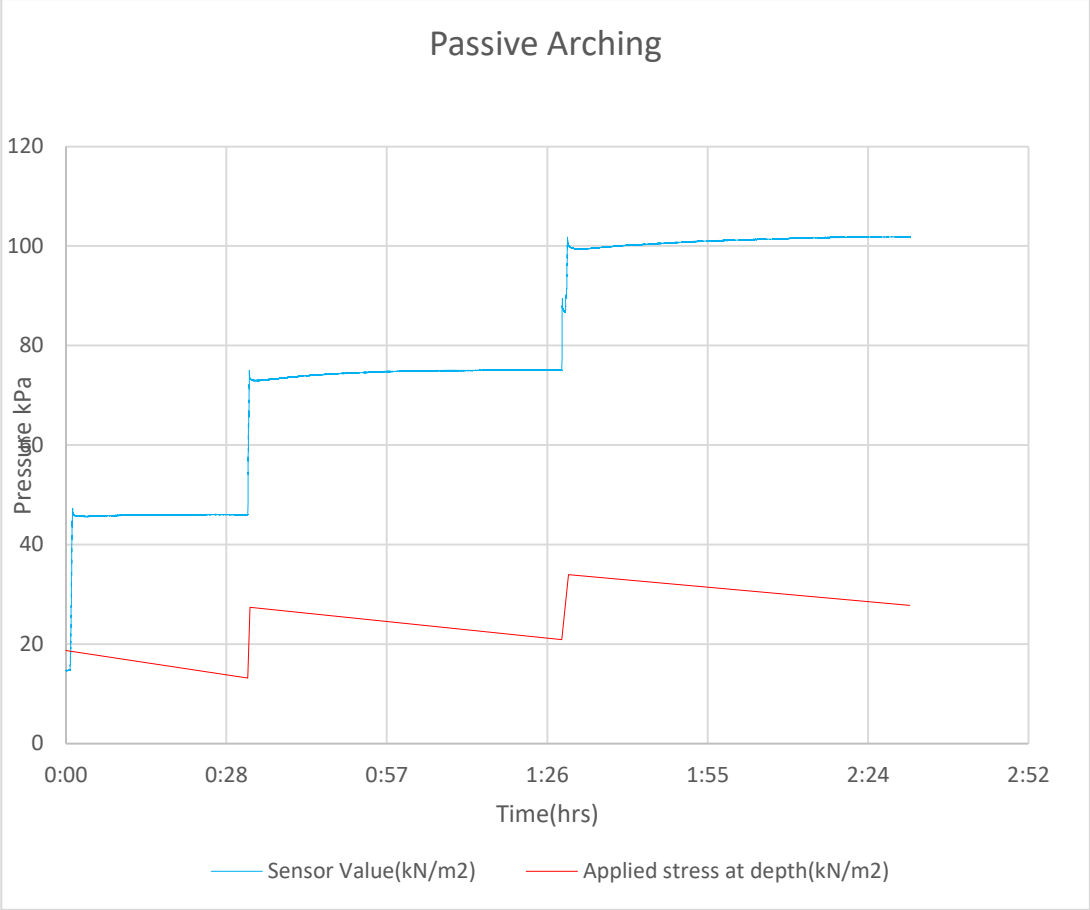

Figure 108: Passive arching in the clayey medium graph

In Figure 108, x-axis of the graph is time in hrs and y- axis of this graph is the sensor output value as a pressure in kPa at that sensor level. The blue line indicates the sensor value and the red line indicates the applied pressure which should be at the sensor level according to the pressure calculations. Initially, sensor values and calculated stress values were behaving identically but when the load is increased, sensor values increased with respect to the calculated value. It clearly indicates that passive arching happened due to the settlement of the clayey doughnut respect to the sand and vies-versa. In addition, it can be seen that more pressure increment occurred for higher loads.

10.4 Evaluation of arching effect with the trap-door model

Previous experiments were carried out with unknown settlements. But the following experiments were focused on evaluating the arching effect with known settlements. To vary the settlement according to the requirement a special setup was made based on the trapdoor model. That apparatus consists with 2-tons scissors jack to adjust the settlement according to the experimental requirements as shown in the following Figure 109. Sensor was placed on top of the moving apparatus.

Figure 109: Jacking Mechanism

To prevent the soil from moving to the inside of the apparatus it was covered with some flexible materials. Other than that, a pipe was provided to take out the rotating rod from the bucket and to rotate easily as shown in the following Figure 110 and Figure 111.

Figure 110: Moving apparatus placed in the bucket

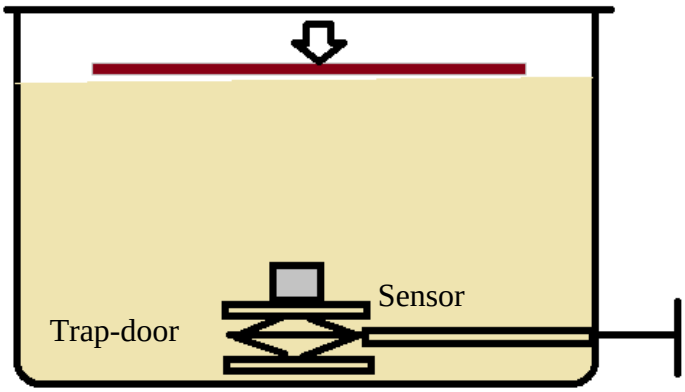

Figure 111: Known settlement arching effect evaluation setup

Trap-door model experiment was carried out as follows. Initially all the tests were carried out for dry sand. Dry sand experiments were also divided into main two cases, first one is the active arching model and second one is the passive arching model. After that experiment was carried out for saturated sand, that was also divided into two cases, first one is the active arching model and second one being the passive arching model. Active arching was created by moving the sensor holding plate in the downward direction and passive arching was created by moving the sensor holding plate in an upward direction. Experiments were carried out in following method as shown in Figure 112.

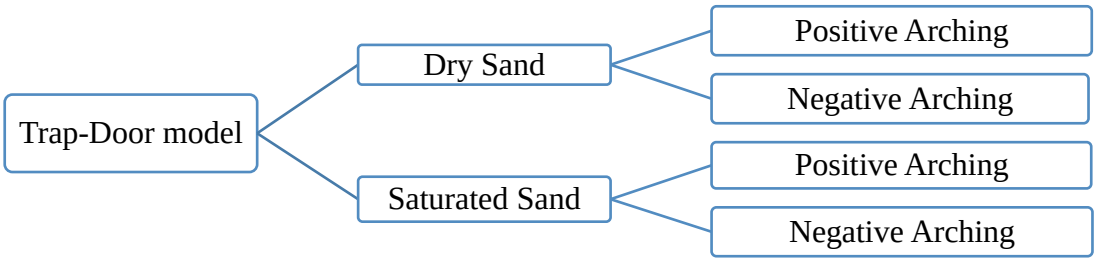

Figure 112: Trap-Door Experimental Method

10.4.1 Active arching effect in dry sand with trap-door method

This experiment was carried out with a known settlement while maintaining a constant load. The settlement was changed in 1mm increments by keeping the constant loading until a stable reading was obtained and similarly 4 mm total settlements were created in 1mm increments. In addition, the same experiment was carried out for 4 stress values.

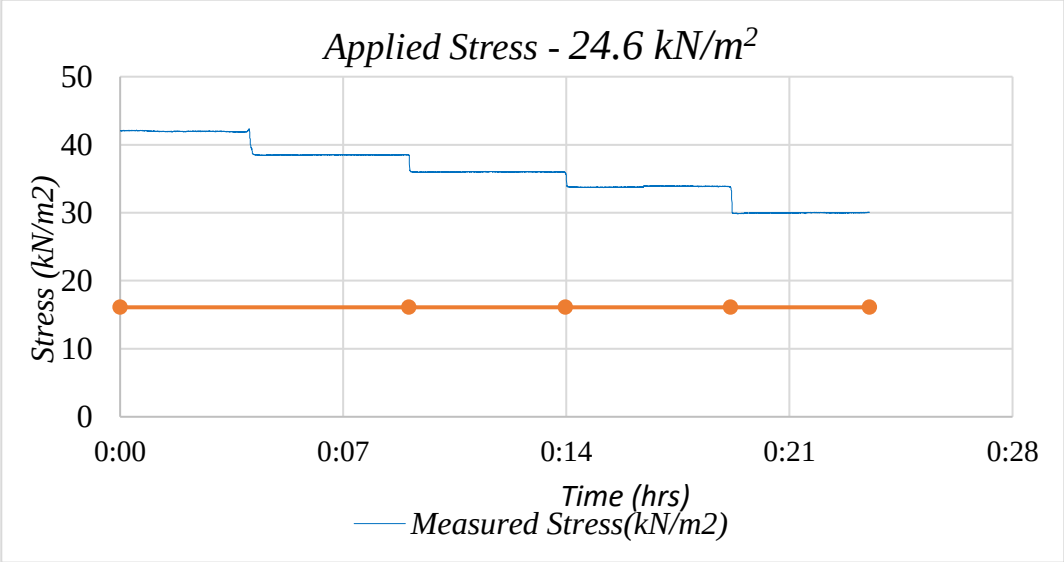

Figure 113: Stress vs time curve of the trap-door active arching model for dry sand (24.6kN/m^2)

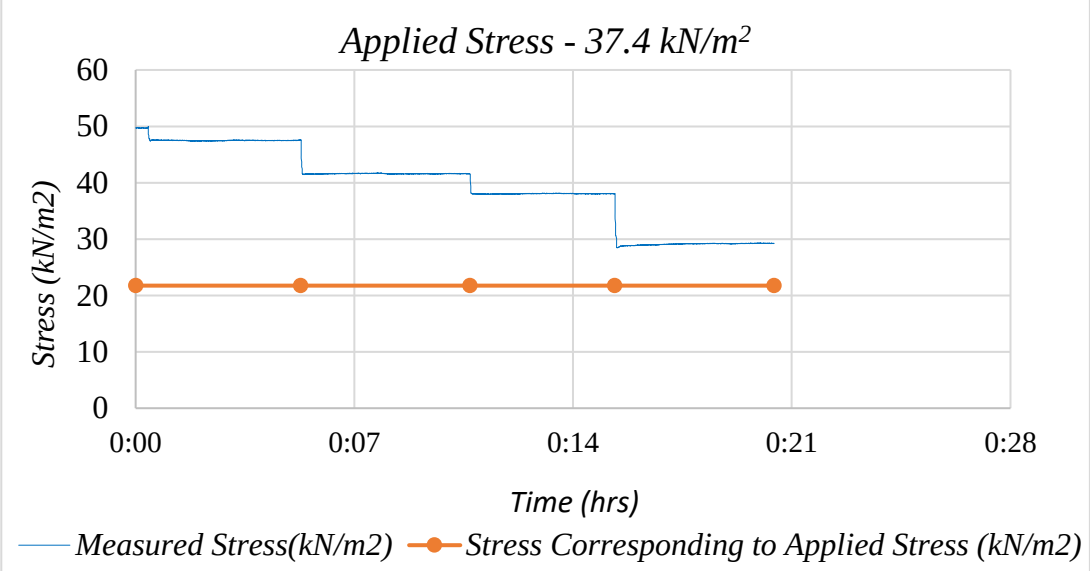

Figure 114: Stress vs time curve of the trap-door active arching model for dry sand (37.4kN/m^2)

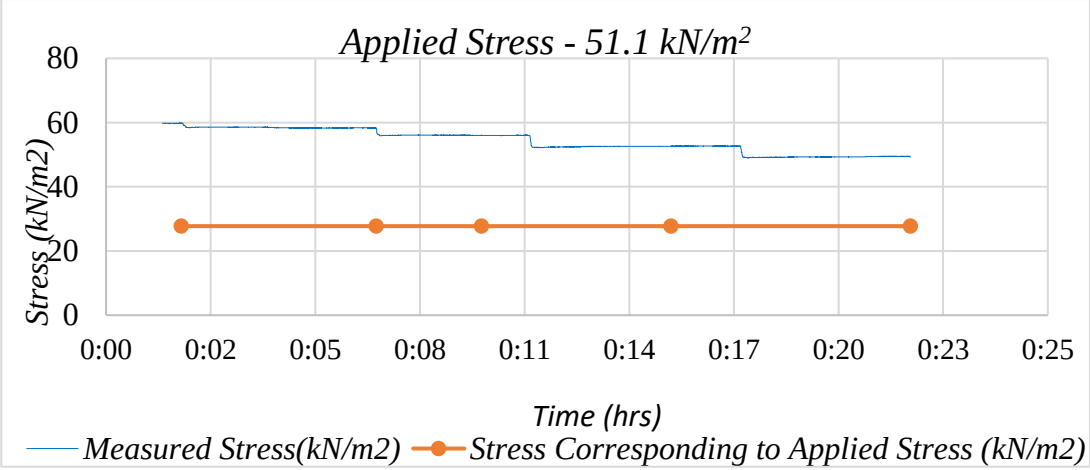

Figure 115: Stress vs time curve of the trap-door active arching model for dry sand (51.1kN/m^2)

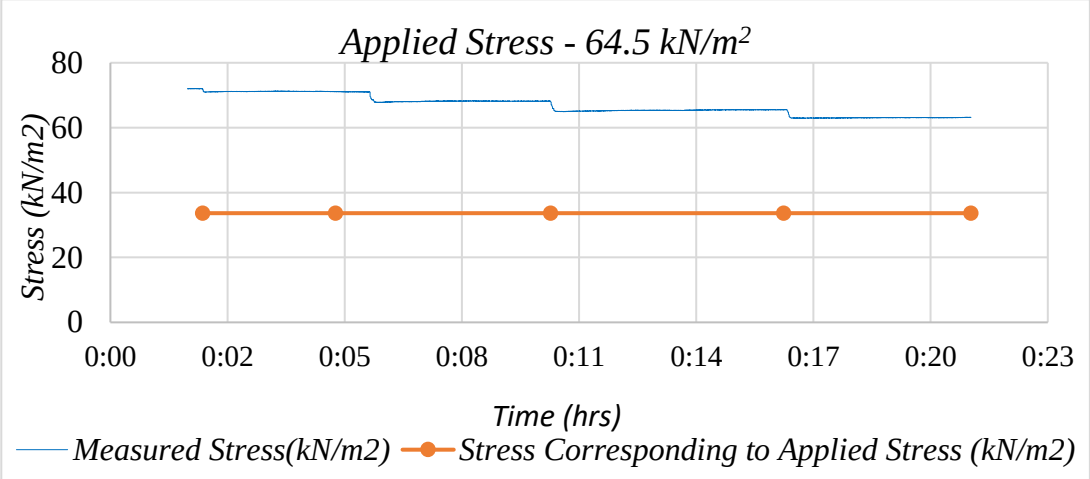

Figure 116: Stress vs time curve of the trap-door active arching model for dry sand (64.5kN/m^2)

In Figure 113, Figure 114, Figure 115 and Figure 116, loads of 24.6kN/m^2, 37.4kN/m^2, 51.1kN/m^2 and 64.5kN/m^2, respectively were applied using a hydraulic jack system. In all graphs x-axis indicate the time of experiments and y-axis indicates the measuring stress at the sensor level or in other words sensor output values. The blue line indicates the sensor value and the red line indicates the applied pressure which should be at the sensor level according to the pressure calculations. At the beginning all measured values are greater than the applied pressure unlike the experiment which was carried out using a clayey medium, because the jacking setup act like a rigid based relative to the surrounding sand layer. Therefore, initially a

passive arching might influence the results. After that, when plate was moved in the downward direction with 1mm displacement, the measuring pressure was reduce by reasonable amount which can be seen in above Figures, due to active arching.

10.4.2 Passive arching effect in dry sand with trap-door method

This experiment is the opposite of the last experiment. In this case, the trap door was moved in the upward direction of the support with respect to the surrounding area. The increment was changed in 1mm increments with time while keeping the loading constant, until a stable reading was observed. A total of 3 mm increment was created with 1mm steps. Then the same experiment was carried out for 4 loading sets.

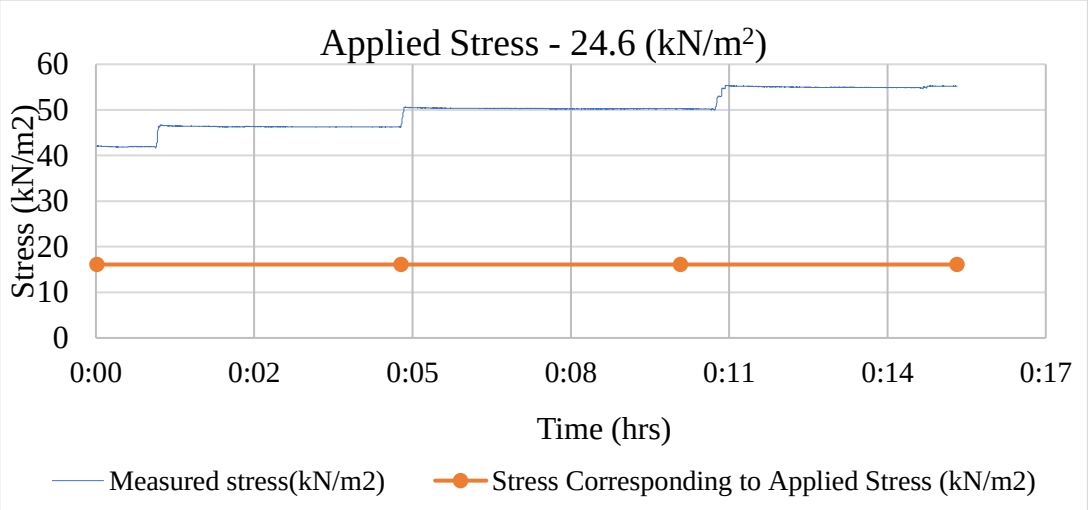

Figure 117: Stress vs time curve of the trap-door passive arching model for dry sand (24.6kN/m^2)

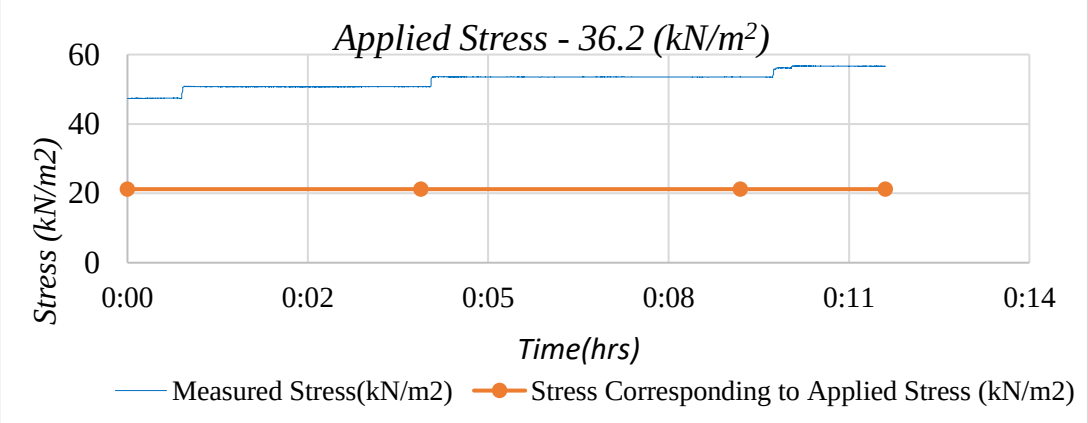

Figure 118: Stress vs time curve of the trap-door passive arching model for dry sand (36.2kN/m^2)

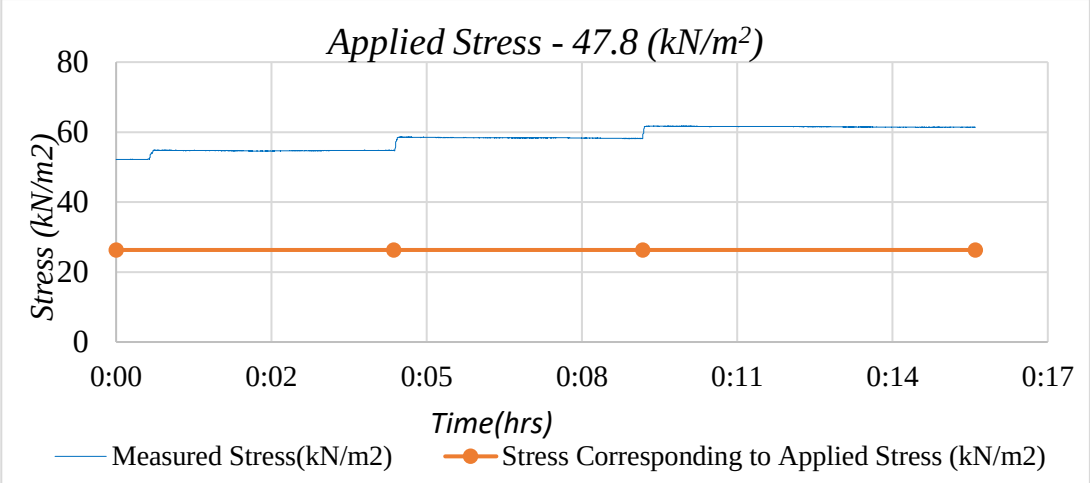

Figure 119: Stress vs time curve of the trap-door passive arching model for dry sand (47.8kN/m^2)

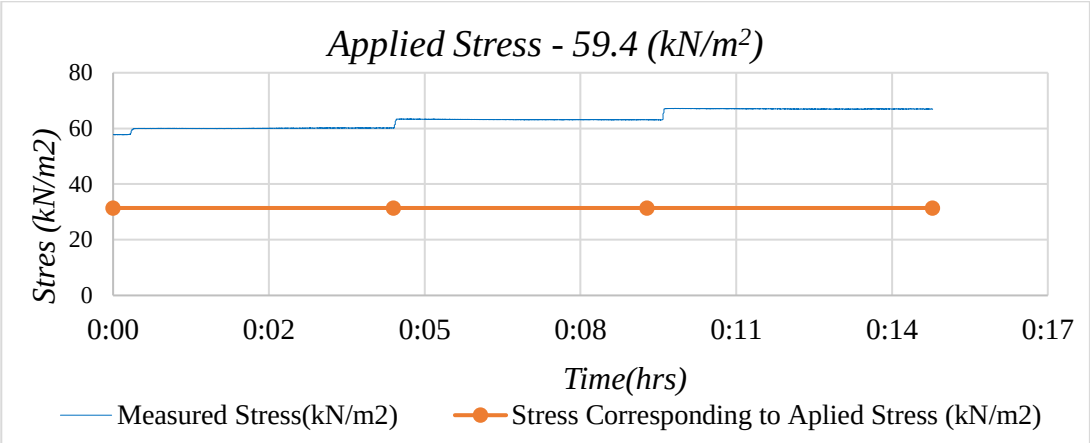

Figure 120: Stress vs time curve of the trap-door passive arching model for dry sand (59.4kN/m^2)

In Figure 117, Figure 118, Figure 119 and Figure 120 loads of 24.6kN/m^2, 36.2kN/m^2, 47.8kN/m^2 and 59.4kN/m^2, respectively were applied using a hydraulic jack system. In all graphs x-axis indicates the time of experiments and y-axis indicates the measured stress at the sensor level or in other words sensor output values. The blue line indicates the sensor value and the red line indicate the applied pressure which should be at the sensor level according to the pressure calculations. Reason for the measured value being higher than the applied one is discussed in the previous section. After that, when the plate was moved in the upward direction in 1mm displacement measured pressure was increased by a reasonable amount which can be seen in the above Figures, due to passive arching.

10.4.3 Active arching effect in saturated sand with trap-door method

From this point onwards, arching effect in saturated sand is discussed. Similar to dry sand trap-door experiments this experiment was also carried out with a known settlement while keeping the loading constant, from hydraulic jack. The settlement was changed in 1mm increments with time by keeping the loading constant, until a stable reading is obtained and similarly 4 mm total settlements were created with 1mm steps. In addition, the same experiment was carried out for 3 loading sets. Other than the previous experiments both total and effective stresses were measured in this case.

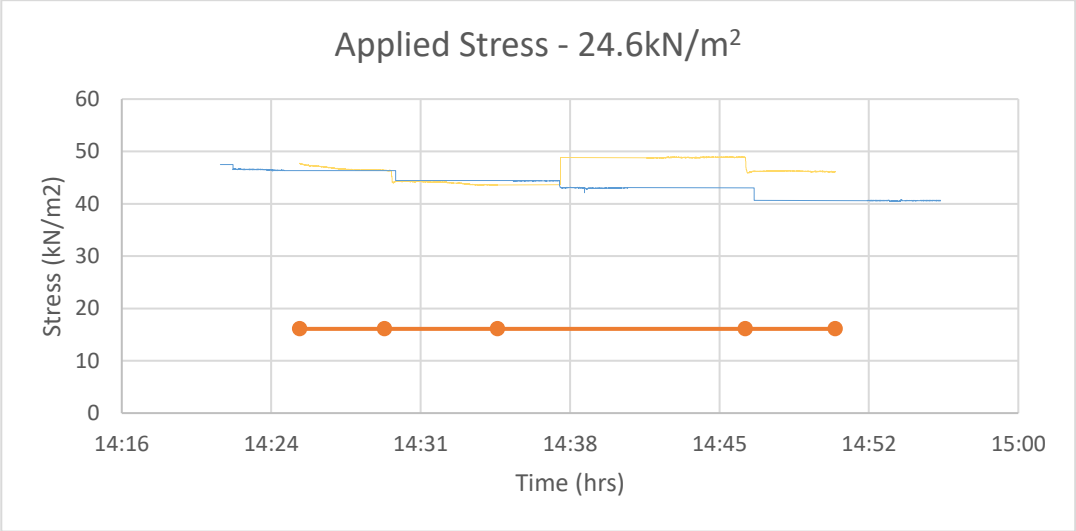

Figure 121: Stress vs time curve of the trap-door active arching model for saturated sand for total and effective pressure (applied pressure 24.6kN/m^2)

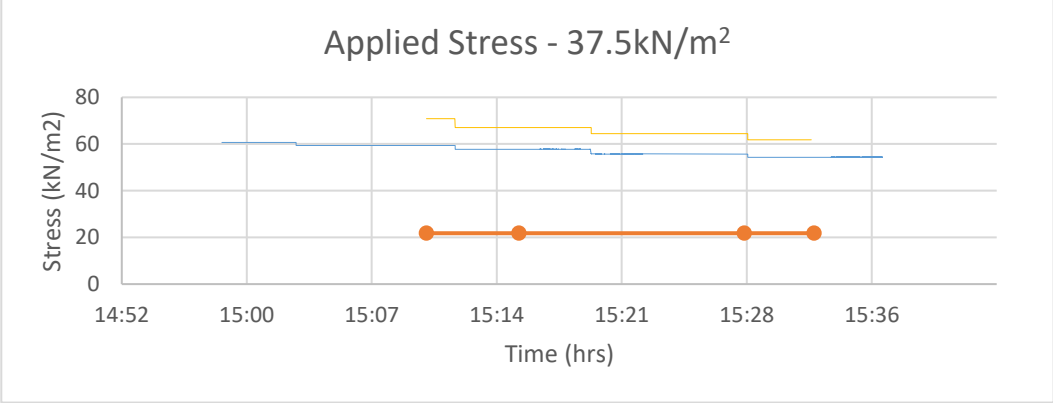

Figure 122: Stress vs time curve of the trap-door active arching model for saturated sand for total and effective pressure (applied pressure 37.5kN/m2)

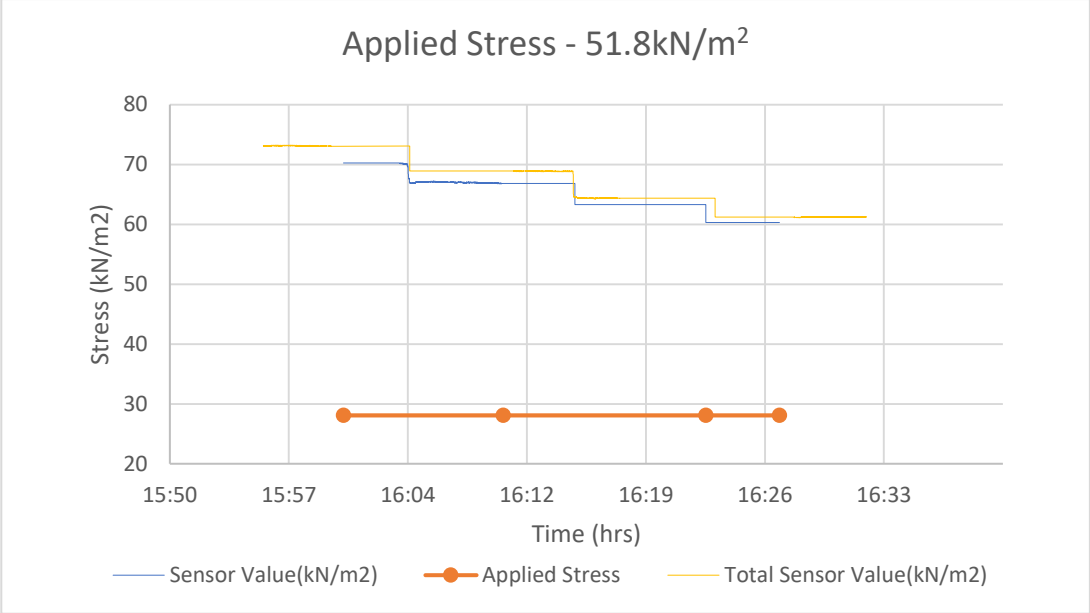

Figure 123: Stress vs time curve of the trap-door active arching model for saturated sand for total and effective pressure (applied pressure 51.8kN/m^2)

In Figure 121, Figure 122 and Figure 123 applied pressure of 24.6kPa, 37.5kPa and 51.8kPa respectively were applied using a hydraulic jack system. In all graphs x-axis indicate the time in hours of the experiment and y-axis indicates that measured stress at the sensor level or in other words sensor output values. The blue line indicates the effective sensor value, yellow line indicates the total sensor value and the red line indicate the applied pressure which should be at the sensor level according to the pressure calculations. Similar to dry sand experiments, around 3kPa value reduction happened for every 1mm settlement.

10.4.4 Passive arching effect in saturated sand with trap-door method

This experiment is quite the opposite to the last experiment. In this case, plate was moved in the upward direction from the support with respect to the surrounding area. Therefore, this experiment was carried out with a known upward movement while keeping a constant loading. Increment was changed in 1mm increment with time maintaining a constant loading until a stable reading was observed and in the same manner, 3 mm total increment were created in 1mm steps. Then the same experiment was carried out for 4 loading sets.

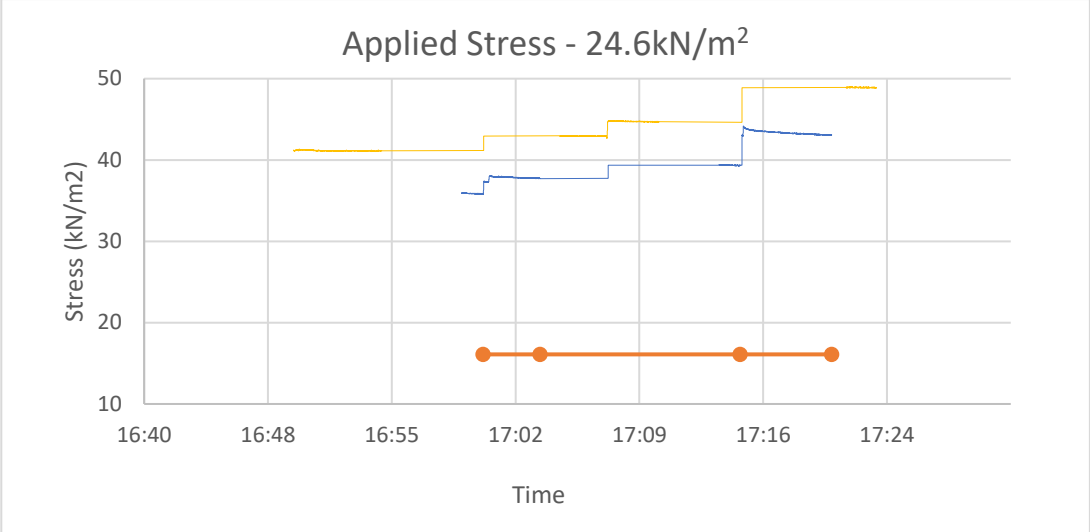

Figure 124: Stress vs time curve of the trap-door passive arching model for saturated sand for total and effective pressure (applied pressure24.6kN/m^2)

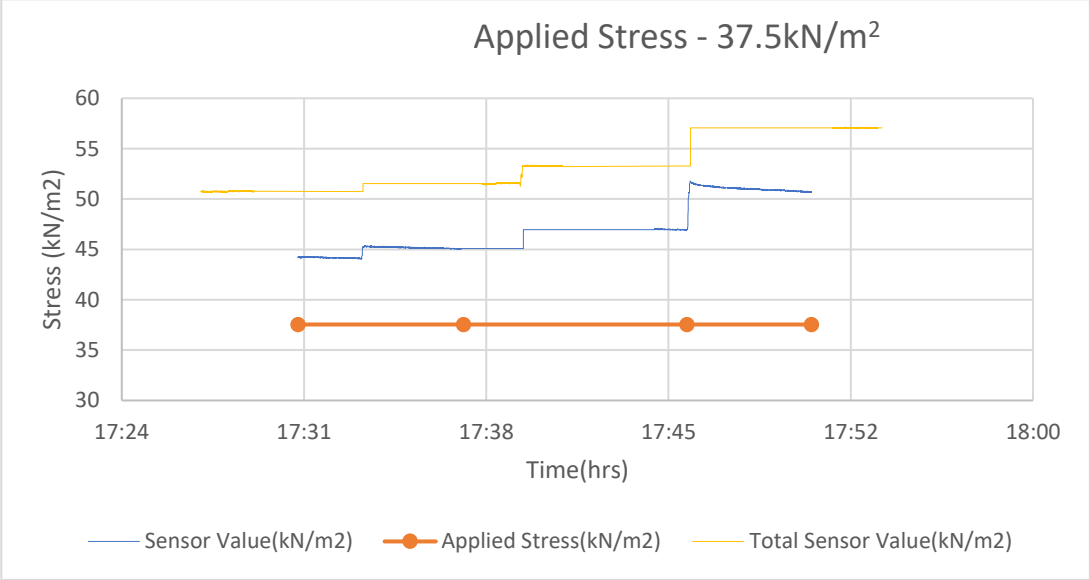

Figure 125: : Stress vs time curve of the trap-door passive arching model for saturated sand for total and effective pressure (applied pressure 37.5 kN/m^2)

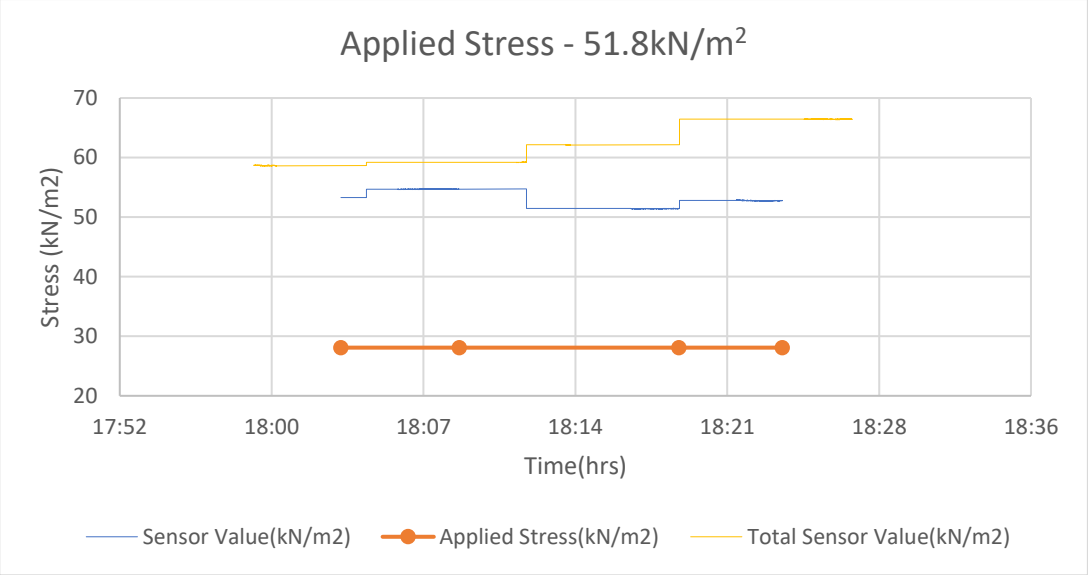

Figure 126: Stress vs time curve of the trap-door passive arching model for saturated sand for total and effective pressure (applied pressure 51.8 kN/m^2)

In Figure 124, Figure 125 and Figure 126 applied pressure of 24.6kPa, 37.5kPa and 51.8kPa respectively were applied using a hydraulic jack system. In all graphs x-axis indicate the time in hours of the experiment and y-axis indicates that measured stress at the sensor level or in other words sensor output values. The blue line indicates the effective sensor value, yellow line indicates the total sensor value and the red line indicate the applied pressure which should be at the sensor level according to the pressure calculations. Measured pressure was increased by a reasonable amount which can be seen in above Figures, due to passive arching

10.5 Discussion

Arching effect test results can be divided in to two cases which are active arching and passive arching. In clayey experiment, it was clearly seen that, active arching effect increases with load increment. In the first load increment, it showed 9% of stress reduction compared to the applied stress, in the second load increment, reduction of stress compared to the applied stress increased 12.5% and it showed 14% stress reduction in final step. When considering the test results of passive arching experiment in clayey medium, sensing stress increased with time in every loading step compared to the applied stress. But in this scenario, stress increment with respect to

the applied load, increment was not much linear. Variation was similar to that of passive arching.

In trap-door test initially it was seen that the applied stress at sensor level is less than the measured valued. The reason behind that is trap door acts like a rigid base. Therefore, passive arching effect influence on the test results. Following graph in Figure 127 is a comparison between the measured values and applied values of first experiment to verify the sensor results with Terzaghi's theory which is discussed in first section of this chapter. It shows passive arching due to the rigid base.

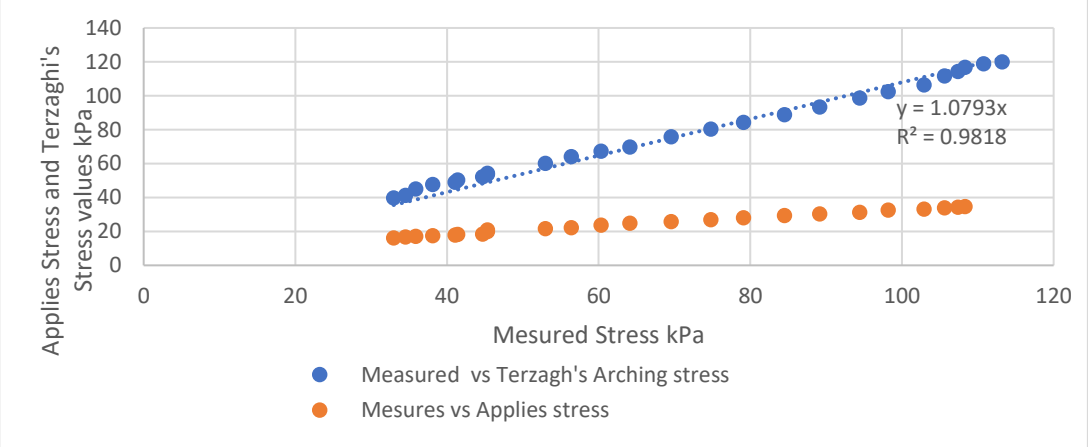

Figure 127: Measured values vs applied values

Trap door experiment is mainly divided in to dry sand test and saturated sand test. Dry sand test and saturated sand test can further be divided in to active and passive arching experiments. Common scenario of this trap door experiment series was that arching effect does not vary with time because in the clayey medium experiment, clay layer settles with time but in this experiment it does not happen. On average, 4 kN/m^2 stress reduction and increment can be obtained from the each 1mm downward movement and upward movement of the trap door. At the end, a total 4mm settlement or increment was obtained. Reduction or increment in stress with respect to the active or passive arching varied from 25% to 12%. But in the saturated test stress range varies by about 2.5 kN/m^2..

11 CONCLUSIONS AND RECOMMENDATIONS

This research was focused on developing an earth pressure cell capable of measuring both total and effective stresses. Initially an earth pressure cell with a maximum load of 150kPa with 1kPa minimum reading to measure the total and effective earth pressure in a single sensor system was developed. This sensor system consists of a data acquisition system. After the developments testing and validation was done for the developed sensor system.

Then, using the developed sensor system, arching effect of the sand was studied. Different types of simulation models were developed to study the arching effect behaviour of the dry sand and saturated sand under different conditions.

The development of the sensor system was carried out mainly in three stages. Initially the proper mechanism to develop the sensors was identified. After that the whole data acquisition system was developed and finally the output results were verified.

11.1.1 Development of the other data acquisition part

• LMP2021MAEVAL instrumentation amplifier evaluation board was selected as the bridge amplifier in this sensor bridge mainly due to 14-bit high precision one. As an analogue to digital converter ADC141s626eb evaluation board is selected.

• Then data were received from the ADC process by the micro-controller based platform.

• There were three ways provided to access the sensor data; first one was real time which can be seen through the display in the main control unit, second option was data collection from the SD card and the last was web platform developed to transfer the real time data via a cloud-based system. Therefore, this system can be used as a real time earth pressure monitoring system.

11.1.2 Testing and validation of the sensor output results.

• According to laboratory experiment which was done using a desktop multi-meter the sensitivity is 1.63 mV/V for per kPa.

• Secondly the temperature characteristic of the earth pressure cell was studied and it showed only 0.5kPa variation for room temperature of 40^0 C.

• Zero drift and hysteresis values also vary between 0 to 0.5kPa range. Therefore, this sensor can be used to measure a minimum pressure of 1kPa value.

• Finally, test was carried out to find the time taken to saturate the earth pressure cell in a sand medium. According to that test result its takes only around 1 minute to saturate and reach the equilibrium state in sand.

11.2 Conclusion of trap-door arching effect experiment

In this study, arching effect test was carried out for two main scenarios including a clayey medium experiment and a trap-door experiment. In both cases active and passive arching action was simulated.

11.2.1 Clayey medium experiments

• First the active arching effect was simulated, for that 10cm x 20cm x 10cm (length, width, height) clay cube was used, and a sensor was place on that. According to the experimental result; initially applied pressure and measured pressure became equal and when increasing the load; measured pressure reduced with different loading stages.

• Secondly the passive arching effect was simulated. For that sensor was placed on a rigid base and doughnut shape clay was placed around the sensor. Initially applied pressure and measured pressure became equal and when increasing the load measured pressure increased with different loading stages.

11.2.2 Trap-door experiment

• Initially that experiment was carried out for dry sand. For that special upward and downward moving setup was developed, and sensor was placed on that, in this case the experiment was done for both the active and passive arcing effects.

• Finally, trap-door experiment was carried out for saturated sand and in this case also the active and passive arching effect was simulated.

11.3 Recommendation for future research

•This sensor system should be developed to measure a pressure higher than the 150kPa and more accurate than the 1kPa minimum reading. Also, should optimize the dimension of the sensor packaging.

•Validation of the sensor output results for different type of soils should be done.

•Experiment should be carried out for different soil type to identify the arching effect behavior in different soil types.

•This experiment should be carried out in a real scale level.

12 REFERENCES

[1] K. Terzaghi, *Theoretical Soil Mechanics*, 2nd ed. New York, 1943.

[2] J. F. Labuz and B. Theroux, "Laboratory calibration of earth pressure cells," *Geotech. Test. J.*, vol. 28, no. 2, pp. 188–196, 2005.

[3] T. N. Dave, "A Review on Pressure Measurement using Earth Pressure Cell," vol. 04, no. 06, pp. 1031–1034, 2011.

[4] G. M. Fitz and T. L. Brandon, "Static and Dynamic Measurements Using Embedded Earth Pressure Cells," *Transp. Res. Rec. J. Transp. Res. Board*, no. 1432, pp. 86–95, 1994.

[5] O. S. Oshati, A. J. Valsangkar, and A. B. Schriver, "Earth pressures exerted on an induced trench cast-in-place double-cell rectangular box culvert," *Can. Geotech. J.*, vol. 49, no. 11, pp. 1267–1284, 2012.

[6] GLÖTZL, "LOAD CELL Models AU, AI and VW," vol. 590, pp. 10–11, 2016.

[7] L. Daigle and J. Zhao, "The influence of temperature on earth pressure cell readings," *Can. Geotech. Journaljournal*, vol. 41, pp. 551–559, 2004.

[8] I. F. Morrison and W. E. Cornish, "Description of a pressure cell for the measurement of earth pressure," *Canad. J. Res. A*, vol. 17, pp. 216–220, 1939.

[9] J. B. Hannon and K. A. Jackura, "Measurement of Earth Pressure," *Transp. Res. Rec. J. Transp. Res. Board*, no. 1004, pp. 6–13, 1985.

[10] M. R. Ahmed and M. A. Meguid, "Patents and Techniques of Contact Pressure Measurement in Geotechnical Engineering," *Recent Patents Eng.*, vol. 3, no. 3, pp. 210–219, 2009.

[11] S. A. Liu and H. L. Tzo, "A novel six-component force sensor of good measurement isotropy and sensitivities," *Sensors Actuators, A Phys.*, vol. 100, no. 2–3, pp. 223–230, 2002.

[12] D. V. D. T. Udayanga, R. Amarasinghe, "Development of a Quantum Tunneling Composite based 1-DOF Tactile Sensor Development of a Quantum

Tunneling Composite based 1-DOF Tactile Sensor," *Int. J. Adv. Inf. Sci. Technol.*, vol. 40, no. 40, 2015.

[13] A. Song, J. Wu, G. Qin, and W. Huang, "A novel self-decoupled four degree-of-freedom wrist force/torque sensor," *Meas. J. Int. Meas. Confed.*, vol. 40, no. 9–10, pp. 883–891, 2007.

[14] M. Sharifzadeh, M. T. Masouleh, and A. Kalhor, "Design, construction & calibration of a novel Human-Robot Interaction 3-DOF force sensor," *Int. Conf. Robot. Mechatronics, ICROM 2015*, pp. 182–187, 2015.

[15] C. Yuan, W. Wang, C. Han, and H. Choi, "A three degree of freedom force/torque sensor to measure foot forces," *Control. Autom. Syst. (ICCAS), 2012 12th Int. Conf.*, pp. 2028–2032, 2012.

[16] R. F. Lind, L. J. Love, J. C. Rowe, and F. G. Pin, "Multi-axis foot reaction force/torque sensor for biomedical applications," *2009 IEEE/RSJ Int. Conf. Intell. Robot. Syst. IROS 2009*, pp. 2575–2579, 2009.

[17] Omega, *Transactions in Measurement and Control Volume 2: Data Acquisition*, vol. 3. 1998.

[18] Geokon, "Model 4800 Series," 2018.

[19] J. E. Jennings and J. B. Burland, "Rand soil-pressure cell for low pressures, high accuracy and long-term stability," *J. Sci. Instrum.*, vol. 37, no. 6, pp. 193–195, 1960.

[20] G. Margason and M. J. Irwin, "Earth Pressure Cell," *Nature*, vol. 201, pp. 464–466, 1964.

[21] M. Talesnick, H. Horany, A. N. Dancygier, and Y. S. Karinski, "Measuring Soil Pressure on a Buried Model Structure for the Validation of Quantitative Frameworks," *J. Geotech. Geoenvironmental Eng.*, vol. 134, no. 6, pp. 855–865, 2008.

[22] Y. I. Rzhavin, "Fiber-optic sensors: Technical and market trends," *Meas. Tech.*, vol. 46, no. 10, pp. 949–953, 2003.

[23] P. Roriz and A. B. Lobo Ribeiro, *Fiber Optical Sensors in Biomechanics*. Elsevier Inc., 2018.

[24] D. Tosi, S. Poeggel, I. Iordachita, and E. Schena, *Fiber Optic Sensors for Biomedical Applications*. Elsevier Inc., 2018.

[25] G. B. Hocker, "Fiber-optic sensing of pressure and temperature," *Appl. Opt.*, vol. 18, no. 9, p. 1445, 1979.

[26] S. S. Chong, A. R. Abdul Aziz, and S. W. Harun, "Fibre optic sensors for selected wastewater characteristics," *Sensors (Switzerland)*, vol. 13, no. 7, pp. 8640–8668, 2013.

[27] B. G. Dandridge, A and Cogdell, "Fiber optic sensors for Navy applications," *IEEE*, 1991.

[28] B. Lee, "Review of the present status of optical fiber sensors," *Opt. Fiber Technol.*, vol. 9, no. 2, pp. 57–79, 2003.

[29] L. Ran, X. W. Ye, G. Ming, and X. B. Dong, "Structural Monitoring of Metro Infrastructure during Shield Tunneling Construction.," *Sci. World J.*, vol. 2014, 2014.

[30] M. Majumder, T. K. Gangopadhyay, A. K. Chakraborty, K. Dasgupta, and D. K. Bhattacharya, "Fibre Bragg gratings in structural health monitoring-Present status and applications," *Sensors Actuators, A Phys.*, vol. 147, no. 1, pp. 150–164, 2008.

[31] B. P. Cosentino, B. Grossman, C. Shieh, S. Doi, H. Xi, and P. Erbland, "Fiber-Optic Chloride Sensor Development," *J. Geotech. Eng.*, vol. 121, no. 8, pp. 610–617, 1995.

[32] F. Ravet, L. Zou, X. Bao, L. Chen, R. F. Huang, and H. A. Khoo, "Detection of buckling in steel pipeline and column by the distributed Brillouin sensor," *Opt. Fiber Technol.*, vol. 12, no. 4, pp. 305–311, 2006.

[33] D. Inaudi, "Overview of Fiber Optic Sensing Technologies for Geotechnical Instrumentation and Monitoring," *Geotech. Instrum. NEWS*, pp. 1–7, 2011.

[34] R. Correia *et al.*, “Fibre Bragg grating based effective soil pressure sensor for geotechnical applications,” vol. 7503, no. October, p. 75030F, 2009.

[35] T. F. H. Legge, P. L. Swart, G. Van Zyl, and A. A. Chtcherbakov, “A fibre Bragg grating stress cell for geotechnical engineering applications,” *Meas. Sci. Technol.*, vol. 17, no. 5, pp. 1173–1179, 2006.

[36] K. Weiss and H. Worn, “The working principle of resistive tactile sensor cells,” *IEEE Int. Conf. Mechatronics Autom. 2005*, no. July, pp. 471–476, 2005.

[37] S. G. Paikowsky, C. J. Palmer, and L. E. Rolwes, “The Use of Tactile Sensor Technology forMeasuring Soil Stress Distribution Samuel,” *Proc. Geocongress 2006*, no. 978, pp. 3–8, 2006.

[38] S. Springman, P. Nater, R. Chikatamarla, and J. Laue, *Use of flexible tactile pressure sensors in geotechnical centrifuges*. 2002.

[39] Y. W. Choo, T. H. Abdoun, M. J. O’Rourke, and D. Ha, “Remediation for buried pipeline systems under permanent ground deformation,” *Soil Dyn. Earthq. Eng.*, vol. 27, no. 12, pp. 1043–1055, 2007.

[40] T. H. Abdoun *et al.*, “Factors influencing the behavior of buried pipelines subjected to earthquake faulting,” *Soil Dyn. Earthq. Eng.*, vol. 29, no. 3, pp. 415–427, 2009.

[41] T. D. O’Rourke *et al.*, “Geotechnics of Pipeline System Response to Earthquakes,” *Geotech. Earthq. Eng. Soil Dyn. IV*, pp. 1–38, 2008.

[42] L. D. Suits, T. C. Sheahan, I. Weidlich, and M. Achmus, *Measurement of Normal Pressures and Friction Forces Acting on Buried Pipes Subjected to Cyclic Axial Displacements in Laboratory Experiments*, vol. 31. 2008.

[43] Y. Xiao and S. Xiaoke, “Soil pressure mini-sensor made of monocrystalline silicon and the measurement of its sensitivity coefficient,” *J. Wuhan Univ. Technol. Sci. Ed.*, vol. 20, no. 4, pp. 135–137, 2005.

[44] C. Redshaw and S. A. Group, “A sensitive miniature pressure cell,” vol. 31, p. 50, 1954.

[45] A. C. Tory and R. W. Sparrow, “The influence of diaphragm flexibility on the performance of an earth pressure cell,” *J. Sci. Instrum.*, vol. 44, no. 9, pp. 781–785, 1967.

[46] V. Askegaard, *Measurement of pressure in solids by means of pressure cells*, no. 28. 1963.

[47] K. R. Peattie, “The Fundamental Action of Earth Pressure Cell,” *J. Mech. Phymia Solid&*, vol. 2, 1954.

[48] W. A. Weiler Jr and F. H. Kulhawy, *Factors affecting stress cell measurements in soil.*, vol. 108. 1982.

[49] S. F. Brown, “STRESSES LAYERED AND DEFORMATIONS PAVEMENT DYNAMIC SYSTEMS LOADS IN FLEXIBLE TO by Thesis for the submitted degree of to the Doctor of of Philosophy , Nottingham,” 1967.

[50] V. Reg, B. A. Sch, W. L. Kraft, D. Unterschied, S. Granit, and W. Abb, “Die bautechnik 7.,” no. April, 1929.

[51] M. Arshad and B. C. O. Kelly, “Use of Miniature Soil Stress Measuring Cells under Repeating Loads,” *in*, pp. 177–182, 2014.

[52] W. Andrew Take, *Lateral earth pressures behind rigid fascia retaining walls*. 2018.

[53] V. Askegaard, “Applicability of normal and shear stress cells embedded in cohesionless materials,” *Exp. Mech.*, vol. 35, no. 4, pp. 315–321, 1995.

[54] N. R. Faces, “Earth Pressure on Retaining Walls,” vol. 113, no. 21544, pp. 586–599, 1987.

[55] C. R. I. Clayton and A. V. . Bica, “The design of diaphragm-type boundary total stress cells,” no. 2, pp. 349–351, 1993.

[56] L. Chen and A. Song, “A novel three degree-of-freedom force sensor,” *2009 Int. Conf. Meas. Technol. Mechatronics Autom. ICMTMA 2009*, vol. 1, pp. 77–80, 2009.

[57] A. Marston and A. O. Anderson, “The Theory of Loads on Pipes in Ditches and Tests of Cement and Clay Drain Tile and Sewer Pipe,” *Iowa State Coll. Agric. Mech. Arts*, vol. 11, no. 31, No.5, 1913.

[58] K. Szechy, *Art of tunnelling*. 1970.

[59] R. L. Handy, “The Arch in Soil Arching,” *J. Geotech. Eng.*, vol. 111, no. 3, pp. 302–318, 1985.

[60] C. Lee, “Computer Analysis of Cross Canyon Culvert,” 1982.

[61] D. O. Potyondy and P. A. Cundall, “A bonded-particle model for rock,” *Int. J. Rock Mech. Min. Sci.*, vol. 41, no. 8 SPEC.ISS., pp. 1329–1364, 2004.

[62] P. P. Balestrassi, E. Popova, A. P. Paiva, and J. W. Marangon Lima, “Design of experiments on neural network’s training for nonlinear time series forecasting,” *Neurocomputing*, vol. 72, no. 4–6, pp. 1160–1178, 2009.

[63] P. A. Cundall and O. D. L. Strack, “A discrete numerical model for granular assemblies,” *Géotechnique*, vol. 29, no. 1, pp. 47–65, 1979.

[64] R. Zhang and G. Jiang, “Numerical Analyses of Soil Arching Mechanism For Passive Laterally Loaded Piles at the Mesoscopic Scale,” vol. 20, pp. 1667–1680, 2015.

[65] N. Oreskes, K. Shrader-frechette, K. Belitz, N. Oreskes, K. Shrader-frechette, and K. Belitz, “Verification , Validation , in Models Numerical and the Confirmation of Earth Sciences,” vol. 263, no. 5147, pp. 641–646, 2010.

[66] J. W. McNulty, “An experimental study of arching on sand,” in *US Army Corps of Engineers Technical Report I-674*, no. 1, 1965.

[67] B. Ladanyi and B. Hoyaux, “A STUDY OF THE TRAP-DOOR PROBLEM IN A GRANULAR MASS,” *Can. Geotech. J.*, vol. 6, no. 1, pp. 1–14, 1969.

[68] G. W. Harris, “A sandbox model used to examine the stress distribution around a simulated longwall coal-face,” *Int. J. Rock Mech. Min. Sci.*, vol. 11, no. 8, pp. 325–335, 1974.

[69] I. Vardoulakis, “Trap-Door Problem with Dry Sand: A Statical Approach Based Upon Model Test Kinematic,” *Int. J. Numer. ANALnICAL METHODS Geomech.*, vol. 5, no. November 1979, pp. 57–78, 1981.

[70] C. H. EVANS, “AN EXAMINATION OF ARCHING IN GRANULAR SOILS by,” 1984.

[71] G. Lglesia, H. H. E. R. V. Whitman, and Sponsored, “Stochastic and Centrifuge Modelling of Jointed Rock,” 1990.

[72] T. Yoshida, F. Tatsuoka, and M. Siddiquee, *Shear banding in sands observed in plane strain compression*. 1994.

[73] H. Tien, “A Literature Study of the Arching Effect,” no. 1990, 1996.

[74] G. Iglesia, H. Herbert, and V. Robert, “Stochastic and Centrifuge Modelling of Jointed Rock,” no. December, 1990.

[75] J. Sadrekarimi and A. Abbasnejad, “Arching effect in fine sand due to base yielding,” *Can. Geotech. J.*, vol. 47, no. 3, pp. 366–374, 2010.

[76] R. Rui, A. F. Van Tol, Y. Y. Xia, S. J. M. Van Eekelen, and G. Hu, “Investigation of soil-arching development in dense sand by 2D model tests,” *Geotech. Test. J.*, vol. 39, no. 3, pp. 415–430, 2016.

[77] Ruuki, *Aluminium AW 6082 T6 round*. 2012.